7-13-2020

Gasoline Production Fischer-Tropsch Synthesis using Bi-Functional Structured Catalytic Reactors

Chunxiang Zhu
University of Connecticut - Storrs, chunxiang.zhu@uconn.edu

Gasoline Production Fischer-Tropsch Synthesis using Bi-Functional Structured Catalytic Reactors

Chunxiang Zhu, PhD

University of Connecticut, 2020

Gasoline accounts for more than half of U.S. transportation energy usage and its consumption continues growing. Crude oil is where gasoline originates from. However, crude oil reserves are limited in most of the countries around the world. U.S. imports thousand barrels of gasoline per day, making it highly dependent on foreign oil import which imposes a threat to U.S. homeland security. To make the U.S. gasoline independent, alternative processes such as Fischer-Tropsch Synthesis process (FTS) can be promising to mitigate high gasoline demand on transportation fuel and increase fuel diversity. However, scalable, selective and more efficient FTS technologies are required to align with the need for high gasoline production.

Energy independence and security are some of the merits of making FTS a more efficient and less centralized process. Among the many challenges in FTS catalysis, selectivity to gasoline-range products is vital to be addressed. FTS uses synthesis gas (syngas, CO and H_2) as feedstock. Normally, it follows the Anderson-Schulz-Flory (ASF) distribution. FTS can be environmentally benign and friendly, since there is no sulfur or nitrogen in the products. While FTS is conceived as a diesel-producing process, using either a cobalt or an iron catalyst. A bifunctional catalyst can be formulated and applied to improve gasoline selectivity via oligomerization, aromatization, and isomerization reactions. This thesis aims at exploring the potential of structured catalysts as candidates for intensified FTS process selective to gasoline production.

Chunxiang Zhu, University of Connecticut, 2020

In this thesis, structured bifunctional catalysts consisting of a monolith support, cobalt catalyst and ZSM-5 with micro- or mesoporosity were synthesized and tested in a fixed bed reactor. Fine tuning of the catalyst and process condition led to desirable gasoline selectivity. However, the CO conversion was hindered due to the mass transfer limitations in the micro-porous zeolite. Mesopores were, thus, introduced later to relax mass transfer limitation. CO conversion increased to near 90%, while maintaining high gasoline selectivity with the introduction of the mesopores. A highly active and selective structured catalyst was formulated. After successful synthesis and testing of the bifunctional structured catalysts, modeling was performed to assess the techno-economic feasibility and potential of the new catalytic process. The experimental data was used in a modular Gas-to-Liquid (GTL) plant to further study the potential of the structured catalysts for an intensified process, aiming to monetize stranded natural gas.

Gasoline Production Fischer-Tropsch Synthesis using Bi-Functional Structured Catalytic Reactors

by

Chunxiang Zhu

B. S., Dalian University of Technology, 2013

A Dissertation Submitted in

Partial Fulfillment of the Requirements for the Degree of

Doctor of Philosophy

At the University of Connecticut

2020

APPROVAL PAGE

Gasoline Production Fischer-Tropsch Synthesis using Bi-Functional Structured Catalytic Reactors

by

Chunxiang Zhu, B.S

Major Advisor: _____
George M. Bollas, Ph.D.

Associate Advisor: _____
Puxian Gao, Ph.D.

Associate Advisor: _____
Brian Willis, Ph.D.

Associate Advisor: _____
Julia A.Valla, Ph.D.

Associate Advisor: _____
Luyi Sun, Ph.D.

University of Connecticut, 2020

DEDICATION

This thesis is dedicated to my family members, my mom, dad, brother and sisters and all the people who love me in the past, the present and the future.

ACKNOWLEDGEMENTS

I would like to first thank my advisor, Prof. George Bollas, for taking me under his wings and teaching me everything he knows about academia research, paper writing, data analysis, critical thinking, so on and so forth, for the countless days and nights he spent on editing our disastrous papers and posters, even conference abstracts, for his hidden love caring for our future and development. He never said anything about that, but it can be felt so deeply. It might be my fate joining his group and I feel so blessed being part of the SOFT lab, with so many awesome lab mates and so much to learn. More than five years of my life have been framed inside and it is a true wealth that will keep me accompany for the rest of my life. I would also like to thank Prof. Brian Willis, Prof. Julia Valla, Prof. Puxian Gao, and Prof. Luyi Sun for serving on my committee. I really appreciate their willingness to take on this responsibility despite their busy schedule. I am also grateful for all the supporting staff at both UCONN ChEG department and C2E2 (Leah, Susan, Amy, Terry and Sheila). Finally, I would also like to extend my gratitude to the C2E2 technical staff, Garry, Pete and Mark, for keeping a safe and organized researching environment. They are more friends than technicians.

Many thanks go to both former and current group members for their help along the way. I was blessed to work alongside Dr. Shoucheng Du, whom as the first generation in Bollas group, made it so much easier for me to adapt and work in the group. He and his wife Ting Jiang offered help for me not only on research, but also on the feeling of a sense of belonging at where I am far away from home. Dr. Han Lu, Dr. Zhiquan Zhou, Dr. Kyle Palmer and Dr. Chen Chen, they are all part of my life and study, thanks to their appearance in my life, making it so colorful. I would like to acknowledge the current group members including Williams Hale, Xi Yang and Brian

Billie, for their help and great memories shared in the lab. Other UCONN graduate students that should not be forgotten Dr. Kevin Lee, and Akie Fujita who have been treating me like a family member. Special thanks go out to Dr. David Gamliel and Dr. Julia Valla for their collaborative work that resulted in my second paper. Last but not least, thanks also go to my close friends Dr. Jin Zhu, Dr. Yang Wu, Dr. Yuan Hao, Dr. Wenxiang Tang and Dr. Xingxu Lu for their accompany and selfless share.

Finally, I would like to thank my family for all their love and support throughout my graduate school career. My mom, Yurong Chen, her encouragement, education and unconditional love played a significant role in shaping me into the person I am today. I am also grateful for my dad, Yongzhou Zhu, sisters, Xiaoyan Zhu, Xiaolin Zhu, Xiaoqing Zhu and my brother Xiaoping Zhu, for their continuous love and care that got me through the journey of graduate school. There was a tough time in my life. Without their selfless love, I could not be here today. I would also like to acknowledge my brother in law Chunbo Yi, for his support, encouragement, sacrifices and contributions to the family. I would also like to give my gratitude to my girlfriend, XihuiWang, who showed up during my toughest time and brought me so much enjoyable time. She has a pure heart.

TABLE OF CONTENTS

APPROVAL PAGE ..... **iv**
DEDICATION ..... **v**
ACKNOWLEDGEMENTS ..... **vi**
TABLE OF CONTENTS ..... **viii**
LIST OF TABLES ..... **xi**
LIST OF FIGURES ..... **xii**
Chapter 1 ..... **1**
INTRODUCTION **1**
1.1 Objectives 1
1.2 Scope of the Dissertation 2
1.3 Crude Oil Status and Rising Gasoline Transportation Fuel Demand 3
1.4 Natural Gas Status 7
1.5 Fischer-Tropsch Synthesis 11
1.5.1 Catalysts used in FTS 12
1.5.2 Reaction mechanism of FTS 14
1.5.3 Commercial FTS reactors and monolithic reactor 21
1.5.4 Gasoline production FTS 24
1.6 Modularization of Gas-to-Liquid Plant 28
Chapter 2 ..... **32**
EXPERIMENTAL PROTOCOLS **32**
2.1 Introduction 32
2.2 Bifunctional Catalysts Preparation Methods 32
2.2.1 Multi-layer Monolith Catalyst Synthesis 33
2.2.2 Hierarchical ZSM-5 preparation 35
2.3 Experimental Apparatus 35
2.3.1 Construction and validation of the setup 35
2.3.2 Calibration of the equipment and products analysis method 37
2.4 Fixed Bed Bifunctional Catalysts Experiment 39
2.4.1 Bifunctional catalysts fixed bed performance 39
2.4.2 Bifunctional catalysts regeneration 40

2.5 Catalysts Characterization Techniques 41
2.5.1 N_2 adsorption/desorption-porosity and surface area 41
2.5.2 FTIR-acid sites quantification and surface species identification 43
2.5.3 Electron microscopy-surface morphology, elemental mapping and particle size .. 43
2.5.4 XRD-material phase and Co particle size 44
Chapter 3 45
GASOLINE SELECTIVE FISCHER-TROPSCH SYNTEHSIS IN STRUCTURED BIFUNCTIONAL CATALYSTS 45
3.1 Introduction 45
3.2 Description of Experimental Facilities and Methods 48
3.2.1 Multi-layer Monolith Catalyst Synthesis 48
3.2.2 Experimental Apparatus and Procedure 49
3.2.3 Gas and Liquid Product Analysis 51
3.3 Catalyst Characterization 53
3.3.1 Characterization of the fresh structured catalysts 53
3.3.2 Structure of the Catalysts 56
3.3.3 Transmission Electron Microscopy and Energy Dispersive X-ray Spectroscopy .. 57
3.4 Results and Discussion 58
3.4.1 ZSM-5 Effect on FTS Performance and Products Selectivity 58
3.4.2 Temperature Effect on ZSM-5 Coated Monolith Catalysts Performance 62
3.4.3 Pressure Effect on ZSM-5 Coated Monolith Catalyst Performance 64
3.5 Conclusions 68
Chapter 4 69
FISCHER-TROPSCH SYNTHESIS IN MONOLITH CATALYSTS COATED WITH HIERARCHICAL ZSM-5 69
4.1 Introduction 69
4.2 Experimental 71
4.2.1 Monolith Catalyst and Hierarchical ZSM-5 Preparation 71
4.2.2 FTS Lab-scale process 73
4.2.3 Product Quantification 75
4.2.4 Characterization Methods 76
4.3 Results 77
4.3.1 Characterization of Meso-ZSM-5 77
4.3.2 SEM and TEM Characterization of the Structure of the 1.1 g-Meso-ZSM-5 co-catalyst 79

4.3.3 FTS with Meso-ZSM-5 Catalyst 81
4.3.4 Meso-ZSM-5 Layer Thickness 85
4.3.5 Pressure Effect on 1.6 g-Meso-ZSM-5 Co-catalysts Performance 88
4.4 Catalyst Deactivation 91
4.4.1 TPO Characterization 92
4.4.2 FTIR Characterization 94
4.4.3 BET Characterization 95
4.4.4 Catalysts in-situ regeneration 96
4.5 Conclusions 98
Chapter 5 99
TECHONO-ECONOMIC ANALYSIS OF A MODULAR GAS-TO-LIQUID PROCESS TO MONETIZE STRANDED NATURAL GAS 99
5.1 Introduction 99
5.2 Simulations 102
5.2.1 Process description 102
5.2.2 Simulation basis 102
5.2.3 Reforming block 104
5.2.4 FTS block 108
5.2.5 Upgrading block 111
5.3 Total Capital Investment and Product Cost Estimation 112
5.4 Preliminary Results and Discussion 114
5.5 Conclusions 119
Chapter 6 120
CONCLUSIONS AND FUTURE PERSPECTIVE 120
6.1 Conclusions 120
6.2 Future Perspective 122
APPENDIX I: MISCELLANEOUS INFORMATION AND COPYRIGHT 125
APPENDIX II: PUBLICATIONS AND PRESENTATIONS 127
REFERNCES 128

LIST OF TABLES

Table 1-1. Stranded natural gas potential 10

Table 1-2. Syncrude compositions representative of low temperature Co-based catalysts, low temperature Fe-based catalysts and high temperature Fe-based catalysts [37] 13

Table 1-3. Major reactions of FTS [39] 15

Table 1-4. Current commercial GTL plants in operation 29

Table 3-1**:** Monolithic Catalysts Preparation Parameters Summary 49

Table 3-2**.** Structure Parameters of the Materials studied 55

Table 3-3. Performance of Monolith Catalyst with and without ZSM-5. Reaction conditions: Temperature: 230 °C, Pressure: 12 bar, H_2/CO: 2:1, Syngas flowrate: 35 ml/min, Catalyst loading: 2.9 g for ZSM-5/Co-Al_2O_3/M and 2.3 g for Co-Al_2O_3/M, Co loading: 3.3 wt.% for ZSM-5/Co-Al_2O_3/M and 6.5 wt.% for Co-Al_2O_3/M, Time of experiments: 48 h* 59

Table 3-4. Conversion and Selectivity Summary of ZSM-5/Co-Al_2O_3/M Catalyst as a Function of Temperature. Reaction conditions: Catalyst loading: 2.9 g, Co loading: 3.3 wt.%, Pressure: 12 bar, H_2/CO ratio: 2:1, Syngas flowrate: 35 ml/min, Time on stream: 48 h. Reference commercial selectivities are reported in Table 3-3 63

Table 3-5. FTS Performance Summary of ZSM-5/Co-Al_2O_3/M Catalyst at Different Pressures. Reaction conditions: Catalyst loading: 2.9 g, Co loading: 3.3 wt.%, T: 230 °C, H_2/CO ratio: 2:1, syngas flowrate: 35 ml/min, Time on stream: 48 h. Reference commercial selectivities are reported in Table 3-3 66

Table 4-1. Monolith co-catalysts synthesized and loading of each catalyst component 73

Table 4-2. N_2 isotherm properties summary for parent Micro-ZSM-5 and Meso-ZSM-5 78

Table 4-3. Phase status in FTS reactor at different pressures 89

Table 4-4. Data summary for fresh 1.1 g-Meso-ZSM-5 catalyst and used co-catalysts with different Meso-ZSM-5 loadings 96

Table 5-1. Fractional conversion of all the carbon species used in FTS block 111

Table 5-2. Six-tenths factors used for bare module equipment cost estimation 112

Table 5-3. Chemical Engineering Plant Cost Index (CEPCI) changing with year [240,241] 112

Table 5-4. Economic assumptions and base case market prices 113

LIST OF FIGURES

Figure 1-1. Percentage of the petroleum products obtained from crude oil [5] 5

Figure 1-2. World transportation consumption by fuel 2012 [7] 6

Figure 1-3. U.S total wet natural gas proved reserves up to 2018 [12] 9

Figure 1-4. Four ways of transporting natural gas to market and the role of GTL in the gas economy [13] 10

Figure 1-5: Overall GTL process using FTS for liquid fuels production 12

Figure 1-6: FTS products selectivity as a function of the chain growth probability 16

Figure 1-7. CO insertion mechanism for FTS proposed by Pichler and Schulz [47]. (A) Initiation mechanism to form $=CH_2$ (H_2 assisted CO activation). (B) Chain propagation to form alcohol and alpha olefin 18

Figure 1-8. Chain growth in the CO insertion mechanism proposed by Masters [49] 19

Figure 1-9. Carbide mechanism [57] 20

Figure 1-10. Oxygenate mechanism offered by Deluzarche et al. [58] 20

Figure 1-11. Another oxygenate mechanism proposed by Sapienza [59] 21

Figure 1-12. Different types of reactors for FTS used in industry [60] 22

Figure 1-13. Three ways of bifunctional FTS catalysts preparation. (a) physical mixture, (b) Co supported on zeolite, (c) layered structure or core-shell structure (red color represents zeolite; blue is Co and green is support)..... 26

Figure 1-14. Flaring of natural gas around the world under a satellite view [95] 29

Figure 2-1. Schematic drawing of the layered structured catalyst with zeolite coating 33

Figure 2-2. Structured bifunctional catalysts preparation flow chart 34

Figure 2-3. Schematic drawing of the fixe bed reactor used in the fixed bed experiments..... 36

Figure 2-4. Repeatability tests to verify the fixed bed set up stability 37

Figure 3-1**.** Schematic drawing of the fixed bed reactor used in this work 51

Figure 3-2. N_2 adsorption-desorption isotherms of the FTS catalysts and baseline materials 54

Figure 3-3. XRD patterns of fresh catalysts: (a) Monolith catalyst coated with Al_2O_3, Co_3O_4, and ZSM-5. (b) Monolith catalyst without ZSM-5 coating..... 56

Figure 3-4. (a) Monolith catalyst coated with Al_2O_3, Co_3O_4, and ZSM-5. (b) Al, Si and Co line mapping along the red arrow from (a) 57

Figure 3-5. Top: TEM image for (a) Co-Al_2O_3/M used catalyst, (b) ZSM-5/Co-Al_2O_3/M used catalyst. Bottom: EDS for ZSM-5/Co-Al_2O_3/M used catalyst 58

Figure 3-6. Overall performance summary for catalyst with and without ZSM-5 coating. Reaction conditions as noted in Table 3-3 59

Figure 3-7. The liquid hydrocarbon distribution. (a) Selectivity of different carbon number species for Co-Al_2O_3/M and ZSM-5/Co-Al_2O_3-M. (b) (c) Paraffin, isomer, olefin selectivity as a function of carbon number for Co-Al_2O_3/M and ZSM-5/Co-Al_2O_3/M. Reaction conditions as noted in Table 3-3 62

Figure 3-8. Overall performance summary of temperature effect for catalyst with ZSM-5 coating. Reaction conditions as noted in Table 3-4 63

Figure 3-9. Liquid hydrocarbons selectivity from FTS at different temperatures. Reaction conditions as noted in Table 3-4 64

Figure 3-10. Overall performance summary of pressure effect for catalyst with ZSM-5 coating. Reaction conditions as noted in Table 3-5 65

Figure 3-11. Liquid hydrocarbon selectivity from FTS at different pressures. Reaction conditions as noted in Table 3-5 67

Figure 4-1. Left: N_2 isotherm for parent Micro-ZSM-5 and Meso-ZSM-5. Right: T-plot for parent Micro-ZSM-5 and Meso-ZSM-5 78

Figure 4-2. DRIFTS-FTIR spectra of Micro-ZSM-5 and Meso-ZSM-5 materials after pyridine titration 79

Figure 4-3. Top: SEM image of the 1.1 g-Meso-ZSM-5 co-catalyst. Bottom: Line EDS mapping along the red arrow indicated in the SEM image 80

Figure 4-4. Left: SEM image of the layered structure of the 1.1 g-Meso-ZSM-5 co-catalyst. Right Top: TEM image of the Meso-ZSM-5 layer. Right Bottom: Elemental mapping of the 1.1 g-Meso-ZSM-5 co-catalyst without the Meso-ZSM-5 layer 81

Figure 4-5. Monolith w/o ZSM-5, 1.1 g-Micro-ZSM-5 and 1.1 g-Meso-ZSM-5 catalysts performance comparison. Reaction conditions: T: 230 °C; P: 12 bar; Syngas flowrate: 35 ml/min; Time on stream: 48 h. (Note: C_5-C_{12}, C_{13+} and Paraffin, Isomer, Olefin in subplot (c) in Figure 4-5 are used to show gasoline, non-gasoline selectivity in the oil phase and the oil quality. Gasoline yield in the subplot (d) was calculated by the weight of gasoline produced divided by the total weight of syngas converted. This note holds for the rest of the plots in the paper.) 82

Figure 4-6. (a) Oil carbon number selectivity and paraffin, isomer and olefin selectivity for (b) monolith w/o ZSM-5. (c) 1.1 g-Micro-ZSM-5, and (d) 1.1 g-Meso-ZSM-5 co-catalysts..... 84

Figure 4-7. Co-catalysts performance with different Meso-ZSM-5 coatings. Reaction conditions: T: 230 °C; P: 12 bar; Syngas flowrate: 35 ml/min; Time on stream: 48 h 86

Figure 4-8. Carbon number distribution in the liquid products from different Meso-ZSM-5 loadings 87

Figure 4-9. Co-catalysts performance of 1.6 g-Meso-ZSM-5 at different pressures. Reaction conditions: T: 230 °C; Syngas flowrate: 35 ml/min; Time on stream: 48 h 90

Figure 4-10. Carbon number distribution of the liquid products from the 1.6 g-Meso-ZSM-5 co-catalysts at different pressures 91

Figure 4-11. 1.6 g-Meso-ZSM-5 CO conversion profile. Reaction condition: T: 230 °C; Pressure: 12 bar; Syngas flowrate: 35 ml/min; Time on stream: 48 h 92

Figure 4-12. TPO and DTG for 1.6 g-Meso-ZSM-5 used co-catalysts 93

Figure 4-13. TPO weight loss and corresponding TPO peak temperature for used co-catalysts with different Meso-ZSM-5 loading 93

Figure 4-14. (a) FTIR spectra for the 1.1 g-Meso-ZSM-5 co-catalysts before and after FTS reaction. (b) Temperature programed FTIR spectra for the used 1.1 g-Meso-ZSM-5 co-catalyst. 94

Figure 4-15. Pore size distribution of fresh 1.1 g-Meso-ZSM-5 co-catalyst and used co-catalysts with different Meso-ZSM-5 loadings. 96

Figure 4-16. Regeneration of the 1.6 g-Meso-ZSM-5 co-catalyst; FTS performance for 250 h on stream. 97

Figure 5-1. Block diagram for the modular modular GTL plant 102

Figure 5-2. Flowchart of the modular GTL plant 104

Figure 5-3. Reformer temperature sensitivity analysis. Left: H_2, CO and CH_4 flowrate; Right: H_2/CO ratio 108

Figure 5-4. Different blocks cost percentage for modular GTL plant 115

Figure 5-5. Total product cost of the modular plant at 5600 BPD scale 116

Figure 5-6. Total capital investment and synthetic oil price change with plant scale 117

Figure 5-7. Cumulative net present value and internal rate of return change with plant scale... 118

Figure 5-8. Sensitivity analysis on the Internal Rate of Return (IRR) at varied costs..... 119

Figure 6-1. The synthesis procedure of raspberry-like silica composite 124

Chapter 1

INTRODUCTION

1.1 Objectives

The overall goal of this dissertation is to explore opportunities and bottlenecks in small-scale FTS in structured catalysts. Bifunctional catalysts were synthesized to drive the FTS selectivity towards gasoline-range hydrocarbons. The effect of structured catalysts properties, such as ZSM-5 loading, film thickness, ZSM-5 pore size, was explored in a novel FTS micro reactors. Micro reactors can intensify FTS and reduce its complexity, offering a technical solution for modularization of GTL processes. After formulation and performance exploration of the structured bifunctional catalysts, the possibility of a modular GTL plant equipped with micro reactors were investigated conceptually combining with up to date technologies to monetize stranded natural gas. The following hypotheses have been proposed and verified:

- ***Hypotheses 1***: Structured catalysts are capable of enhancing FTS conversion and selectivity. Relaxation of mass and heat transfer limitations in microreactors and isothermality can lead to better FTS product selectivity.
- ***Hypotheses 2***: Multilayered structured catalysts which are supported transition metals and zeolite catalyst films of tuned thickness can control the chain-growth and isomerization of the FTS products.
- ***Hypotheses 3***: Zeolites of small-diameter pores are capable of driving process selectivity to gasoline-range products, while reducing coke formation at FTS conditions.
- ***Hypothesis 4***: Increasing of the zeolites pore size can relax heat and mass transfer which will improve FTS activity and productivity.

- ***Hypotheses 5***: Structured bifunctional catalysts can intensify conventional GTL process, offering technical solution to reduce capital investment and monetize stranded natural gas.

1.2 Scope of the Dissertation

Within the scope of this dissertation, monolithic structured catalysts are synthesized and evaluated to study the advantages of structured catalysts in terms of product selectivity and catalyst activity. This dissertation has 6 chapters following the Introduction in Chapter 1. Chapter 2 includes the main experimental methods used, including N_2 adsorption/desorption, X-ray diffraction (XRD), Fourier transform infrared spectrometer (FTIR) and electron microscopy. In Chapter 3, a monolithic bifunctional catalyst is formulated by using dip-coating method. The structured catalyst is composed of three layers, a cordierite monolith as skeleton template, a Al_2O_3 supported Co active sites layer and a zeolite out-layer. Long hydrocarbons are produced on Co active sites and then diffuse out through the zeolite out-layer undergoing cracking and isomerization reaction, thus increasing gasoline selectivity and quality. The monolith substrate provides high heat and mass transfer, achieving high CO conversion even with very low loading of active materials. Temperature and pressure effects are investigated to further understand and optimize the process. Chapter 4 presents a modification of the bifunctional catalysts synthesized in Chapter 3. The bifunctional catalyst discussed in Chapter 3 uses zeolite with micropores as the outer layer. With this type of bifunctional catalysts the process accomplishes high gasoline selectivity, however a penalty in CO conversion is also observed compared to the structured catalysts without the zeolite outer layer. The mass transfer limitations in the miropores are responsible for the lower CO conversion. Therefore, mesoporous ZSM-5 is synthesized with the desilication method. The modified bifunctional catalysts showed elevated CO conversion while maintaining high gasoline selectivity. With that, thickness of the meso-ZSM-5 out-layer and

pressure are varied to maximize gasoline production. In Chapter 5, a modular GTL plant using the optimized bifunctional catalysts parameters is modeled using ASPEN PLUS, aiming to monetize stranded natural gas. A techno-economic analysis is performed to verify its possibility. Sensitivity analysis is carried out to see the profitability regarding to the change of market and resources, such as natural gas price, total capital investment and plant scale. Chapter 6 summarizes work from each chapter to formulate a comprehensive understanding of the proposed process. Advantages and drawbacks of current structured bifunctional catalysts are discussed. Finally, suggestions for future work are offered.

1.3 Crude Oil Status and Rising Gasoline Transportation Fuel Demand

Petroleum has been utilized since ancient times. More than 4000 years ago, petroleum was used in the construction of the walls and towers of Babylon and for medicinal and lighting in the upper levels of ancient Persian; not only in western world, later in ancient China, evidence showed that the Chinese were the first to record the use of petroleum as fuel. Surprisingly, distillation of crude oil has been also invented and performed by Persian chemists in the old times. Tar was used to pave road and hundreds of hand-dug wells were developed to produce crude oil for daily use and military purpose. In the early stage of crude oil application, the ways of usage were simple and production was low. Motivated by the world increasing population and energy demand, the commercialization of modern oil refinery was firstly realized in the world by partnership of Young & Meldrum and Edward William Binney. During 19^{th} and 20^{th} century, with the invention of internal combustion engine and the rise in commercial aviation, and the rules the petroleum played in industrial organic chemistry, crude oil demand boosted and the oil industry entered a new era. Nowadays, the products come from crude oil are everywhere, plastics, fertilizers, solvents,

pesticides, cosmetics and even food additives. With that, petroleum has become the blood to neutralize world economy, politics and technology [1].

The crude oil has become more and more import in modern society. With the crude oil playing such a vital role in the world, this also means that a little bit change of oil price and reserves can alter economic and political stability throughout the world. There were two major oil crises after World War II. The first one was caused by the Arab members of the Organization of the Petroleum Exporting Countries (OPEC). Oil price was quadrupled to almost $12 a barrel. With the global capitalist economy suffering difficulties at the same time, these actions established a steep recession accompanied by rising inflation. This crisis forced many capitalist countries to undergo an economic reconstruction in order to reduce their dependency on oil and continuous stagnate of economy lasted throughout the 1970s. Another major oil crisis occurred in 1979 which was caused by the Iranian Revolution. Due to years of wars, the oil industry was severely damaged, causing drastic oil output reduction. The oil price more than doubled to $39.5 per barrel. This oil crisis triggered the economic recessions in the United States and other countries and the oil prices did not subside to pre-crisis level until the mid-1980s [2].

Fossil fuels as coal, crude oil and natural gas are the main energy sources for modern society, however, with the fast development of global economy, shortage of the fossil fuels and the related environmental pollutions cannot be ignored. Although the oil reserves are increasing year by year, the oil consumption rate is also increasing. OPEC has an estimation that the oil demand will grow by 7.3 million barrel per day (bpd) from 2019-2023, and 14.5 billion bpd from 2019-2040 which means that by 2040, 42 billion bpd of oil will be consumed around the world. Compared with the oil reserves the world has left, as 1.497 trillion barrels of 2018, the oil will be depleted within several decades [3]. Besides, according to the data from OPEC [4], 79.4% of the

world's proven oil reserves are located in OPEC Member Countries and within which 64.5% is in the Middle East. What is worse is that the estimated oil reserves are not 100 % available. Due to political, economic and security effects, the real number could be far less. As the blood to pump nutrition to economy and society, crude oil can be poisonous at the same time. Environmental problems related to crude oil have gained increasing attention. Burning of crude oil can generate significant amount of greenhouse gases and acid gases causing sever air pollution. Oil spill are destroying ecosystem and killing millions of wild lives. What is worse is that toxic chemicals related to oil process are causing sickness of human beings. It will be hard and time consuming to find and establish a new portfolio of energy usage, but energy shift from fossil fuels to clean energy is urgent and inevitable.

After the extraction of crude oil, a refining process is carried out to achieve different, and useful petroleum products. Different refining products percentage from crude oil can be seen in Figure 1-1. Among all of the refining products, gasoline accounts for as high as 43% in volume [5] which is about 73 liters gasoline out of 159 liters of crude oil.

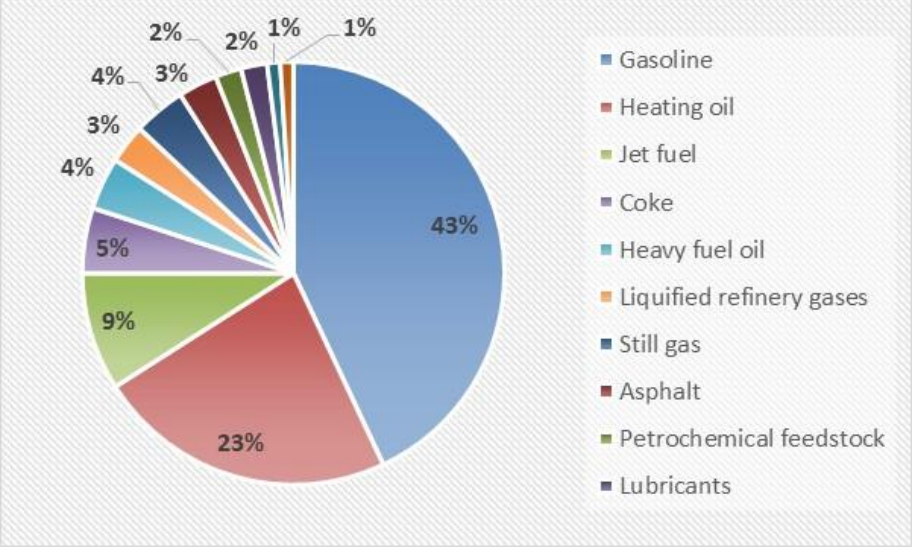

Figure 1-1. Percentage of the petroleum products obtained from crude oil [5]

Due to the high octane number and heat capacity of gasoline, it fits perfectly for internal combustion engine of light-duty vehicles. Besides, the abundance reserve of crude oil also makes gasoline price highly competitive. Ethanol was once an alternative of gasoline for its cleaning energy characteristics, higher octane number and the compatibility with internal combustion engine, but gasoline later dominated due to cheaper price realized by the vast discoveries of large oil wells boosted gasoline production. Ethanol gradually lost it advantages due to the scares of feedstocks which are mainly from crops, causing competition with food supply. Besides the feedstock shortage, highly paid tax to federal was another burden and crushed the use of ethanol in automotive fuel. Gasoline has become one of the major consumed fuels in United States. According to EIA report [6], Americans used about 143 billion gallons of motor gasoline which is 391 million gallons per day which accounts for about 58% of the total transportation sector energy mainly consumed by light-duty vehicles. Household and industry also use large amount of gasoline. In 2012 EIA report shown in Figure 1-2 [7], 71% of petroleum was consumed by transportation among which gasoline occupied about 40%.

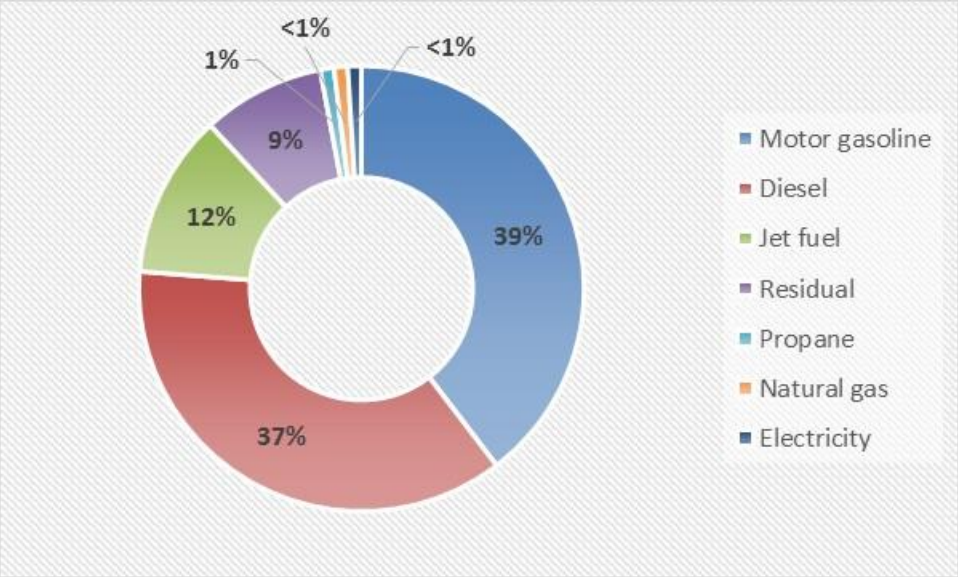

Figure 1-2. World transportation consumption by fuel 2012 [7]

As aforementioned, oil crisis can happen due to the sensitivity of oil price which can be easily affected by wars, policies change of OPEC countries and it is so devastating to world economy. Changing of crude oil price can cause the fluctuation of gasoline price which affects every one of us eventually. What is more is that gasoline has established such an unchangeable position in world energy portfolio. The long established infrastructure, gasoline supplying system, huge number of gasoline powered vehicles and oil companies make the adaption of a new type of energy slow and difficult. Thus, without the invention of groundbreaking technologies, gasoline will still be the main energy used in transportation. To mitigate oil crisis and satisfy the high gasoline demand, one promising solution is to use natural gas as an alternative fuel, considering the enormous reserves of natural gas and mature Gas-to-Liquid (GTL) technologies. Using natural gas to produce liquid fuels can be stable and price competitive.

1.4 Natural Gas Status

Natural gas is a mixture of many different compounds: methane, carbon dioxide, water, sulfur and other impurity gases. Methane is the most abundant component of natural gas. The volume percentage of methane in natural gas can vary between 70-90% [8]. Based on the methane content, natural gas can be dry or wet. Dry natural gas is almost completely methane with the removal of all the liquefied hydrocarbons and non-hydrocarbon impurities, while wet natural gas contains less than 85% methane and has higher percentage of liquid natural gases [9]. Usually, the natural gas that discussed in the media is referring to dry natural gas. Natural gas production usually comes with crude oil drilling. Although they are used in different energy forms, crude oil is mostly used as liquid fuels or in chemicals production and natural gas is mainly used for generating electricity and heating. Crude oil and natural gas still compete in many fields depending on the prices. Compared to crude oil, besides the price advantage, natural gas usage as fuel has many other advantages. Natural gas is a cleaner energy compared to crude oil, containing less harmful chemicals as sulfur or nitrogen compounds and lower CO_2 emissions [10]. There is no soot or ash formation after the burning. Because it is in gas state, there is no eco-system damage as oil spill. The vast reserve makes it super reliable and price competitive and it can also diversify energy

portfolio of U.S. and reduce the dependence on foreign oils. Thus, natural gas has gained more and more attention now to be used in current infrastructure.

Shale gas exploitation increased the natural gas production significantly due to the use of new technologies such as horizontal drilling and hydraulic fracturing. The proved wet natural gas reserves can be viewed in Figure 1-3. As shown, there was a sharp increase of natural gas reserves triggered by the newly developed technologies in 2008 and the trend has been increasing over the last decade. According to EIA 2020 Annual Energy Outlook [11], as of January 1, 2018, there were about 2,828.8 trillion cubic feet (Tcf) of technically recoverable (proved and unproved reserves) of dry natural gas in the United States enough to last about 92 years. Meanwhile, the dry natural gas production reached about 3,000 billion cubic feet (Bcf) monthly in 2020, while the consumption rate is about 80 million cubic feet (Mcf) per day. Considering the total natural gas reserves of 504.5 Tcf at 2018, the production only accounts for less than 10% of the reserves. Natural gas energy is far from fully used, not only to mention that there is also an around 9% production increase annually.

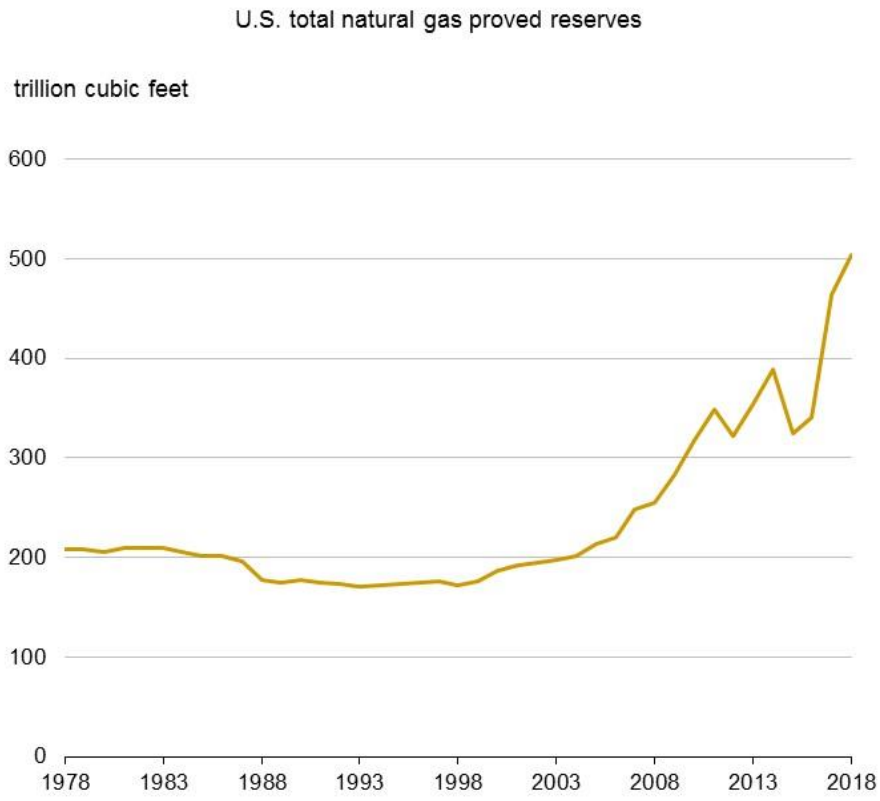

Figure 1-3. U.S total wet natural gas proved reserves up to 2018 [12]

Natural gas usually comes with the production of crude oil and oil wells most times are located in the remote areas which makes the direct usage of natural gas difficult. There are many ways to take advantage of the remote natural gas [13], as listed in Figure 1-4. Natural gas can be compressed and pipelined, but the high cost of the pipeline construction limits the distance between supply and market to less than 5000 km. To make the long distance transportation of natural gas profitable, natural gas can be liquefied to form liquefied natural gas (LNG) and be shipped to market using tanks. A regasification process is needed for the natural gas usage in conventional markets. Different from the former two physical methods of transforming natural gas, gas to liquid (GTL) process uses natural gas as feedstock and transforms it into value added liquid products, then the liquid products will be shipped to market via trucks or ships. Another possible way is

transporting natural gas by wire. Electricity is generated at the point of the source and transported by DC voltage. Because of the high cost of the power grid, the gas by wire method has limited application for distances smaller than 5000 km. Among the aforementioned techniques, each of them has their own advantages and disadvantages depending on the purpose of the application.

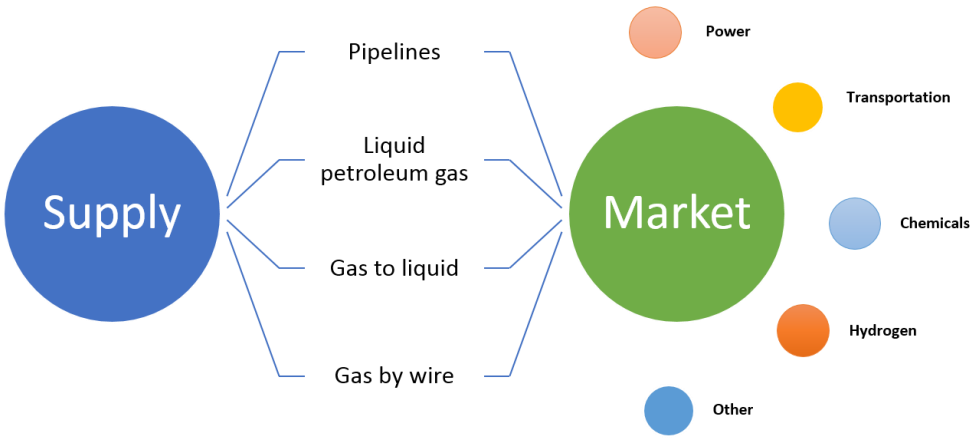

Figure 1-4. Four ways of transporting natural gas to market and the role of GTL in the gas economy [13]

Besides remote natural gas, stranded natural gas has become one of the hot topics among industry [14–17]. Stranded natural gas is the gas that is wasted and trapped, due to the small size or remote locations of natural gas reserves which cannot be developed economically from sizable population centers [18]. Sources of the stranded natural gas including associated gas reserves, deep offshore gas reserves, marginal gas fields and remote gas reserves. There are plenty of natural gas reserves with this situation and the total stranded natural gas reserves are enormous. The potential of using stranded natural gas is huge. As shown in

Table 1-1, the total reserve of stranded nature gas can be as high as 6000 trillion cubic meter. Based on the energy scarcity of some local districts, it will be highly beneficial to transform those stranded natural gas into useful liquid fuels.

Table 1-1. Stranded natural gas potential

Source	10^{12} m^3
Associated gas	12

Deep offshore	8
Marginal fields	5
Remote gas fields	24 to 40
Total	49 to 65

As mentioned earlier, there are many ways of taking remote natural gas supply to market. From the point of using remote natural gas and stranded natural gas, GTL processes can show many advantages compared to other methods. The technologies of GTL process have been applied in industry for more than 100 years. Products obtained from GTL process are liquid fuels which can be easily stored and used in the existing infrastructure. Besides, variety of chemicals can be produced from GTL process, methanol, dimethyl ether, olefins, paraffins and wax. Monetization of stranded gas is not only good for economy, but also for the efficient usage of energy. Stranded natural gas is basically free which can reduce enormous amount of operating cost of GTL process. Among different GTL technologies, Fischer-Tropsch Synthesis (FTS) has gained high reputation for its wide range of products and flexibility, making it easily adaptable according to market fluctuation. Besides, the operation conditions of FTS are relative mild, making the process much safer compared to high pressure process. However, conventional FTS suffers from low products selectivity and catalysts deactivation. In order to make FTS a process for gasoline production aiming to monetize stranded natural gas, an intensified catalysts is needed to reduce GTL plant size and capital cost.

1.5 Fischer-Tropsch Synthesis

FTS process was discovered by German scientists Franz Fischer and Hans Tropsch at the Kaiser-Wilhelm-Institut für Kohlenforschung in Mülheim an der Ruhr in 1925 [19]. It is a collection of chemical reactions that convert a mixture of hydrogen and carbon monoxide into liquid fuels. As further development, it has become a crucial part in both coal liquefaction and GTL process. The GTL process using FTS to transform biomass, coal or natural gas into liquid can be

schematically depicted in Figure 1-5, basically composed of three steps [20,21]. During the process, pre-cleaned biomass, coal or natural gas are converted into synthesis gas (also called syngas which composed of H_2 and CO) first by steam-reforming, partial oxidation or auto-thermal reforming [22,23]. Syngas then is used as the feedstock for FTS to produce liquid hydrocarbons. Depending on the quality or application requirements, an upgrading process is carried out to achieve the desired range of transportation fuels. FTS was intensively studied after its discovery and several large GTL plants incorporating FTS have been constructed in Germany during World War II to meet the high liquid fuel demand. Crude oil then dominated during the postwar time due to the vast reserve and low price. Recent years, FTS has redrawn attention due to crude oil crisis, the environmental issues related, and the establishment of energy diversity [24–26].

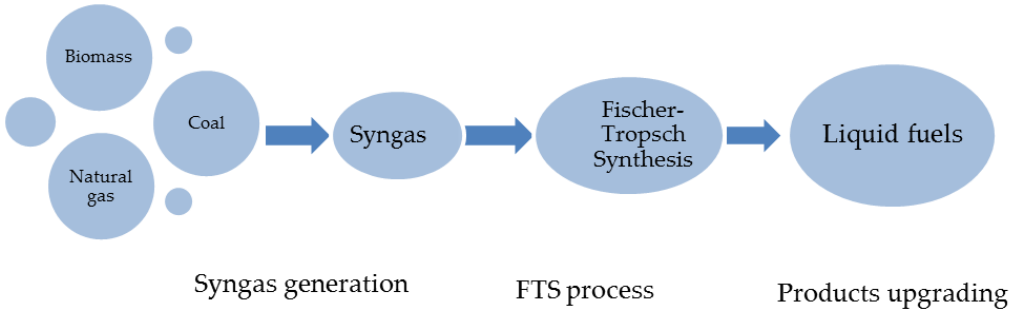

Figure 1-5: Overall GTL process using FTS for liquid fuels production

1.5.1 Catalysts used in FTS

FTS is catalyzed by transition metals, such as Fe, Co, Ni, and Ru [27–30]. Ni is not used in industry due to its high selectivity towards methane. Ru has high activity for CO hydrogenation and is capable of working at low temperatures (<150 °C) to produce long-chain hydrocarbons even without promoters [31]. However, its application for industrial-scale is hindered due to the low reserve and high price. Fe and Co are the common active materials used in industry. There are many differences between these two types of catalysts. Depending on the catalyst used, high-temperature (330-350 °C-Fe [32]) or low temperature (200-240 °C-Co [32–34]) processes are defined.

Co-based catalysts are highly active and has low WGS activity. While Fe-based catalysts is cheap and has high flexibility toward synthesis gas ratio. For syngas ratio, Co catalysts require H_2/CO ratio of ~2. While Fe-based catalysts require H_2/CO ratio close to unity, due to the strong Water-Gas-Shift (WGS) activity which can transformed excess H_2 into CO. This makes Fe-based catalysts attractive for Coal-to-Liquid (CTL) or Biomass-to-Liquid (BTL) technology. Co-based catalysts possess higher chain growth probability compared to Fe-based catalysts. Therefore, Co is the preferred active material for long paraffins production, while Fe is a better choice for short olefin production. A syncrude composition comparison from Co and Fe-based catalysts is summarized and shown in Table 1-2. FTS products are mainly paraffins and olefins. Small amount of alcohols can also be produced. For cobalt-based catalysts, heavier hydrocarbons tend to form with carbon number bigger than 11+. Only small amount of aromatic, oxygenate and carbonyl will be produced. Thus cobalt type catalysts are suitable to generate value added chemicals in the range of wax or diesel fuel. While for Fe-based catalysts, it is suitable for the production of middle distillate which also contains large amount of aromatics and oxygenate. Fe-based catalysts are also proved to be superior for olefin production [35,36].

Table 1-2. Syncrude compositions representative of low temperature Co-based catalysts, low temperature Fe-based catalysts and high temperature Fe-based catalysts [37]

Product fraction	Carbon range	Compound class	Syncrude composition (mass%)		
			Co-LTFT	***Fe-LTFT***	***Fe-HTFT***
Gas phase					
Tail gas	C_1	Alkane	5.6	4.3	12.7
	C_2	Alkene	0.1	1	5.6
		Alkane	1	1	4.5
LPG	C_3–C_4	Alkene	3.4	6	21.2
		Isomer	1.8	1.8	3
Oil and wax phases					
Naphtha	C_5–C_{10}	Alkene	7.8	7.7	25.8
		Alkane	12	3.3	4.3
		Aromatics	0	0	1.7
		Oxygenate	0.2	1.3	1.6
Distillate	C_{11}–C_{22}	Alkene	1.1	5.7	4.8
		Alkane	20.8	13.5	0.9
		Aromatics	0	0	0.8
		Oxygenate	0	0.3	0.5
Residue	C_{22+}	Alkene	0	0.7	1.6
		Alkane	44.6	49.2	0.4
		Aromatics	0	0	0.7
		Oxygenate	0	0	0.2
Aqueous phase					
Reaction water	C_1–C_5	Alcohol	1.4	3.9	4.5
		Carbonyl	0	0	3.9
		Carboxylic acid	0.2	0.3	1.3

1.5.2 Reaction mechanism of FTS

The reaction mechanism of FTS is very complicated. Many assumptions have been formulated trying to explain the chemistry, however no consensus has been made yet. But, typical reaction patterns have been described. The major reaction patterns of FTS are summarized in Table 1-3. Linear paraffin and olefin production are the dominant reactions, while Water-Gas-Shift (WGS) reaction is an undesirable side reaction. Small amounts of branched hydrocarbons and oxygenates are also produced. FTS is a highly exothermic reaction. Good control of the catalyst bed temperature is crucial, since FTS products are extremely sensitive to temperature change. High temperature is favorable for light hydrocarbons production with high CO conversion. However,

increased temperature also elevates methane and CO_2 production which will decrease overall process liquid hydrocarbons yield. FTS is a polymerization reaction with a chain growth probability of α. The products distribution can be expressed by the Anderson-Schulz-Flory (ASF) distribution [38] as shown in Eq 1. Among the equation, w_n represents weight fraction of hydrocarbon with n carbon number, and n is the carbon number. While α is the chain growth probability.

$$w_n = n(1-\alpha)^2\alpha^{n-1} \quad (1)$$

Table 1-3. Major reactions of FTS [39]

Major reactions in the FTS	
Main reactions	
1. Paraffins	$(2n+1)H_2 + nCO \rightarrow C_nH_{2n+2} + nH_2O$
2. Olefins	$2nH_2 + nCO \rightarrow C_nH_{2n} + nH_2O$
3. WGS reaction	$CO + H_2O \rightleftharpoons CO_2 + H_2$
Side reactions	
4. Alcohols	$2nH_2 + nCO \rightarrow C_nH_{2n+2}O + (n-1)H_2O$
5. Catalysts oxidation/reduction	(a) $M_xO_y + yH_2 \rightleftharpoons yH_2O + xM$
	(b) $M_xO_y + yCO \rightleftharpoons yCO_2 + xM$
6. Bulk carbide formation	$yC + xM \rightleftharpoons M_xC_y$
7. Boudouard reaction	$2CO \rightarrow C + CO_2$

Figure 1-6 shows FTS products distribution with the increase of chain growth probability, following an ASF distribution. When chain growth probability is small, the main products are light hydrocarbons. With desired large chain growth probability, heavy hydrocarbons tend to form. However, to get a certain range of products, such as gasoline or diesel, chain growth probability must be carefully controlled. It is important to realize that chain growth probability and other products selectivity, such as olefin to paraffin ratio, WGS reactivity, can be influenced by the catalyst properties and the process conditions [40]. Due to the polymerization-like growth mechanism, FTS product selectivity for certain range of products will always be limited. According to the ASF distribution, gasoline range (C_5-C_{12}) hydrocarbons have a maximum mass

selectivity of 48 %. This selectivity is too low for successful industrial application of FTS to produce gasoline. A potential solution to this problem is the use of materials and process conditions with large chain growth probability. A large amount of wax can be produced, then the wax can be subsequently cracked to fuel range products using a hydrocracker unit. Shell uses this technology in its Shell Middle Distillate Synthesis (SMDS) process [41,42]. More of the gasoline production FTS will be discussed later and it is also the scope of this dissertation.

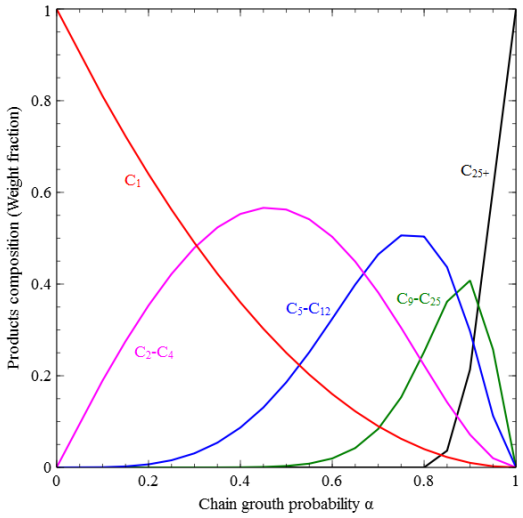

Figure 1-6: FTS products selectivity as a function of the chain growth probability

Exact mechanisms for FTS are still not clear, but there are several types of mechanism proposed which can explain experimental results quite well [43]. As listed in the following:

1. Enol mechanism

   For enol mechanism, CHOH was considered as monomer and initiator. However, extensive work showed that although alcohols can initiate FTS reaction, it cannot act as propagators, especially for Co-based catalysts. Other studies on Fe and Co catalysts found proof showing that it is alcohols and aldehydes that form alkoxide not CHOH. Thus, it can be concluded that for Fe and Co catalsyts, alcohols or aldehydes can form alkoxide structure to initiate hydrocarbon chain growth.

2. CO insertion mechanism

CO insertion mechanism has been extensively studied theoretically using density function theory (DFT) and many studies derived well kinetics equations based on this mechanism [44–46]. A possible CO insertion mechanism proposed by Pichler and Schulz [47] is shown in Figure 1-7. In this mechanism, CO chain growth initiation is first achieved by H_2 assisted adsorption and $=CH_2$ formed on the catalysts surface (shown in Figure 1-7(A)). Then, chain propagation is realized first by a hydrogenation of $=CH_2$ and followed by CO insertion. Olefin and paraffin products can be produced with O alleviation, while direct hydrogenation after CO insertion will result in aldehyde and alcohols (shown in Figure 1-7(B)). This type of CO insertion mechanism can cover all of the products formed in FTS. Because chain propagation occurs by CO coupling to a RCH_2 group, no high surface concentration of $-CH_2$ group is needed to ensure fast chain growth rate. However, DFT simulation from Meng-Ru Li and co-workers [48] showed that the energy barrier for CO insertion into a CH_3 group is as high as 182 kJ/mol on a Co(0001) surface, making CO insertion into RCH_2 group unlikely. More work needed to be done to fully understand the CO insertion mechanism, since there is no panacea, considering the complexity of the surface properties of catalysts and surface active species.

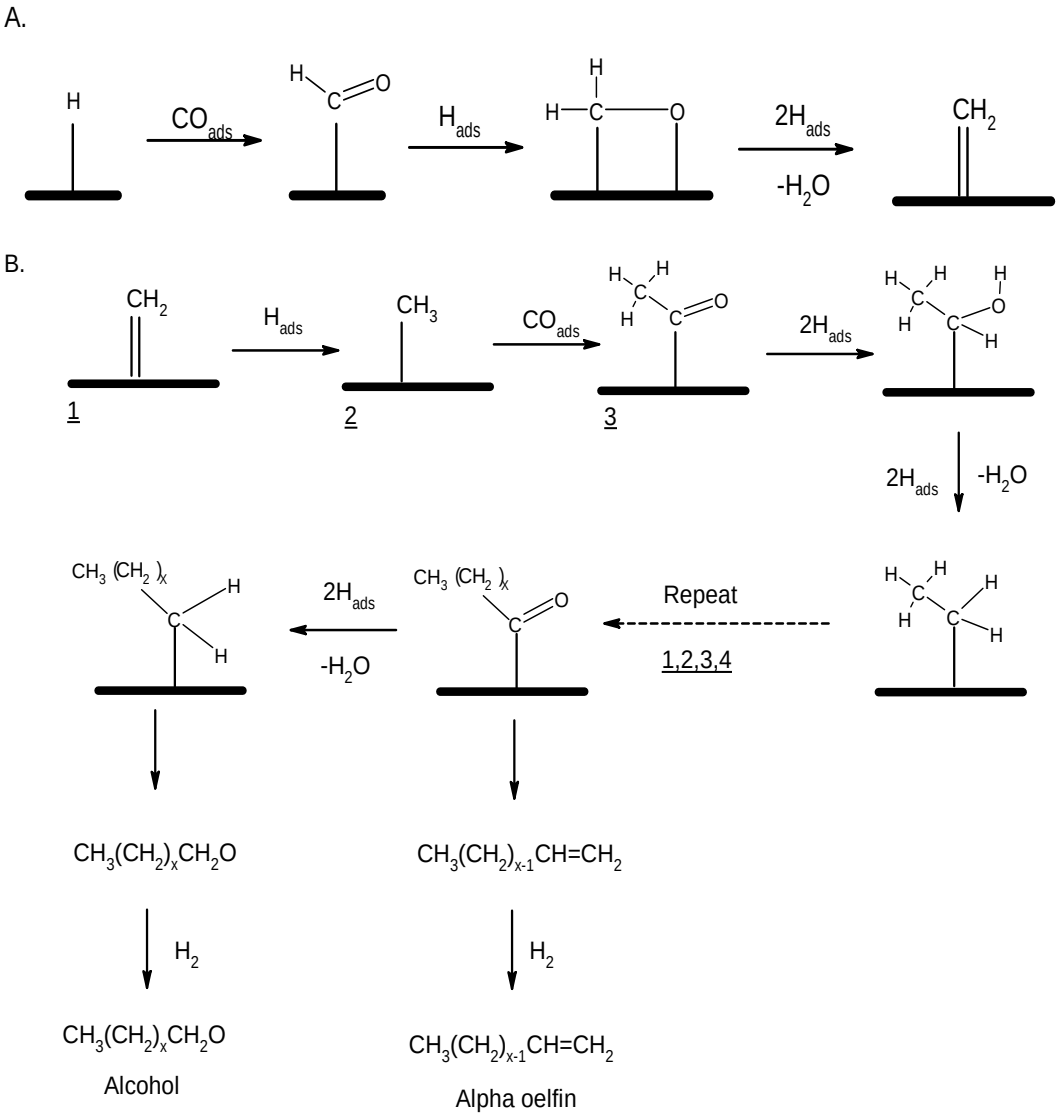

Figure 1-7. CO insertion mechanism for FTS proposed by Pichler and Schulz [47]. (A) Initiation mechanism to form $=CH_2$ (H_2 assisted CO activation). (B) Chain propagation to form alcohol and alpha olefin.

Another possible route for CO insertion mechanism was proposed by Masters [49], shown in Figure 1-8. In his theory, CO insertion instead of happening to RCH_2 group, is actually to RCH groups. After the formation of surface $=CH_2$ species, CO insertion happens directly. There is no hydrogenation of $=CH_2$ to begin with. CO insertion mechanism has been supported by many radiotracer experiments by Emmett and co-workers [50,51] and Davis et al. [52]. On the basis of their work, carbide

and CO insertion mechanism play a vital role in FTS. However, work from Brady and Pettit [53] showed different opinions. No consensus has been reached yet for CO insertion mechanism which is not surprising based on the complex reactions of FTS

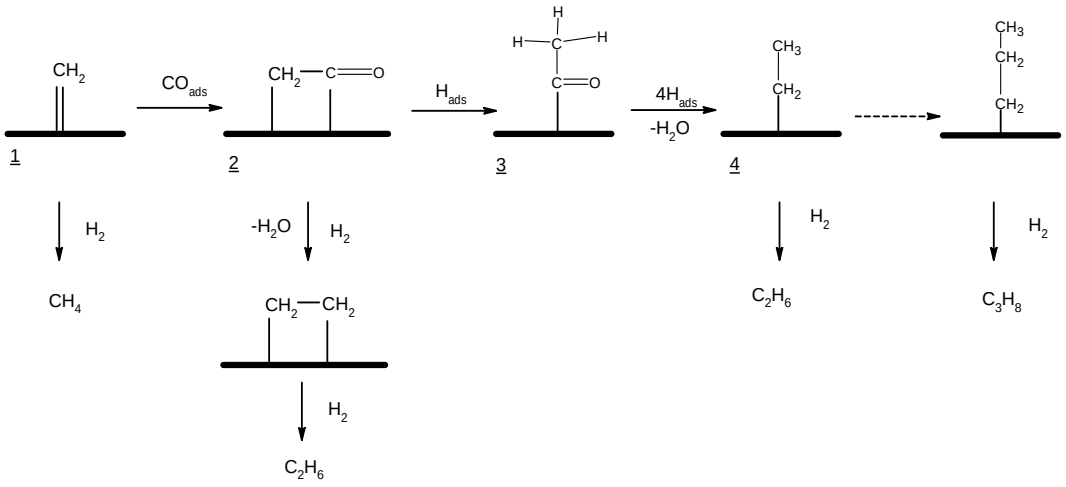

Figure 1-8. Chain growth in the CO insertion mechanism proposed by Masters [49]

3. Carbide mechanism

In this mechanism, as shown in Figure 1-9, a metal carbide is the initial surface species in the formation of carbenes. As a result of many workers, this carbide mechanism was named as Fischer-Tropsch-Brady-Pettet-Biloen-Sachtler mechanism. The work from Pettit et al. used CH_2N_2 as a reactant. They concluded that the methylene groups to be formed is the addition of hydrogen to adsorbed carbon which was produced by CO dissociation. Their conclusion was verified by Biloen and Sachtler using ^{13}C [53]. Indirect evidence for carbide mechanism was also acquired by Bell [54]. Using cyclohexenes and syngas as reactants over a ruthenium catalyst, norcarane and alkyl cyclohexenes were produced which was the result of the added compound reacting with surface CH_2 groups. Other works [55,56] also proved the same phenomenon.

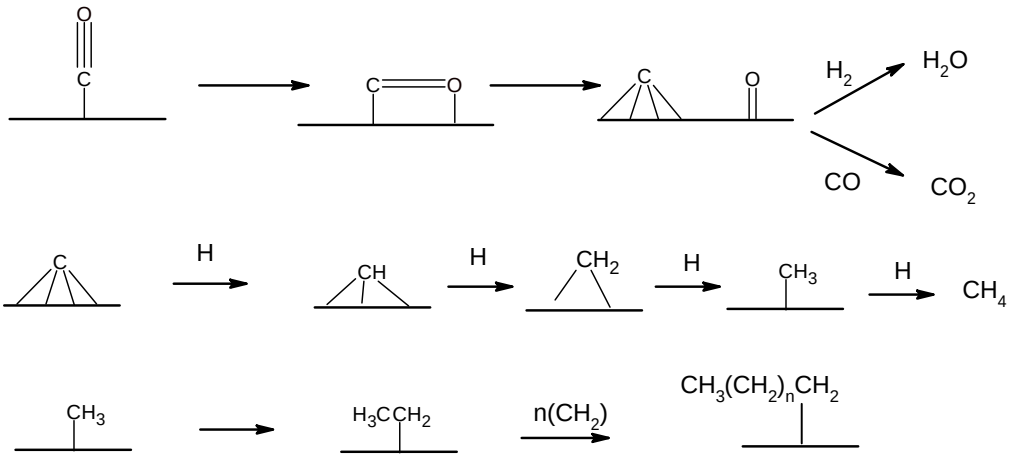

Figure 1-9. Carbide mechanism [57]

4. Oxygenate mechanism

For oxygenate mechanism of FTS, one possible reaction steps is shown in Figure 1-10. Different from CO insertion and carbide mechanism, an oxygen surface species forms on metal. Then CO inserts between the O and H bond of the adsorbed –OH. This advanced mechanism was first proposed by Deluzarche et al. [58].

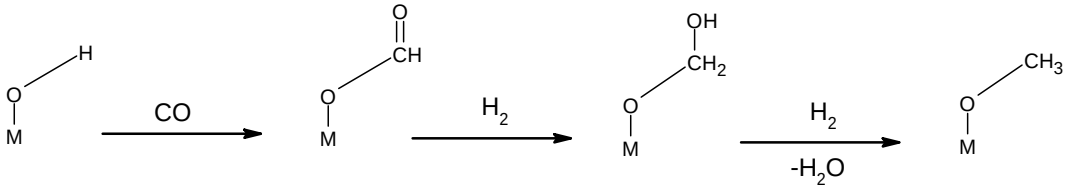

Figure 1-10. Oxygenate mechanism offered by Deluzarche et al. [58]

Another even more unique mechanism for oxygenate mechanism was proposed by Sapienza and co-workers, shown in Figure 1-11. In this theory, CO and H_2 were adsorbed both on metal surface, then C was hydrogenated and O is bonded.

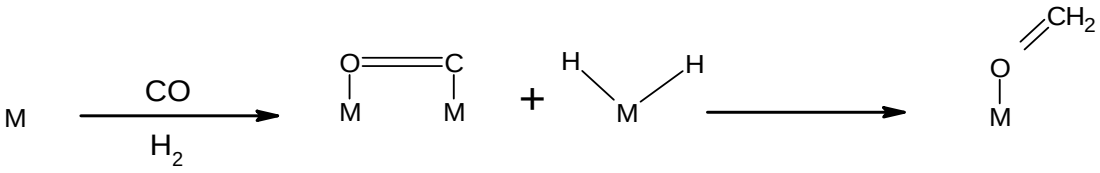

Figure 1-11. Another oxygenate mechanism proposed by Sapienza [59]

Tons of work has been done trying to shed some light on the reaction mechanism of FTS. However, there is no single and simple method that can be used due to the complexity of FTS with so many factors affecting the reaction, such as reaction conditions, material used, promoters and so on. To better understand a specific phenomenon for a specific type of FTS, a comprehensive mechanism review should be carried out before making any conclusions.

1.5.3 Commercial FTS reactors and monolithic reactor

FTS is a highly exothermic process, where temperature gradients are responsible for low selectivity. Therefore, FTS reactors must operate isothermally. There are several different types of reactors been used in commercial FTS plant, as shown in Figure 1-12. Early FTS designs were based on multi-tubular fixed bed reactors (SASOL ARGE) [41], dipped in boiling water for heat removal. However, fixed-beds imposed limits on the minimum applicable catalyst particle size, leading to a compromise between diffusion lengths and acceptable pressure drop. In slurry bed column reactors (SASOL), the bubbling flow ensures good mixing and isothermality. Diffusion limitations are relaxed by using small catalyst pellets. However, the separation of the waxy product from the catalyst particles is a major limitation. In fluidized-bed reactors (SASOL) [41], small particle size relaxes mass transfer limitations, but the liquid FTS products cause catalyst particle agglomeration and disturb fluidization. Therefore, operating temperatures above the hydrocarbons dew point must be chosen, resulting in chain length growth probability of ~0.7 and selectivity to

lighter hydrocarbons. Circulating fluidized bed reactors (Sythol) suffer from attrition, temperature gradients and difficulties in separating waxes from solid catalysts.

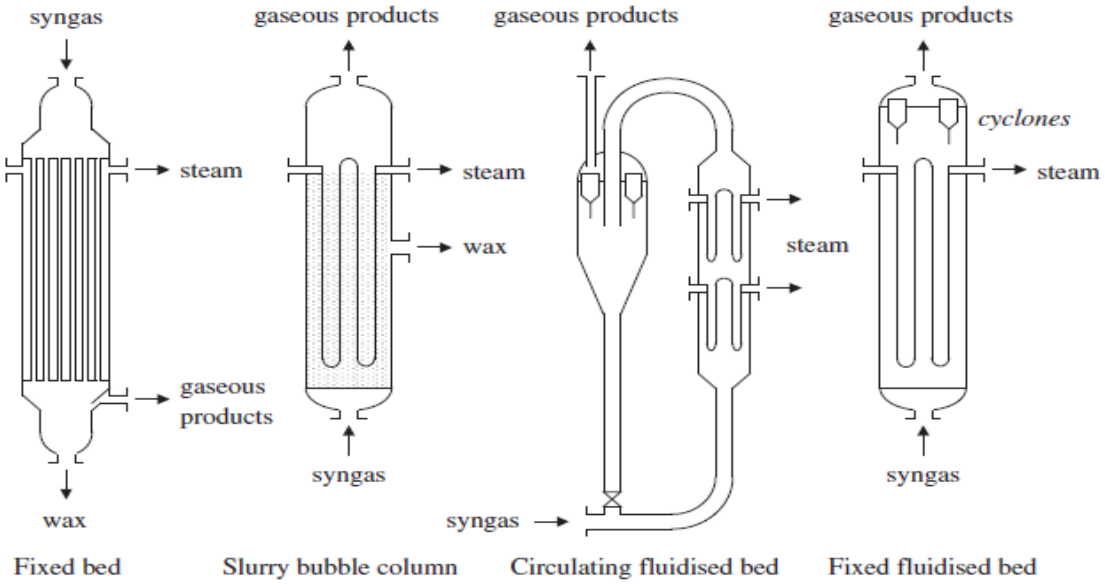

Figure 1-12. Different types of reactors for FTS used in industry [60]

As mentioned, no reactors are perfect so far, suffering from different types of design problems. Thus, a great amount of research and development effort has been devoted to novel type of reactor development. Monolithic structured reactors are a promising solution. Monolithic reactors are well know from gas-solid applications to solve environment related problems, especially the three-way catalytic converter in the field of car exhaust cleaning, but the application of monolith reactors is rather new to gas-liquid-solid reactions [61]. In contrast to other industrial reactors, monolithic structured reactors can operate at low pressure-drop, high geometric surface-area, high mass-transfer coefficients, and short diffusion lengths. The thickness of cell wall can be adjusted to achieve effectiveness factors close to unity [62–64]. Because of the honeycomb structure with active phase attached on the cell wall, wax separation and catalyst attrition are not of significant concern. Structured catalysts are typically operated adiabatically, resulting in low radial heat transfer and temperatures gradients, but Moulijn and coworkers [61,65,66] and Güttel et al. [67,68]

suggested recycling the liquid product and removing reaction heat externally. Almeida et al. [69] explored FTS in aluminum foams, honeycombs and micro monoliths and measured C_{5+} selectivity of over 50%. They underlined the importance of the catalytic layer thickness of the FTS catalysts. Visconti et al. [64] showed that heat conduction in structured aluminum catalysts can be exploited to effectively remove heat. Liu et al. [70,71] showed that C_5–C_{18} selectivity and olefinicity obtained by FTS in monolith catalysts are better than their packed-bed equivalents. They reported high one-pass conversions (~95%) at very low CH_4 selectivity (<10%), which was not possible using conventional fixed beds. In general, structured FTS reactors show superior activity and selectivity, but the importance of temperature profile flattening, through internal or external heat removal is emphasized.

A monolithic reactor consists of thin parallel straight channels of different shapes, through with the gas, containing the reactants, flows [72]. Catalysts are coated on the channel walls. When reactants flow into the channels, they are diffused through convective flow and mass diffusion toward the walls. At the meantime, products also diffuse back to the gas phase and carried away by the convective flow. Many parameters can affect the monolithic reactor performance, temperature, geometry, wash-coat properties and catalysts coating. Therefore, it is important to find a suitable method for monolithic catalysts preparation. There are many ways to make a monolithic catalyst. For massive production of monoliths, extrusion is the most extensively employed method in industry [73]. There are two types of monolith according to the material used, ceramic and metallic. Ceramic monolith can resist high temperature, corrosion and relative harsh reaction environment, while metal monolith is superior on mechanical resistance and thermal conductivity. Bare monolith usually possess a low surface area, thus an active catalytic layer with high surface area and active material is needed. Wash-coating and direct synthesis are the two

main methods used to coat the active materials on bare monolith template. In wash-coating process, usually a slurry is prepared with the active and supporting materials. The wash-coat quality highly depends on the properties of slurry which can be tuned by carefully control the properties of solid particles, the solvent and the solid wt.% used. After the coating of the active materials, thermal treatment can be carried out to stabilize the structure [74]. Direct synthesis can provide a stronger adhesion of the coating to the support, however the process is considerably complex. Without precise control, a dense layer can be formed with small intercrystalline structure, causing severe diffusion limitations. For FTS, conventional catalysts are usually prepared by impregnation of active phase on a highly porous sphere support. This type of catalysts suffer from high pressure drop due to the densely packed pattern in the reactor. Besides, the small inter particle distance and the intra particle pore tortuosity can trigger serious mass and heat transfer barriers, causing low catalysts performance. What is more is that the separation of products and catalysts also need tremendous amount of work. In terms of tackling those drawbacks of conventional FTS catalysts. Monolithic catalysts offer a good alternative. Since the application of the monolithic catalysts in gas-liquid-solid reaction is still quite new, investigating its performance for FTS can be instructive and valuable.

1.5.4 Gasoline production FTS

Tremendous effort has been devoted to gasoline production FTS due to the decline of oil reserves and the high gasoline demand for transportation fuel. Compared to conventional crude oil derived fuels, syncrude produced through FTS is cleaner, containing almost no sulfur and nitrogen compounds. It could be a sustainable process and achieve zero carbon emission if the syngas used is produced from renewable resources like biomass [75,76]. Besides, it is a good alternative to energy diversity and to reduce oil dependency for countries without enough crude oil reserves but with

abundance of renewable resources. Aforementioned, FTS products follow an ASF distribution, guided by one chain growth probability α. For Co-based catalysts, α is usually around 0.8 which means that the carbon chains tend to grow and form long, heavy hydrocarbons [38,77]. Thus, GTL process using FTS with cobalt-based catalysts needs to have an upgrading unit at the end, breaking the long wax products into middle distillates. In this way, the FTS products will show a two chain growth probability trend. Zeolite or zeolite-like materials are the typical active phase used in the upgrading unit, same as what is applied in crude oil processing. Zeolites are crystalline aluminosilicate with both Lewis and Bronsted acidity which are the active sites for reactions like isomerization, oligomerization, aromatization, hydrogenation and hydrocracking [78–80]. These type of materials have well-organized structure which can be tuned to control products selectivity, chemical resistance and thermal stability. However, there are drawbacks of using fluid catalytic cracking (FCC) process with zeolite material as an upgrading unit. The whole process is a stand along unit requiring high energy input and capital investment.

To intensify GTL process, a bifunctional catalyst is proposed. Bifunctional catalysts combine FTS active phase and zeolite into one component. Upgrading of FTS products can happen in-situ without FCC unit. Many efforts have been devoted to developing highly efficient bifunctional catalysts for gasoline production. There are mainly three ways of preparing a bifunctional catalyst, as shown in Figure 1-13. The easiest way is by physical mixing of cobalt catalysts with zeolite. A. Martinez and co-workers [81] studies the performance of hybrid catalysts using Co/SiO_2 physically mixed with medium-pore zeolite. Different zeolites with 10 membered ring structure showed varied deactivation behavior. The presence of zeolite elevated the gasoline yield by about 20-40% and enhanced the isoparaffin and olefin content through isomerization and cracking reactions. Results showed that the zeolite acidity had a proportional relation with the

initial yield of branched hydrocarbons. However, coke formation was also detected. They concluded that the morphologies and structure differences were the main factors affecting coke amount and its location, rather than the differences on acidity. Due to the poor active materials usage and zeolite confinement, physically mixed hybrid catalysts are used as a benchmark most of times which has low zeolite efficiency and uncompleted heavy hydrocarbon cracking.

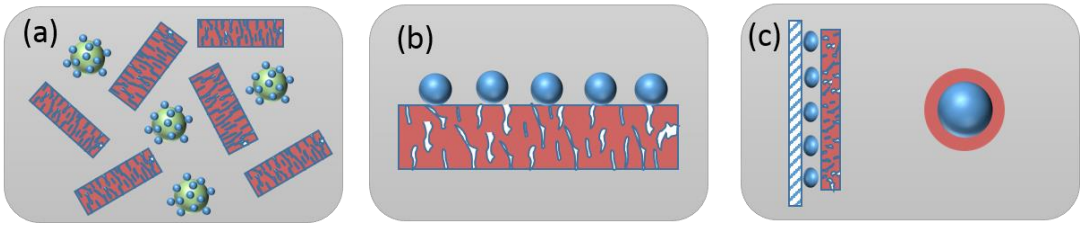

Figure 1-13. Three ways of bifunctional FTS catalysts preparation. (a) physical mixture, (b) Co supported on zeolite, (c) layered structure or core-shell structure (red color represents zeolite; blue is Co and green is support)

Compared to physical mixed hybrid catalysts. Zeolite supported Co-based catalysts are more widely used formula, prepared using dry or wet impregnation methods. A sequence of reactions can happen in order with this type of layout. Hydrocarbons are formed on the active sites and then diffuse to adjacent acid sites undergoing cracking, isomerization and hydrogenation reaction. This allows an intimate position for the active materials and zeolite resulting a relative full conversion of heavy hydrocarbons. Xiao-gang Li et al. [82] developed a novel physical sputtering equipment which successfully synthesized a hybrid catalyst with narrow distributed Co particles well dispersed on H-ZSM-5. The hybrid catalysts showed superior performance on gasoline selectivity and iso-paraffin content due to the weak metal-support interactions and highly disperse cobalt particles which accelerated n-paraffin diffusion. A. Martinez and co-workers [83] prepared a KFeCo FTS catalysts by co-precipitation method. The influence of the ZSM-5 composition (Si/Al ratio, Ga and Pd additives) and crystal size on the gasoline production was investigated. Results showed that the presence of ZSM-5 improved gasoline production. With the increase of Bronsted

acidity, isoparaffins and aromatics selective increased. While, the crystallite size had an important effect on the catalysts activity. Catalysts life was elongated with decreasing crystallite size mainly due to increased diffusion of aromatics which prevented coke formation. Addition of Pd showed positive effect on catalysts longevity, while addition of Ga favored coke formation. Extensive work on zeolite supported Co-based catalysts have been done by Tsubaki et al. [84–87]. Gasoline selectivity and quality were significantly boosted at normal FTS reaction conditions.

Zeolite supported hybrid catalysts showed high gasoline selectivity due to the intimate contact of Co active phase and zeolite acid sites. However, heavy hydrocarbons are still not fully converted due to a lack of full confinement. Wax can diffusion through the gaps without undergoing cracking and isomerization reactions. To further improve gasoline selectivity and quality, structured catalysts, such as layered and core-shell, are formulated. In the work of J. Prech et al. [88] , a three steps preparation method was utilized to entirely encapsulate the metal nanoparticles inside the zeolite matrix. High amount of isoparaffins was observed with the shell coating of ZSM-5. They concluded that the proximity between the metal and acid sites was a crucial factor for high gasoline selectivity. Xingang Li and co-workers [89] developed a one-step synthesis of H-β zeolite-enwrapped Co/Al_2O_3 catalyst. A H-β zeolite shell was directly synthesized over Co/Al_2O_3 pellets to form a core-shell structure which has no pinholes or cracks. Results showed that the molar ratio of C_{iso}/C_{paraf} increased about 64% than that of the products obtained from a physical-mixed catalyst. They draw a conclusion that the elevated gasoline and isomers selectivity was due to the spatial confinement effect and molecule shape selectivity. Many other work with similar conclusions have been done [87,88,90,91], proving that structured catalysts are superior according to the space confinement.

Aforementioned in the monolithic reactor part, monolithic reactors have many advantages used as a structured reactor. However, there is a lack of application in the field of FTS. As known, FTS is highly exothermic reaction and products selectivity is super sensitive to temperature. Thus, quick heat remove and well temperature control are crucial to ensure a good catalysts' performance. Use of monolith as a catalyst support could be promising, considering its high mass and heat transfer properties.

1.6 Modularization of Gas-to-Liquid Plant

GTL process uses syngas produced from natural gas to generate liquid fuel. Compared to hydrogen, nuclear and solar energy, it has the advantages of matching directly with the conventional fuel markets without any modifications to the existing infrastructure. Besides, natural gas has stable stock from the vast reserve. The GTL process offers a good solution for countries that have scarce oil reserves but abundant of natural gas. At present, there are five commercial-scale GTL plants in operation [92]. Detailed data for the five commercial GTL plants is summarized in Table 1-4. As shown in the table, production scale of commercial GTL plants has to be gigantic in order to be profitable, the least capacity in the table is 14,700 barrel per day of liquid fuels. The reason is that, as the larger the GTL plants are, the cheaper one barrel of fuels production cost will be due to the size economy [93].

Table 1-4. Current commercial GTL plants in operation

Plant	Capacity (bpd)	Location	Capital (Billion$)	Year	Developed by
Mossel Bay GTL	36,000	South Africa	--	1992	PetroSA
Bintulu GTL	14,700	Malaysia	0.9	1993	Shell
Oryx GTL	34,000	Qatar	6	2007	Sasol, Qatar Petro
Pearl GTL	140,000	Qatar	19	2011	Shell, Qatar Petro
Escravos GTL	33,000	Nigeria	10	2014	Chevron, Sasol

One of the drawbacks of large commercial GTL plant is that it needs vast reserve of natural gas as feedstock. However, natural gas wells that are large enough to support a gigantic commercial plant account for less than 1% of the total natural gas wells [94]. The truth is that those natural gas resources from small wells are either flared or remain undeveloped due to the commercial and technical challenges of transporting gas to markets. Building pipelines and liquefaction of those remote

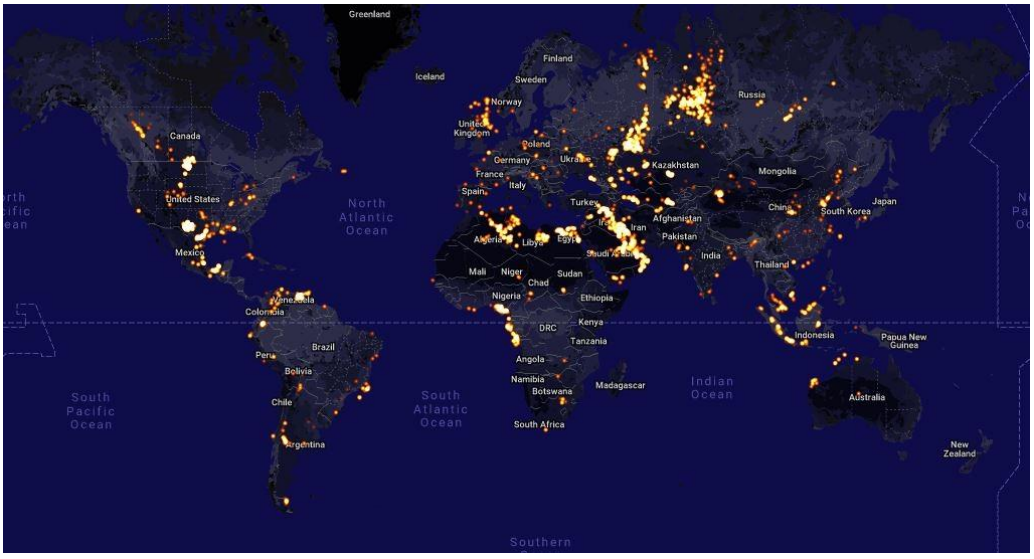

Figure 1-14. Flaring of natural gas around the world under a satellite view [95]

natural gas can be extremely expensive [96]. Those unrecovered natural gas is either called associated gas produced as a by-product of oil production or stranded gas where the accumulation is predominantly or completely composed of gas. Flaring and reinjection are the two conventional disposal options for associated natural gas. Nevertheless, flaring of natural gas is basically a waste of energy and can cause a considerable environment problem with millions tons of CO_2 emissions. Natural gas reinjection is used for oil recovery, but the high pressure characteristic requires complicated equipment and possesses high risk. A satellite map of natural gas flaring around the world is shown in Figure 1-14. Flaring of natural gas is all over the world, concentrating at Russia and Saudi Arab. According to the World Bank estimates, around 5 trillion cubic feet of natural gas is flared annually which is equivalent to the 20% of the entire U.S. gas consumption. The natural gas flared in Nigeria alone is equivalent to a revenue of 2.5 billion dollar per year. The development options for stranded natural gas are limited due to technology availability and commercial limitations, such as infrastructures. CompactGTL who has been devoting efforts to micro scale GTL has identified over 2,000 potential global problematic gas wells with over 500 trillion cubic feet gas, equivalent of 7.8 million barrels per day of GTL oil.

Monetization of stranded and associated natural gas has gained increasing attention due to nearly zero feedstock cost. Modular GTL plant offers a feasible technical solution. The main breakthrough of modular GTL is compact and intensified reactors, making the process highly efficient with reduced scale. Modular GTL plants are usually constructed offsite. The modularized blocks can then be shipped to the natural gas wells and installed onsite. After full use of the resource, the GTL plant can be disassembled and reused on other locations. Several companies have devoted many efforts for modular GTL plant. CompactGTL and Velocys are the two leading companies. In 2010, CompactGTL successfully delivered a commercial demonstration plant to

Brazil and commissioned. In 2014, the world's first small scale commercial GTL pant started construction in Kazkhstan [97]. Microchannel reactors have the potential to meet all of the requirements to make modular GTL process possible. Microchannel reactors contain numerous small channels in the millimeter dimension, providing a high surface-to-volume ratio which enables faster heat and mass transfer compared to conventional fixed-bed reactors and achieving essential isothermal conditions [98–100]. Besides, high feedstock conversion at high space velocity and reduction in reactor volume can be achieved in microchannel reactor due to the improved heat and mass transfer.

With the aim of producing high quality gasoline from FTS and offering a solution for intensified modular GTL FTS reactor, the idea of formulating a structured bifunctional catalyst will be investigated in the dissertation.

Chapter 2

EXPERIMENTAL PROTOCOLS

2.1 Introduction

Depending on the active materials used, FTS can be high-temperature (Fe-based catalysts) or low-temperature (Co-based catalysts) process. It is highly exothermic. Well temperature control is important to maintain high catalysts activity and products selectivity. In this dissertation, a monolithic structured micro-reactor coated with Co-based catalyst was formulated and studied to achieve high gasoline selectivity while tackle heat and mass transfer limitations. The key of high gasoline selectivity and heat transfer is the use of monolith honey comb structure, Co active phase and zeolite which yields a bifunctional catalyst. Monolithic template supported with Co is used as a highly active FTS catalyst, while zeolite serves as a consecutive cracking and isomerization catalyst. Homemade fixed bed reactor setup was used to systematically study the bifunctional catalysts. Different characterization methods were applied to understand the bifunctional catalysts properties and the mechanism behind the performance.

2.2 Bifunctional Catalysts Preparation Methods

Two types of bifunctional catalysts were prepared in this dissertation, bifunctional catalysts coated with ZSM-5 with miroporosity and ZSM-5 with mesoporosity. The schematic drawing of the bifunctional catalyst can be viewed in Figure 2-1. Monolithic catalysts without ZSM-5 coating were also synthesized and used as a benchmark. Besides structured catalysts, conventional Co supported on spherical Al_2O_3 catalysts were prepared by dry and wet impregnation methods to validate the homemade fixed bed setup by closing mass balance with a $\pm$ 5% error. The wet and

dry impregnation methods will not be elucidated in the dissertation and can be learned from references [101–104].

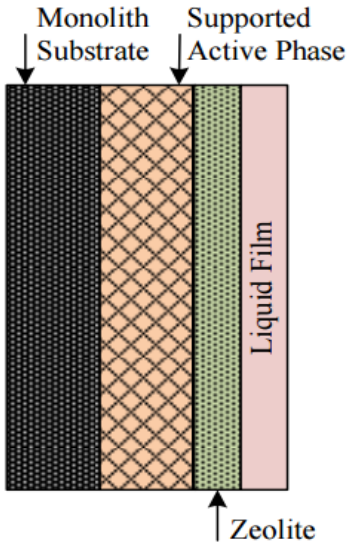

Figure 2-1. Schematic drawing of the layered structured catalyst with zeolite coating

2.2.1 Multi-layer Monolith Catalyst Synthesis

The whole bifunctional catalysts preparation process is shown in Figure 2-1. The structured catalysts were synthesized on cordierite monolith substrates ($2MgO:2Al_2O_3:5SiO_2$, Corning, 200 cpsi, L: 7.5 cm), shaped to fit in the 0.5'' ID reactor. Alumina wash-coating solution was prepared, by adding 5 g Boehmite (Al_2O_3, 20% in H_2O, Alfa Aesar) and 30 g deionized water into 25 g γ-Al_2O_3 (99.97%, 3-micron APS powder, 80-120 m^2/g surface area, Sigma Aldrich). The mixture was stirred well to achieve homogeneous slurry. The monoliths, pretreated at 120 °C, were immersed in the wash-coating solution for 1 min, and the excess solution was gently blown off with pressurized air. After wash-coating, the monoliths were dried at 120 °C for 4 h and calcined at 400 °C for 12 h. Wash-coating was repeated to tune the thickness of the Al_2O_3 layer. After wash-coating, the active material was deposited by immersing the monolith into a $Co(NO_3)_2•6H_2O$ solution, prepared by dissolving 33.3 g $Co(NO_3)_2•6H_2O$ (98%, Sigma-Aldrich) in 25.6 ml DI

water, for 1 min. The excess solution was blown off gently. The catalyst was then dried at 120 °C for 4 h and calcined at 400 °C for 12 h. The final ZSM-5 coating was applied by dip coating the monolith into a NH_4-ZSM-5 slurry, prepared by mixing 20 g NH_4-ZSM-5 (Zeolyst International, 418 m^2/g surface area, Si/Al = 80) with 31 ml DI water. The excess solution was again blown off, and the previously described drying and calcination protocols were repeated. Two wash-coatings of Al_2O_3 and a single Co impregnation produced approximately 5 wt.% Co_3O_4 loading on the monolith. Multi-step wash-coating in dilute solutions and careful inspection of the final zeolites reduced or eliminated the potential of axial gradients in the composition and quality of the structured catalysts. Characterization of these catalysts is discussed in Section 3. In the remaining of this article, the notation for the catalyst represents the coating sequence. For instance, ZSM-5/Co-Al_2O_3/M describes that Al_2O_3, Co and ZSM-5 coated the monolith (M) from interior (bare monolith surface) to exterior (final structured catalyst surface). The bare Co-Al_2O_3/M catalyst was used as a baseline to which the ZSM-5 coated catalysts were compared in terms of performance and selectivity. The monolith supported bifunctional catalysts with meso-ZSM-5 were prepared using the same protocol as bifunctional catalysts with micro-ZSM-5. The only difference is the porosity of ZSM-5.

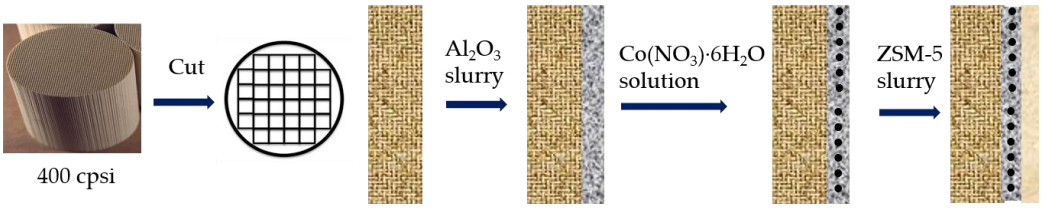

Figure 2-2. Structured bifunctional catalysts preparation flowchart

The bifunctional catalysts composed of micro-ZSM-5 showed high gasoline selectivity with significant amount of isoparaffins and olefins, however, the catalysts suffered a decrease of CO conversion which was caused by the micro-ZSM-5 out-layer with mass and heat transfer

barriers. To tackle the mass and heat transfer limitations posed by the presence of micro pores in the ZSM-5, a hierarchical ZSM-5 possesses mesoporosity was prepared by using desilication method which is going to be elucidated in the following part.

2.2.2 Hierarchical ZSM-5 preparation

Mesoporous ZSM-5 (Meso-ZSM-5) was prepared by alkaline mediated desilication of the parent ZSM-5 zeolite (Zeolyst International CBV8014, 418 m^2/g surface area, Si/Al = 80. Prior to alkaline treatment, the parent ZSM-5 was calcined in air at 550 °C for 6 h. Alkaline treatment was accomplished by mixing the calcined zeolite and 0.2 M NaOH at 60 °C for 30 min, followed by three times centrifuging and washing with DI water. The material was converted to the ammonia form by triple-ion exchange in 2 M NH_4NO_3 solution followed by drying at 80 °C for 12 h. The final material was obtained in the H- form by calcination in air at 550 °C.

2.3 Experimental Apparatus

2.3.1 Construction and validation of the setup

Figure presents the FTS microreactor configuration used in this dissertation. A custom-designed fixed bed reactor consisting of a 0.5'' ID and a 12'' long stainless-steel tube (Swagelok) was used. The whole process starts with two high pressure mass flow controllers (MFC, BROOKS 5850S) which can work under high pressure up to 1500 psi. Argon was controlled by a 50 ml/min MFC with ±1.0% accuracy, serving as an internal standard. While premixed syngas (H_2/CO ratio equals 2, Airgas, UHP) was controlled by a 100 ml/min MFC. A relief valve was installed right before the fixed bed reactor inlet to prevent sudden pressure increase, preventing pressure buildup. A K type thermocouple was inserted right at the top of the monolith catalyst for accurate temperature control. The fixed bed reactor was heated using a tube furnace (Thermo Fisher Scientific). A two traps system was applied for collecting wax, light oil and water products. The

wax trap was kept at 120 °C with a heating tape, while the water trap was kept at room temperature. The reaction pressure was controlled by an Equilibar precision back pressure regular which used a separate gas pressurizing system. To assure security, all of the equipment aforementioned was contained by a large metal box with a vent on the top. A Micro GC 4900 (Agilent, equipped with a PPQ column-10 m and a molecular sieve 5 column-10 m) with thermal conductive detector (TCD) was set up right next the FTS work station to collect gas composition on line. A stand along Agilent GC 6890 (HP-5 column) equipped with a flame ionized detector (FID) was used to do analysis for liquid hydrocarbons.

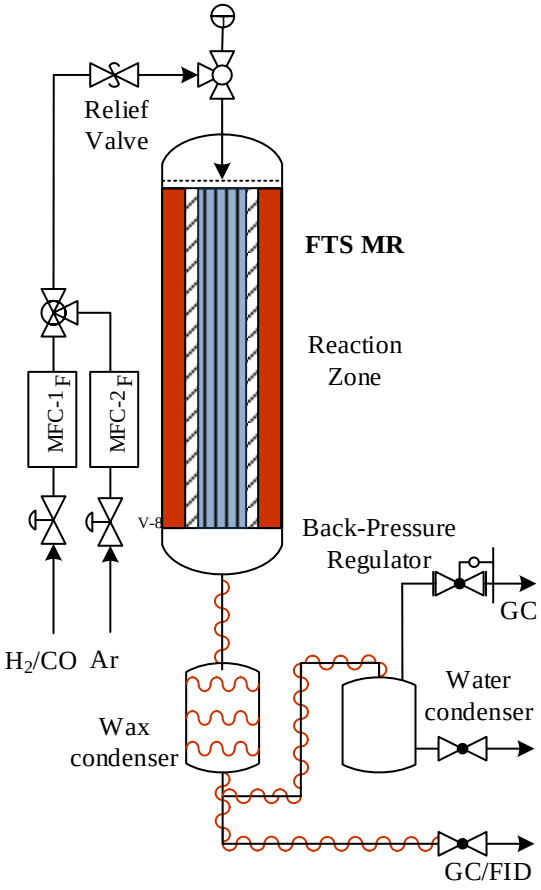

Figure 2-3. Schematic drawing of the fixe bed reactor used in the fixed bed experiments

After the construction of the whole set up, leak check was performed by pressurizing the system with Argon to 30 bar. Pressure was controlled by using a back pressure regulator. If there

was no pressure drop for the system after a night, leak check was completed. Liquid soap was used to identify the leaking spots. Leaking joints will be replaced. Leak check will be performed until there is no pressure drop. After finishing all of the security check, the system was validated by using a convention Co/Al_2O_3 catalyst with 20 wt% Co loading. Mass balance calculation and products analysis were conducted and repeated to verify the stability of the system. Stability test (more than three times) with error bar is shown in Figure 2-4.

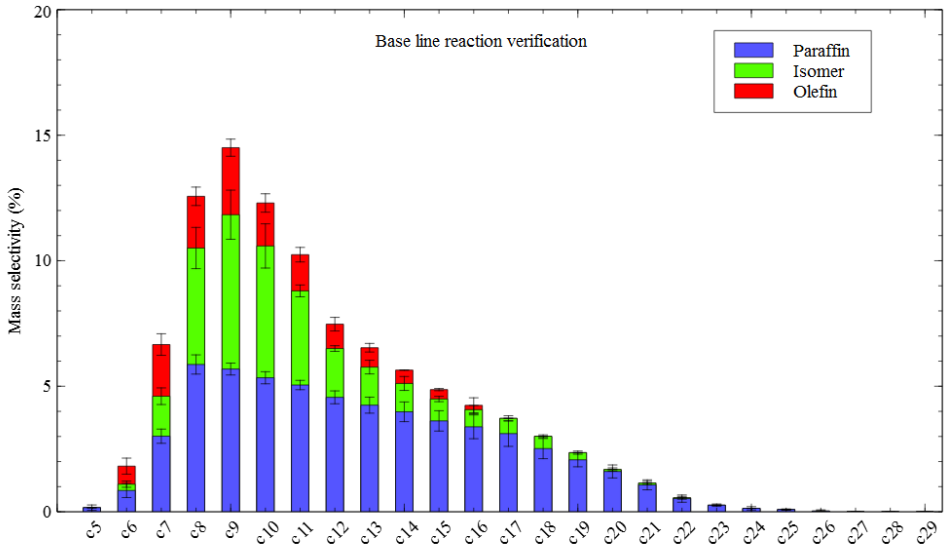

Figure 2-4. Repeatability tests to verify the fixed bed set up stability

2.3.2 Calibration of the equipment and products analysis method

The gas products (H_2, CO, CO_2, C_1-C_4 paraffin, and olefin gasses) were analyzed on-line with gas chromatography. Calibration for all gasses was conducted with gas standards (UHP300 Airgas). Different known amount of standard gas was mixed with Ar to achieve desired gas percentage. For H_2, CO and CO_2, 5%-90% range was calibrated. While for C_1-C_4 paraffins, 1%-10% range was calibrated to make sure the calibration curve fit into the normal FTS products range for good accuracy. All of the gas components showed a linear calibration curve. The calibration of each paraffin gas was assumed to hold for its corresponding olefin. Ar as an internal standard,

the flowrate was kept as 10 ml/min for every experiment. Then, the total gas out flowrate of each experiment F_{tot}^{out} was calculated using Eq.(2.1): $\underline{F_{Ar}}$ is 10 ml/min; f_{Ar} is the fraction of Ar in the total outlet flowrate calculated by using its calibration curve. Outlet flowrates for each species *i* was calculated using Eq.(2.2). CO conversion was then calculated from the difference of CO flowrates measured at the inlet and the outlet of the reactor, as shown in Eq.(2.3):

$$F_{tot}^{out} = \frac{F_{Ar}}{f_{Ar}} \tag{2.1}$$

$$F_i = F_{tot}^{out} \times f_i \tag{2.2}$$

$$X_{CO} = \frac{F_{co}^{in} - F_{CO}^{out}}{F_{CO}^{in}} \times 100\%, \tag{2.3}$$

where F_{co}^{in} and F_{CO}^{out} are the inlet and outlet volumetric flowrates of CO respectively. F_{co}^{in} is the flowrate controlled by MFC, while F_{CO}^{out} is calculated from Eq.(2.2). Three types of selectivity are used in this dissertation: the molar selectivity to each product based on carbon number (C%); the mass selectivity (wt.%) of gasoline range hydrocarbons (C_5-C_{12}) and C_{13+} in the oil phase; and the mass selectivity (wt.%) of paraffins, isomers and olefins in the oil product. Moreover, the overall gasoline yield was calculated as a fraction of the C_5-C_{12} weight over the total syngas mass fed. C% selectivity was used for peer paper comparison [35,105,106]. Mass selectivity were used to describe the gasoline selectivity and quality in the oil, as is typical in refinery applications. Gasoline selectivity was calculated to provide a direct and clear metric of the effectiveness of the proposed process in its intended application (production of gasoline). The molar selectivity was calculated with the following equations:

$$S_{c_i} = \frac{n_i F_{C_i}}{F_{CO}^{in} - F_{CO}^{out}} \times 100\%, \tag{2.4}$$

$$S_{c_{5+}} = (1 - \sum_i \frac{n_i F_{c_i}}{F_{CO}^{\text{in}} - F_{CO}^{out}}) \times 100\%. \quad (2.5)$$

Eq.(2.4) was used to calculate molar selectivity to CO_2 and C_1-C_4 species. F_{C_i} is the outlet volumetric flowrate of species C_i. n_i is the number of carbon atoms in each species. Eq.(2.5) was used to calculate C_{5+} selectivity. For the liquid products analysis process, at the end of each experiment, the liquid products were collected from the wax and cold traps and weighed. Oil and water were separated by decanting with a pipette and were quantified separately. The oil product was dissolved in CS_2, and analyzed with an Agilent GC 7890 equipped with HP-5 column (0.25 micron, 30 m x 0.320 mm, -60 to 350 °C) and FID. C_5-C_{40} calibration was performed with C_5-C_8 and C_8-C_{40} alkane calibration standards (Sigma-Aldrich). In the liquid GC-FID analysis, oxygenates, alcohols and branched paraffins (here lumped together and termed as isomers) were detected as the peaks before the calibrated alkane peak. α-olefins and other olefins were detected as the peak right before and the peak subsequent to the corresponding alkane peaks, respectively [106].

2.4 Fixed Bed Bifunctional Catalysts Experiment

2.4.1 Bifunctional catalysts fixed bed performance

To evaluate the catalysts performance, the bifunctional monolithic catalyst was held in place with quartz wool at both ends of the reactor. The reactor was heated with a tube furnace. A thermocouple at the top of the reactor was used to monitor the reactor entrance temperature and a thermocouple placed at the middle of the outer reactor wall was used to measure and control the reactor temperature. After loading, the catalyst was reduced in situ at 400 °C, with a ramp rate of 5 °C/min and 1 atm for 16 h with 50 ml/min pure H_2 flow. Thereafter, the reactor temperature was decreased to 180 °C and 100 ml/min of Ar was used to purge the reactor for 10 min, getting rid of

any H_2 residue. The reactor was then pressurized with the same flowrate of Ar to 12 bar, controlled by an Equilibar precision back pressure regulator (500 psig max, Cv: 0.07). After stabilization of the pressure at set-point, a premixed 35 ml/min syngas feed, with H_2 to CO ratio of 2:1, was introduced to the reactor. Simultaneously, the temperature was increased to 230 °C at 2 °C/min ramp rate. A slow heating rate is crucial for a well-controlled bed temperature. Carbon formation and side reactions tend to happen with a quick temperature increase. Ar at 10 ml/min was fed continuously to serve as an internal standard. All the gasses were controlled with high-pressure mass flow controllers (BROOKS 5850S). Liquid products were collected in a two-trap system. The wax trap was maintained at 120 °C with temperature-controlled heat tape, while the water condenser was set to room temperature. Verification of the cold trap temperature was conducted using a dry ice trap, showing no further products condensation. Gases were analyzed online with gas chromatography (Agilent Micro GC 4900 equipped with PPQ column - 10 m, molecular sieve 5 column - 10 m, and TCD). Liquid products were collected from experiments performed for 48 h at steady state. Liquid analysis was performed offline with gas chromatography (Agilent GC 6890 equipped with FID). The mass balance was calculated for each test to ensure the validity of the analysis and only results that were within 5 wt.% mass balance error were accepted. Experiments were repeated at least three times or as many required to meet the mass balance requirement. Error bars were calculated using the standard deviation of the repeated experiments.

2.4.2 Bifunctional catalysts regeneration

In-situ regeneration of the bifunctional catalysts was also performed to investigate the bifunctional catalysts' stability. Purging and *in-situ* regeneration of the catalysts was performed by first lowering the system pressure to atmospheric and cooling the temperature to 180 °C, followed by 10 min 100 ml/min Ar purging. After purging, 50 ml/min of Air was fed to the fixed

bed reactor, while the furnace temperature was increased from 180 °C to 400 °C with 5 °C/min ramp rate and maintained at 400 °C for 1 h to assure the full depletion of liquid hydrocarbon products. The regeneration temperature was carefully chosen based on FTIR and TPO results shown in Chapter 4, catalysts deactivation part. After regeneration, the reactor was cooled down to 180 °C and pressurized with Ar and syngas to 12 bar for another FTS test. This completed one regeneration cycle. A total of 4 regeneration cycles were conducted which added up to 250 h on stream.

2.5 Catalysts Characterization Techniques

Characterization of chemical and physical properties of catalysts can not only provide us the information of morphologies and arrangement, but also the hidden catalysis mechanics behind the performance. Thus, it is crucial to use proper techniques to accurately showcase the catalysts' properties. To better understand the structured bifunctional catalysts and providing profound insights, techniques such as N_2 isotherm, X-ray diffraction (XRD), Fourier Transform Infrared Spectroscopy (FTIR), electron microscopy were used. Temperature programmed oxidation (TPO), Thermo Gravimetric Analysis (TGA) and Differential Thermo Gravimetric (DTG) were also used to study the bifunctional catalysts deactivation. But they will not be elucidated here, details of the operations can be found in Chapter 4 characterization methods part.

2.5.1 N_2 adsorption/desorption-porosity and surface area

The quantification of surface area, pore size, pore size distribution and the corresponding volume is one of the most fundamental practice of catalysis. Surface area and pores are the environment where active phases stay. Their properties are closely related to the catalysts performance. Pore size and volume determine surface area, which play a key role in the dispersion of active metals. The most common method for determining the internal surface area and pore size

of catalysts is by gas adsorption. The surface area of the bifunctional catalysts, the collected gas adsorption data were processed using a Brunauer-Emmett-Teller (BET) adsorption method. The BET theory is a widely accepted method for analyzing adsorption of gas molecules on a solid surface. The BET theory uses Langmuir model and the following assumptions are made:

(1) Langmuir theory holds true for every layer

(2) Interaction of gas molecules only exists with adjacent layers

(3) Infinite physisorption of gas molecules can happen on solid surface

(4) Enthalpy of adsorption for the first layer is highest

(5) All other layers have the same adsorption energy

The derived BET equation is shown in Eq. 2.6:

$$\frac{1}{v[(p_0/p)-1]} = \frac{c-1}{v_m c}\left(\frac{p_0}{p}\right) + \frac{1}{v_m c} \tag{2.6}$$

Where p_0 and p are the equilibrium and saturation pressures of gas adsorbate; v is the amount of adsorbed gas; v_m is the amount of monolayer adsorbed gas and c is the BET constant defined by Eq. 2.7:

$$c = exp\left(\frac{E_1 - E_L}{RT}\right) \tag{2.7}$$

where E_1 is the heat of adsorption of the first layer and $E_L$is that for the subsequent layers. To obtain information about the pore structure, the process is extended to allow the gas to condense in the pores. Further increase in the gas pressure will cause the pores to be completely filled. The Brunauer-Emmett-Teller (BET) surface area and pore volume were determined using N_2 adsorption/desorption. With the theory validated, the N_2 Isotherms were gathered using a Micromeritics ASAP 2020 Physisorption Analyzer at 77 K. Prior to analysis, samples were

degassed at 150 °C for 12 h. Isotherms were gathered for both fresh and spent catalysts to determine the effects of wax formation on pore blockage and catalysts deactivation.

2.5.2 FTIR-acid sites quantification and surface species identification

Diffuse Reflectance Fourier Transform Spectroscopy (DRIFTS) was used to investigate the deposition of extra-framework alumina (EFAL) and determine the relative Brønsted and Lewis acidity of the Meso-ZSM-5, compared to the parent. IR spectra were obtained using a Thermo Nicolet 6700 Fourier-transform Infrared Spectroscopy (FTIR) equipped with a Harrick Praying Mantis DRIFTS accessory and reaction chamber. KBr was used as the background for zeolite spectra, and all spectra were recorded using 32 scans at a resolution of 4 cm^{-1}. Calcined samples were degassed at 550 °C under vacuum for 1 h, then cooled to room temperature for analysis. At that point, the samples were heated to 130 °C, and a new background was taken. Pyridine was then dosed into the cell until saturation, followed by evacuation and then heating to 230 °C, to remove physisorbed pyridine. Brønsted and Lewis acidity were determined from the area under the peaks at 1550 cm^{-1} and 1450 cm^{-1}, respectively, and corrected using the extinction coefficients provided by Emeis [107]. Temperature programmed FTIR was conducted with the same set-up. Characterization was carried out at 25 °C, 100 °C, 150 °C, 300 °C, 500 °C and 600 °C respectively for 3 min with N_2 purging.

2.5.3 Electron microscopy-surface morphology, elemental mapping and particle size

The layered co-catalysts morphology and elemental properties were characterized with Scanning Electron Microscopy (SEM) and Transmission Electron Microscopy (TEM). For SEM a FEI EFEM Quanta 250 was used equipped with an EDAX Genesis EDS for elemental analysis. TEM was performed in a FEI Talos F200X operating at 200 KV. The co-catalysts were cut with a razor blade and coated with gold prior to SEM imaging. Coating of gold was crucial for a sharp

image, because monolith and Al_2O_3 are poor electron conductive materials. Line elemental mapping was used to showcase each element's distribution along with the layered structure. Preparation of SEM material with intact layer structure was tricky, since the cordierite monolith was fragile. For TEM imaging, micro and mesopores of the ZSM-5 can be validated. Elemental mapping was also performed to see the active phase distribution. Particle size was acquired by direct visualization of the active phase under high magnification.

2.5.4 XRD-material phase and Co particle size

A Scintag model XDS 1000 was used for X-ray diffraction (XRD) characterization. The scan angle range was set to 5° - 80° with 2°/min scan speed. Voltage of 40 kV and current of 44 mA were applied. After XRD pattern was established, the material phase was acquired by using a build in D8 software package. Fitting will be ended until all of the characteristic peaks were matched. The crystalline structure information was acquired based on the Bragg's equation:

$$n\lambda = 2d \sin\theta \tag{2.8}$$

Where n is an integral number of reflection; λ is the wavelength of the beam; d is the distance between the crystal planes and θ is the Bragg angle. After getting the phase information, the Scherrer equation was used to calculate the crystallite size of Co_3O_4 in each catalyst

Chapter 3

GASOLINE SELECTIVE FISCHER-TROPSCH SYNTEHSIS IN STRUCTURED BIFUNCTIONAL CATALYSTS

3.1 Introduction

According to the U.S. Department of Energy [108], the high gasoline demand in the U.S. creates a market for high-octane hydrocarbons from alternative domestic sources. The U.S. transportation infrastructure relies heavily on gasoline as the prime liquid fuel. Given the limited success in converting biomass selectively to biofuels [109,110], the dependency of the US transportation sector on foreign petroleum seems unavoidable [111,112]. The shortage of transportation fuels can be mitigated with gas/coal/biomass to liquids (XTL) processes. This is in part due to the newly discovered vast reserves of domestic natural gas, which provides a versatile resource for fuels production and energy generation. Among the various options for the conversion of gas to liquids, Fischer-Tropsch Synthesis (FTS) is a proven process for the production of linear hydrocarbons in the diesel range, from synthesis gas (produced via the reforming or partial oxidation of natural gas). In that context, it is of interest to explore FTS in terms of its capacity for substantial gasoline production, if modifications are to be made to improve its gasoline selectivity and quality.

The recent need for utilization of stranded natural gas from remote locations producing shale oil or shale gas has refocused research on GTL processes, specifically Fischer-Tropsch Synthesis (FTS), as a prime candidate for process intensification and modular manufacturing. However, Fischer-Tropsch is normally a very large-scale process involving complex heat transfer

and separation steps. Review of FTS reactor designs, reveals a past trend to design very complex reactors with focus on providing excellent isothermality. Temperature gradients are the major reason of low FTS selectivity. Therefore, FTS reactors include multi-tubular fixed bed reactors dipped in boiling water; slurry bed column reactors, in which synthesis gas is bubbled through a slurry of heavy liquid products and catalyst particles; and gas-solid fluidized-bed reactors or circulating fluidized bed reactors, which offer excellent capacities but suffer from attrition, temperature gradients and difficulty to separate waxes from solids. In this context, FTS intensification or modularization may sound as an oxymoron. Prior work [61,62,113] has shown excellent results with intensified rectors, such as microreactors, structured reactors and fixed beds with advanced core-shell catalyst loading. FTS is one gas-to-liquids (GTL) process which can be a solution to the transportation issues associated with stranded natural gas and certainly a major challenge to overcome lies in its scalability and uncertainty in its inputs.

FTS using cobalt catalysts has been studied extensively for diesel production in various reactor configurations [20,114,115]. Despite its commercial success, many challenges still exist in conventional FTS reactors. Fixed bed FTS reactors exhibit large pressure drops, catalyst deactivation, and inefficient control of the reactor temperature [34,61,116]. Fluidized bed FTS reactors experience challenges in the separation of the products from the catalyst, along with catalyst attrition and deactivation [34,41,61]. Conventional sphere or pellet catalysts pose diffusion limitations to the FTS process, which can lead to high local H_2 concentrations, favoring unwanted light hydrocarbons, linear olefins, and paraffins of low octane number [117,118]. To address these issues, Guettel et al. [119] conducted experiments with cobalt-based monolithic catalysts. They concluded that due to the slug flow regime of monolithic catalysts, higher reaction rates at comparable methane selectivity are feasible. Moulijn and coworkers [74,113] extensively studied preparation

methods for coated monolithic FTS catalysts. By tuning the coating thickness, selective FTS with high olefin to paraffin ratios was shown to be feasible. Monolithic catalysts can be operated at low pressure-drops, high geometric surface-areas, high mass-transfer coefficients, and short diffusion lengths, thus relaxing the mass and heat transfer limitations of spherical and pellet catalysts and decreasing olefin reabsorption [31,61,62,113,117].

Targeting specific carbon number groups is not feasible with the use of advanced reactor designs alone. The Anderson-Schulz-Flory (ASF) distribution poses an upper bound on the theoretical FTS selectivity to gasoline (C_5-C_{12}) at ~48 wt.% in conventional reactors [39,120–122]. Tsubaki and co-workers [87,123–128] tried to overcome this barrier by depositing ZSM-5 as an outer shell on conventional FTS catalysts. Their hypothesis was that the ZSM-5 membrane could force the long-chain FTS products to diffuse out through the zeolitic shell and thus have a high probability of undergoing secondary acid-catalyzed reactions. Different types of catalysts were synthesized in their work, such as: core-shell catalysts prepared by hydrothermal coating of HZSM-5 on Co/Al_2O_3 pellets; capsule catalysts by direct coating of HZSM-5 on Co/SiO_2 pellets; Co/SiO_2 + ZSM-5 as the first reaction step catalyst and Pd/SiO_2 + ZSM-5 as the second step catalyst; and hybrid catalysts comprising ZSM-5 and Pd/SiO_2. These catalysts were observed to be capable of direct synthesis of middle range iso-paraffins from syngas. In order to achieve high CO conversion, a higher temperature of 260 °C was recommended, with a concomitant penalty of high CH_4 and CO_2 selectivity.

In this work, we explore the feasibility of combining the advantages of monolithic catalysts and ZSM-5 membrane coating to formulate a highly active and gasoline selective catalyst. We build on the advantages of micro-reactors in scaling and control, which translates to rapid technology transfer and commercialization. In contrast to conventional catalysts, structured

catalysts offer low pressure drop, high geometric surface area, high mass transfer coefficients, and short diffusion lengths. The thickness of the catalyst layer can also be adjusted to achieve catalyst effectiveness factors close to unity [61,62,117]. The hypothesis of this work is that the use of bifunctional catalysts, containing FTS active sites and acid catalysts in a bi-layered arrangement in monolith reactors, can improve gasoline selectivity via oligomerization, aromatization, and isomerization reactions without sacrificing CO conversion. Therefore, we explore the potential of structured bifunctional catalysts as candidates for intensified FTS processes selective to high-quality gasoline production. The effectiveness and selectivity of these catalysts were studied in a range of pressures and temperatures. As shown in the following, highly active structured catalysts, capable of enabling high selectivity to branched hydrocarbons in the C_5-C_{12} range, were synthesized and tested.

3.2 Description of Experimental Facilities and Methods

3.2.1 Multi-layer Monolith Catalyst Synthesis

The structured catalysts were synthesized on cordierite monolith substrates ($2MgO:2Al_2O_3:5SiO_2$, Corning, 200 cpsi, L: 7.5 cm), shaped to fit in the 0.5'' ID reactor. Alumina wash-coating solution was prepared, by adding 5 g Boehmite (Al_2O_3, 20% in H_2O, Alfa Aesar) and 30 g deionized water into 25 g γ-Al_2O_3 (99.97%, 3-micron APS powder, 80-120 m^2/g surface area, Sigma Aldrich). The mixture was stirred well to achieve homogeneous slurry. The monoliths, pretreated at 120 °C, were immersed in the wash-coating solution for 1 min, and the excess solution was gently blown off with pressurized air. After wash-coating, the monoliths were dried at 120 °C for 4 h and calcined at 400 °C for 12 h. Wash-coating was repeated to tune the thickness of the Al_2O_3 layer. After wash-coating, the active material was deposited by immersing the monolith into a $Co(NO_3)_2•6H_2O$ solution, prepared by dissolving 33.3 g $Co(NO_3)_2•6H_2O$ (98%, Sigma-Aldrich)

in 25.6 ml DI water, for 1 min. The excess solution was blown off gently. The catalyst was then dried at 120 °C for 4 h and calcined at 400 °C for 12 h. The final ZSM-5 coating was applied by dip coating the monolith into a NH_4-ZSM-5 slurry, prepared by mixing 20 g NH_4-ZSM-5 (Zeolyst International, 418 m^2/g surface area, Si/Al = 80) with 31 ml DI water. The excess solution was again blown off, and the previously described drying and calcination protocols were repeated. Two wash-coatings of Al_2O_3 and a single Co impregnation produced approximately 5 wt.% Co_3O_4 loading on the monolith. Multi-step wash-coating in dilute solutions and careful inspection of the final zeolites reduced or eliminated the potential of axial gradients in the composition and quality of the structured catalysts. Characterization of these catalysts is discussed in the following Section 3.3. In the remaining of this article, the notation for the catalyst represents the coating sequence. For instance, ZSM-5/Co-Al_2O_3/M describes that Al_2O_3, Co and ZSM-5 coated the monolith (M) from interior (bare monolith surface) to exterior (final structured catalyst surface). The bare Co-Al_2O_3/M catalyst was used as a baseline to which the ZSM-5 coated catalysts were compared in terms of performance and selectivity. All catalysts were synthesized and characterized thrice and their average properties are reported in Table 3-1.

Table 3-1**:** Monolithic Catalysts Preparation Parameters Summary

Catalyst	Catalyst loading (g)	Monolith (g)	Al_2O_3 (g)	Co_3O_4 (g)	ZSM-5 (g)
Co-Al_2O_3/M	2.26 ± 0.08	1.42 ± 0.03	0.54± 0.06	0.20± 0.06	0
ZSM-5/Co-Al_2O_3/M	2.93 ± 0.03	1.42 ± 0.03	0.40± 0.08	0.13± 0.02	1.03± 0.04

3.2.2 Experimental Apparatus and Procedure

Figure 3-1 presents the FTS microreactor configuration used in this work. A custom-designed fixed bed reactor consisting of a 0.5'' ID and a 12'' long stainless-steel tube (Swagelok) was used for all FTS experiments. Monoliths weighing a total of 2.90 g with ~5 wt.% Co_3O_4 were loaded in the reactor, held in place with quartz wool at both ends of the reactor. The reactor was

heated with a tube furnace. A thermocouple at the top of the reactor was used to monitor the reactor entrance temperature and a thermocouple placed at the middle of the outer reactor wall was used to measure and control the reactor temperature. After loading, the catalyst was reduced in situ at 400 °C and 1 atm for 16 h with 50 ml/min pure H_2 flow. Thereafter, the reactor temperature was decreased to 180 °C and Ar was used to purge the reactor. The reactor was pressurized with Ar to 12 bar, controlled by an Equilibar precision back pressure regulator (500 psig max, Cv: 0.07). After stabilization of the pressure at set-point, a premixed 35 ml/min syngas feed, with H_2 to CO ratio of 2:1, was introduced to the reactor. Simultaneously, the temperature was increased to 230 °C at 2 °C/min ramp rate. Ar at 10 ml/min was fed continuously to serve as an internal standard. All the gasses were controlled with high-pressure mass flow controllers (BROOKS 5850S). Liquid products were collected in a two-trap system. The wax trap was maintained at 120 °C with temperature-controlled heat tape, while the water condenser was set to room temperature. Gases were analyzed online with gas chromatography (Agilent Micro GC 4900 equipped with PPQ column - 10 m, molecular sieve 5 column - 10 m, and TCD). Liquid products were collected from experiments performed for 48 h at steady state. Liquid analysis was performed offline with gas chromatography (Agilent GC 6890 equipped with FID). The mass balance was calculated for each test to ensure the validity of the analysis and only results that were within 5 wt.% mass balance error were accepted. Experiments were repeated at least three times or as many required to meet the mass balance requirement. Error bars were calculated using the standard deviation of the repeated experiments.

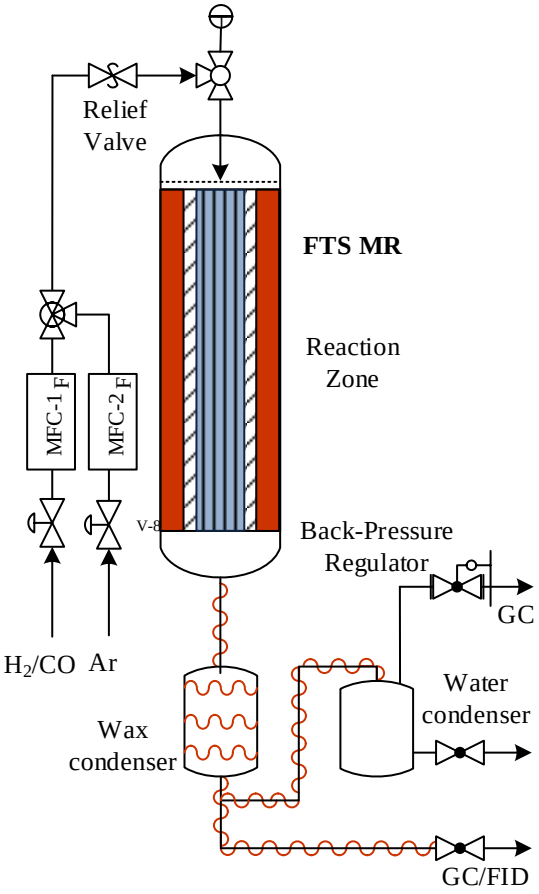

Figure 3-1**.** Schematic drawing of the fixed bed reactor used in this work

3.2.3 Gas and Liquid Product Analysis

The gas products (H_2, CO, CO_2, C_1-C_4 paraffin, and olefin gasses) were analyzed on-line with gas chromatography. Calibration for all gasses was conducted with gas standards (UHP300 Airgas). The calibration of each paraffin gas was assumed to hold for its corresponding olefin. Gas flowrates out of the reactor were calculated using Ar as internal standard. CO conversion was calculated from the difference of CO flowrates measured at the inlet and the outlet of the reactor using Ar as internal standard, as shown in Eq.(3.1):

$$X_{CO} = \frac{F_{co}^{in} - F_{CO}^{out}}{F_{CO}^{in}} * 100\%, \tag{3.1}$$

where F_{co}^{in} and F_{CO}^{out} are the inlet and outlet volumetric flowrates of CO respectively. Three types of selectivity are reported in this paper: the molar selectivity to each product based on carbon

number (C%); the mass selectivity (wt.%) of gasoline range hydrocarbons (C_5-C_{12}) and C_{13+} in the oil phase; and the mass selectivity (wt.%) of paraffins, isomers and olefins in the oil product. Moreover, the overall gasoline yield was calculated as a fraction of the C_5-C_{12} weight over the total syngas mass fed. C% selectivity was used for peer paper comparison [35,105,106]. Mass selectivities were used to describe the gasoline selectivity and quality in the oil, as is typical in refinery applications. Gasoline selectivity was calculated to provide a direct and clear metric of the effectiveness of the proposed process in its intended application (production of gasoline). The molar selectivity was calculated with the following equations:

$$S_{c_{1-4}} = \frac{n_{1-4}F_{C_{1-4}}}{F_{CO}^{\text{in}} - F_{CO}^{out}} \times 100\%, \tag{3.2}$$

$$S_{c_{5+}} = (1 - \sum_i \frac{n_i F_{c_i}}{F_{CO}^{\text{in}} - F_{CO}^{out}}) \times 100\%. \tag{3.3}$$

Equation (3.2) was used to calculate molar selectivity to CO_2 and C_1-C_4 species. F_{C_i} is the outlet volumetric flowrate of species C_i. n_i is the number of carbon atoms in each species. Equation (3.3) was used to calculate C_{5+} selectivity. At the end of each experiment, the liquid products were collected from the wax and cold traps and weighed. Oil and water were separated by decanting with a pipette and were quantified separately. The oil product was dissolved in CS_2, and analyzed with an Agilent GC 7890 equipped with HP-5 column (0.25 micron, 30 m x 0.320 mm, -60 to 350 °C) and FID. C_5-C_{40} calibration was performed with C_5-C_8 and C_8-C_{40} alkane calibration standards (Sigma-Aldrich). In the liquid GC-FID analysis, oxygenates, alcohols and branched paraffins (here lumped together and termed as isomers) were detected as the peaks before the calibrated alkane peak. α-olefins and other olefins were detected as the peak right before and the peak subsequent to the corresponding alkane peaks, respectively [106].

3.3 Catalyst Characterization

The synthesized monolithic catalysts were ground to a fine powder in an agate mortar for characterization. The Brunauer-Emmett-Teller (BET) surface area of the prepared catalysts was measured with a Micromeritics ASAP 2020 using N_2 physisorption at 77 K. Samples were degassed at 120 °C for 12 h at 10 °C/min. FEI EFEM Quanta 250 SEM and EDAX Genesis EDS were used for Scanning Electron Microscopy (SEM) imaging and Energy Dispersive Spectroscopy (EDS) mapping to determine textural and elemental properties. Prior to characterization, the monolith catalysts were cut with a razor blade and sputter-coated with gold. Line EDS spectrums were taken using 500 ms dwell time and 59 points per line. A Scintag model XDS 1000 was used for X-ray diffraction (XRD) characterization. The scan angle range was set to 5° - 80° with 2°/min scan speed. Voltage of 40 kV and current of 44 mA were applied. The Scherrer equation was used to calculate the crystallite size of Co_3O_4 in each catalyst. Transmission electron microscopy (TEM) and Energy Dispersive X-ray Spectroscopy (EDS) were collected using a FEI Talos F200X operating at 200 KV. TEM characterization was performed after completion of the FTS experiments, to assess the properties of the catalysts after reaction.

3.3.1 Characterization of the fresh structured catalysts

The N_2 sorption isotherms of the catalysts prepared are shown in Figure 3-2. The isotherm of pure ZSM-5 is also shown to provide an upper bound for the surface area of the materials prepared. For comparison of the surface area change, the raw monolith and a catalyst with cobalt directly supported on the monolith were also characterized. As shown Figure 3-2, adsorption of N_2 increases sharply at P/P0 0-0.1 and 0.9-1 for the ZSM-5, ZSM-5/Co-Al_2O_3/M, and Co-Al_2O_3/M catalysts, confirming a typical type IV isotherm which exhibits micro (0 Å to 20 Å) and macro (>500 Å) porosity. The physisorption isotherm of the monolith is small and flat, indicating a low

surface area. The isotherm of the monolith is slightly inaccurate in its shape, probably due to its very small surface area, which is within the error margin of the BET. From Figure 3-2, it is clear that coating with Al_2O_3 and ZSM-5 significantly increases the surface area of the monolith support. The shrinking of the adsorption-desorption hysteresis loop from the monolith to the Co/M and Co-Al_2O_3/M materials indicates that the pores of the raw monolith are partially filled with Co and Al_2O_3.

Adsorption data measured for each material is summarized in Table 3-2. The surface area of the materials studied decreases in the order: ZSM-5 > ZSM-5/Co-Al_2O_3/M > Co-Al_2O_3/M > Co/M > Monolith. By coating the monolith with Al_2O_3, the surface area increased by 25 times, providing a better substrate for active material dispersion and increased catalyst activity, which is also verified later in this work (cf. Table 3-3). The extensive micro-porosity observed in the ZSM-5 coated material is a clear indication of the membrane formed around the Al_2O_3 layer. This was further confirmed in SEM and EDS analyses, discussed in the following.

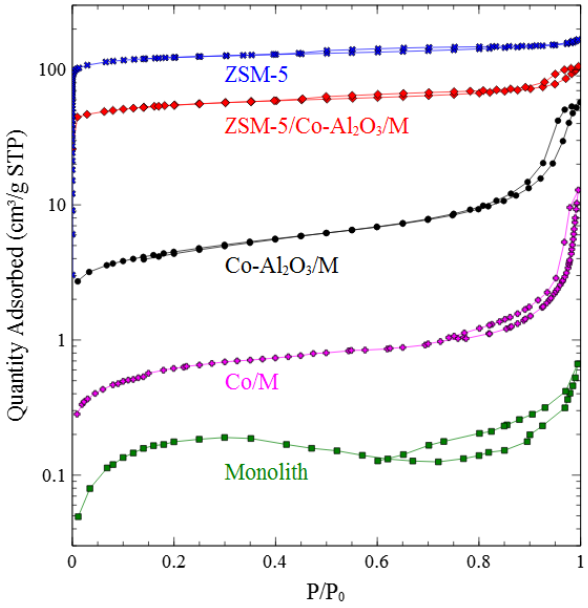

Figure 3-2. N_2 adsorption-desorption isotherms of the FTS catalysts and baseline materials

Table 3-2. Structure Parameters of the Materials studied

Material	S_{BET} (m^2 g^{-1})[a]	V_{total} (cm^3 g^{-1})[b]	V_{micro} (cm^3 g^{-1})[c]	D (nm)[d]	D (nm)[e]
Monolith	0.7	0.0008	0	--	--
Co/M	2.3	0.02	0	--	--
Co-Al_2O_3/M	16.2	0.09	0.0006	14.6	16.0
ZSM-5/Co-Al_2O_3/M	188.3	0.15	0.05	12.8	13.3
ZSM-5	418.8	0.25	0.14	--	--

[a] Surface area obtained from Brunauer-Emmett-Teller (BET) measurements (S_{BET}). [b] BJH desorption pore volume (V_{total}). [c] t-plot micro-volume (V_{micro}). [d] Scherrer's crystallite size (D) of Co_3O_4. [e] Average particle size (D) Calculated from TEM.

Figure 3-3 shows the XRD pattern of the fresh structured catalysts (a) ZSM-5/Co-Al_2O_3/M and (b) Co-Al_2O_3/M. XRD peaks were fitted using the D8 EVA software package. The diffraction peaks at 10.45, 18.16, 21.27, 26.37, 28.43, 29.48, 33.93 and 54.3° correspond to the cordierite monolith ($2MgO:2Al_2O_3:5SiO_2$). The peaks at 7.82, 8.76, 13.83, 14.65, 23.06, 23.76, 24.31 and 29.16° are attributed to the ZSM-5 phase. Peaks at 31.27, 36.85, 38.54, 65.24° belong to Co_3O_4 phase. Co signals are very low due to the small loading. ZSM-5 peaks were very clear for the ZSM-5/Co-Al_2O_3/Mc catalysts. The signals associated with the cordierite monolith dropped for the ZSM-5/Co-Al_2O_3/M catalysts compared to Co-Al_2O_3/M which was caused by the introduction of ZSM-5 (about 33 wt%, Table 1). The Co_3O_4 crystallite size was calculated as shown in Table 3-2.

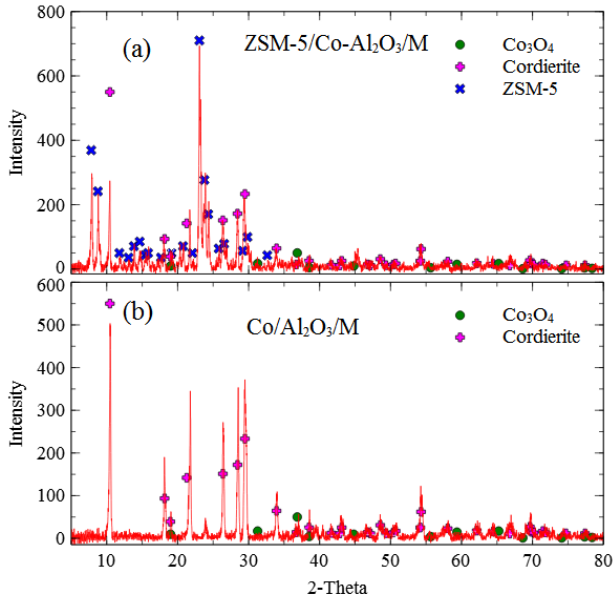

Figure 3-3. XRD patterns of fresh catalysts: (a) Monolith catalyst coated with Al_2O_3, Co_3O_4, and ZSM-5. (b) Monolith catalyst without ZSM-5 coating.

3.3.2 Structure of the Catalysts

Figure 3-4(a) shows the SEM image of the cross-section of a monolith support coated with Al_2O_3, Co_3O_4, and ZSM-5. The corresponding elemental line mapping is shown Figure 3-4(b). It is clear in Figure 3-4(a) that Al_2O_3 and ZSM-5 form two distinct layers on the monolith with the Al_2O_3 layer directly on the monolith and the ZSM-5 formed on the outer layer. A thicker and round layer forms at the corner of the monolith channel. The elemental mapping in Figure 3-4(b) confirms the presence and relative concentration of Al, Si and Co along the red arrow. The Co and Al signals appear and disappear almost at the same scan length. This indicates that Co coexists with the porous Al_2O_3 layer. The Si signal has a sharp increase at 200 µm, while the Co and Al signals have a sharp drop. This indicates that ZSM-5 forms as a distinct outer layer and there is no Co diffusion into the ZSM-5 layer. From Figure 3-4(a), the alumina layer thickness was estimated at about 50 µm, while the ZSM-5 layer is about 150 µm thick.

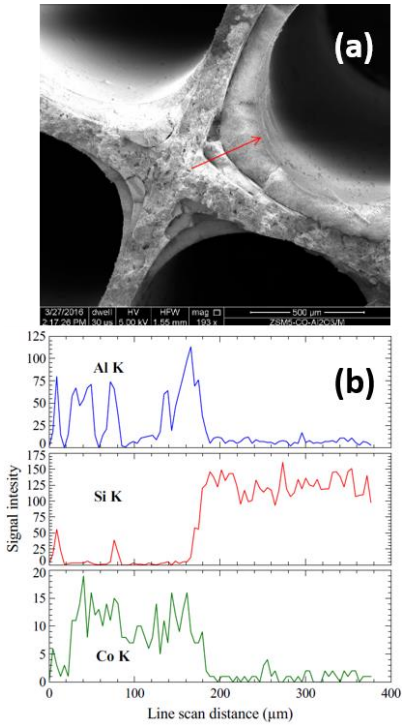

Figure 3-4. (a) Monolith catalyst coated with Al_2O_3, Co_3O_4, and ZSM-5. (b) Al, Si and Co line mapping along the red arrow from (a)

3.3.3 Transmission Electron Microscopy and Energy Dispersive X-ray Spectroscopy

TEM images of the Co-Al_2O_3/M and ZSM-5/Co-Al_2O_3/M used catalysts and EDS of the ZSM-5/Co-Al_2O_3/M used catalyst are shown in Figure 3-5. The top images show TEM of the Co-Al_2O_3/M and ZSM-5/Co-Al_2O_3/M used catalysts. The bottom images show the EDS of the ZSM-5/Co-Al_2O_3/M used catalyst. The EDS of Co-Al_2O_3/M is not shown here because its surface was contaminated by heavy hydrocarbons. This indicates that the Co-Al_2O_3/M catalyst surface was fouled with heavy hydrocarbons, which were not removed during the reactor purging. The catalysts with ZSM-5 coating did not indicate heavy hydrocarbon fouling in EDS. From Figure 3-5(a), the average particle size of dispersed Co (dark spots in Figure 3-5(a)) was estimated at ~16 nm, which agrees well with the XRD characterization (Table 2). From Figure 3-5(b), the average Co particle size of the ZSM-5/Co-Al_2O_3/M used catalyst was estimated at ~13.3 nm. This indicates that ZSM-

5 coating has no effect on catalyst particle size. Co particles are well distributed on both catalysts. The bottom images of Figure 3-5 show the EDS of the used ZSM-5/Co-Al_2O_3/M catalyst. Co is supported on the Al_2O_3 layer deposited at the surface of the monolithic substrate, while ZSM-5 (indicated by the rich Si signal) is a separate region without Co deposition.

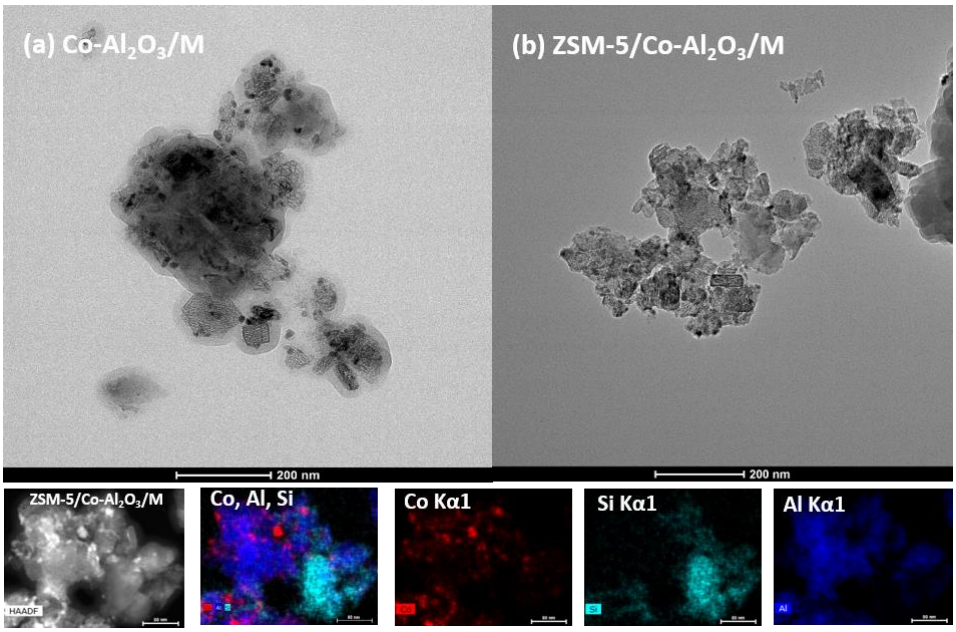

Figure 3-5. Top: TEM image for (a) Co-Al_2O_3/M used catalyst, (b) ZSM-5/Co-Al_2O_3/M used catalyst. Bottom: EDS for ZSM-5/Co-Al_2O_3/M used catalyst

3.4 Results and Discussion

3.4.1 ZSM-5 Effect on FTS Performance and Products Selectivity

The functionality of the ZSM-5 coating was analyzed in terms of its capacity to enhance cracking and isomerization reactions, as well as its capability to control the size of the hydrocarbons produced. FTS was performed using catalysts with and without ZSM-5 coating to test this hypothesis. Table 3-3 presents the performance of monolithic catalysts with and without ZSM-5 coating at the same reaction conditions. The data was also used in Figure 3-6 to illustrate the corresponding trend.

Table 3-3. Performance of Monolith Catalyst with and without ZSM-5. Reaction conditions: Temperature: 230 °C, Pressure: 12 bar, H_2/CO: 2:1, Syngas flowrate: 35 ml/min, Catalyst loading: 2.9 g for ZSM-5/Co-Al_2O_3/M and 2.3 g for Co-Al_2O_3/M, Co loading: 3.3 wt.% for ZSM-5/Co-Al_2O_3/M and 6.5 wt.% for Co-Al_2O_3/M, Time of experiments: 48 h*

Catalyst	CO conv (%)	Product selectivity (C%)				Oil phase (wt.%)		Oil product selectivity (wt.%)			Mass balance (%)
		CH_4	CO_2	C_2-C_4	C_{5+}	C_5-C_{12}	C_{13+}	Paraffins	Isomers**	Olefins	
Co-Al_2O_3/M	81.7	20.0	3.8	16.3	60.0	63.3	35.8	68.4	26.3	4.8	95.9
	± 2.6	± 0.5	± 1.8	± 0.7	± 3.3	± 4.0	± 2.8	± 5.1	± 3.9	± 1.3	± 0.6
ZSM-5/Co-Al_2O_3/M	78.7	10.9	1.5	12.1	75.5	93.3	6.5	28.9	49.8	21.3	96.0
	± 3.7	± 1.1	± 1.4	± 2.8	± 0.7	± 2.1	± 1.8	± 1.7	± 4.0	± 2.3	± 0.3

* Reference commercial FTS selectivity with Co-based catalysts is reported by de Klerk [129] in wt% {CH4: 5.6, C2-C4: 6.3, C5+: 86.5, (C5-C10)/C5+: 23}, Dry [20] in C% {CH4: 4, C2-C4: 8, C5+: 87, (C5-160 C)/C5+: 22}, and Enger et al. [130] in C% {CH4: 8-11, C5+: 72.4-86.7}. ** The lump of isomers includes the oxygenated products (if any).

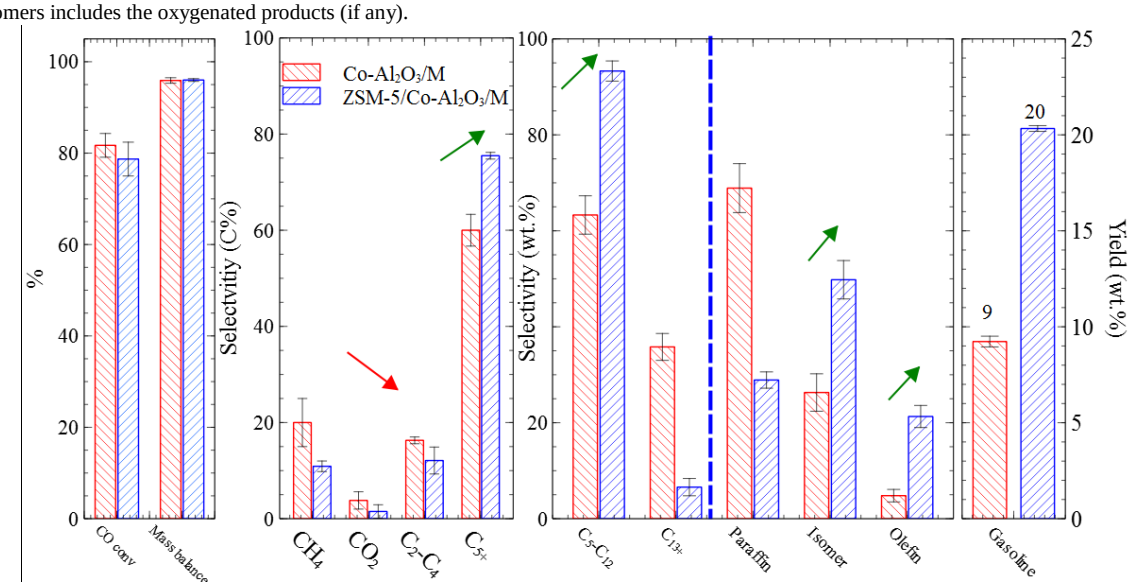

Figure 3-6. Overall performance summary for catalyst with and without ZSM-5 coating. Reaction conditions as noted in Table 3-3

ZSM-5 coating was responsible for a slight drop in CO conversion in the experiments with ZSM-5/Co-Al_2O_3/M. Since the loading of Co in the Co-Al_2O_3/M catalyst was slightly higher than that in the ZSM-5/Co-Al_2O_3/M (Table 3-1), it can be concluded that the ZSM-5 coating does not significantly alter the catalyst activity. This is in contrast to previously studied synthesis methods of ZSM-5 core-shell catalysts, which showed active site loss from the pretreatment process [131]. It is noteworthy that the CH_4 selectivity decreased to almost half with the use of the ZSM-5 coating.

This observation is in agreement with prior work [127,132,133] and has been explained as the result of altered water fugacity due to the hydrophilicity of the zeolite layer [127]; re-adsorption of the zeolite-produced intermediate isomers and olefins and recombination with CH_2 intermediates [127]; balancing of local temperature gradients between exothermic FTS and endothermic zeolite-catalyzed reactions [132]; and the fact that consumption of long-chain FTS products in the zeolite layer may shift FTS selectivity to higher carbon-number products [133]. Sartipi et al. [134] note that hydrogenolysis may increase selectivity to CH_4 in the presence of a zeolite, but they note that literature on this matter is inconsistent. Duyckaerts et al. [135] showed that the presence of CO restores the intrinsic activity of the zeolite for oligomerization of short-chain (α-)olefins, leading to chain-growth and reduction of the overall yield to undesired gas products (C_{1-4}). However, relevant work by Jacobs et al. [130], Rytter et al. [136], and Igelsia [137,138] shows that diffusion limitations (presumably induced by the zeolite layer in this work) change the H_2/CO fugacity ratio on the catalyst surface, leading to excessive chain termination and higher light product selectivities. Overall, the change in H_2/CO local ratios, water fugacity and the impact of isomerization, cracking and hydrogenolysis reactions on the localized temperature gradients needs to be better understood in reactor configurations that, unlike the one presented here, focus on local phenomena, instead of reactor-level results. A possible explanation for the lower selectivity to C_2-C_4 hydrocarbons is provided by Halmenschlager et al. [139] and Ismagilov et al. [140] who conducted research on ZSM-5 oligomerization with FTS tail gas. Their analysis showed that ZSM-5 can oligomerize light hydrocarbons, especially ethylene and butylene into liquid hydrocarbons, such as, dimers and trimers, thus decreasing light hydrocarbons selectivity. Most importantly, Figure 6 shows that the mass selectivity to C_5-C_{12} (Gasoline range) range product increased significantly with the ZSM-5/Co-Al_2O_3/M catalyst. The C_5-C_{12} liquid product selectivity reached 93.3 wt.% (Table 3-3),

which is comparable with the results of Sun et al. [141] and Bao et al. [127]. In Figure 3-6, the gasoline yields for catalysts with and without ZSM-5 coating are shown (last plot in Figure 3-6). Gasoline yield for catalysts coated with ZSM-5 reached 20 wt.% which is double that of catalysts without ZSM-5 coating. The reason for the yield improvement is the cracking, isomerization, and oligomerization reactions over the ZSM-5 catalyst membrane. Hydrocracking and isomerization reactions shifted the selectivity of heavy hydrocarbons ($>C_{12}$) to lighter products (C_5-C_{12}), while oligomerization reactions decreased the C_2-C_4 selectivity and favored products in the desired C_5-C_{12} range [87,142]. It can be concluded that the combination of a structured support with a ZSM-5 membrane resulted in a highly active and gasoline selective FTS catalyst.

The liquid product distribution as a function of carbon number is shown in Figure 3-7. The Co-Al_2O_3/M catalyst was selective to heavy hydrocarbons up to C_{28}, which is in good agreement with earlier reports [87,135,143–145]. As shown in Figure 3-7(a), ZSM-5 coating led to a shift of selectivity from heavy hydrocarbons ($>C_{15}$) to light hydrocarbons. The selectivity peak for the ZSM-5/Co-Al_2O_3/M catalyst was at C_8, which indicates a high-octane and a high-quality gasoline product. The same conclusion can be drawn from Figure 3-7(b) and (c). The selectivity to isomers reached 49.8 wt.% (Table 3-3), which is about 15 wt.% higher than previously reported values for FTS [123]. Hydrocracking and isomerization over the ZSM-5 coated catalysts were very extensive, as shown by the increased isomer and olefin content. In summary, monolith catalysts coated with ZSM-5 membrane showed high activity and high selectivity towards gasoline range products under normal FTS conditions.

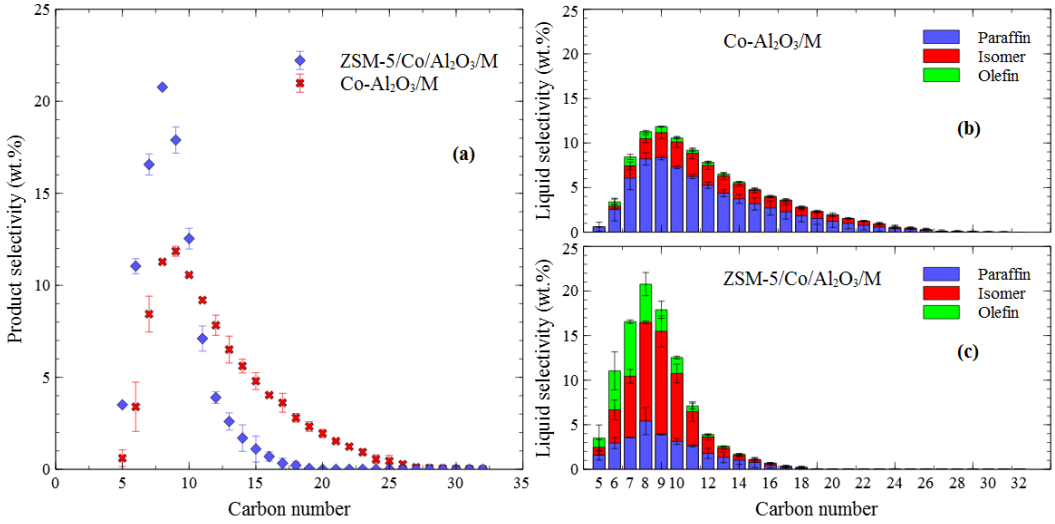

Figure 3-7. The liquid hydrocarbon distribution. (a) Selectivity of different carbon number species for Co-Al_2O_3/M and ZSM-5/Co-Al_2O_3-M. (b) (c) Paraffin, isomer, olefin selectivity as a function of carbon number for Co-Al_2O_3/M and ZSM-5/Co-Al_2O_3/M. Reaction conditions as noted in Table 3-3

3.4.2 Temperature Effect on ZSM-5 Coated Monolith Catalysts Performance

The performance of the ZSM-5/Co-Al_2O_3/M catalyst at different temperatures is summarized in Table 3-4 and plotted in Figure 3-8. CO conversion increased significantly with temperature in the 210-230 °C range. Further increasing the temperature did not affect CO conversion, indicating that a kinetic limit between competing reactions had been reached. CH_4 selectivity was lowest at the intermediate temperature of 230 °C. CO_2 selectivity increased slightly with the temperature increase, which could be attributed to the water-gas shift reaction at higher temperatures over the Co catalysts [39,143]. Selectivity to C_2-C_4 did not change significantly with the change in temperature in the range studied. The ZSM-5/Co-Al_2O_3/M catalyst showed better cracking and isomerization activity at elevated temperatures. This can be seen from the substantial increase in the selectivity to isomers and the corresponding decrease in C_{13+} selectivity. Industrial hydrocrackers operate in the temperature range of 350-440 °C [146], and the temperatures studied here were selected as a compromise between optimal FTS and refinery operations. The selectivity

to C_{5+} reached a maximum at 230 °C (Figure 3-8), while it decreased when temperature increased to 250 °C. This is anticipated for the effect of temperature on FTS, where elevated temperatures lead to higher CH_4 and C_2-C_4 selectivity [39]. At the low temperature studied cracking and isomerization were limited. At high temperature, unfavored short chain hydrocarbons were formed. Within the three temperatures tested, gasoline yield reached highest at 230 °C.

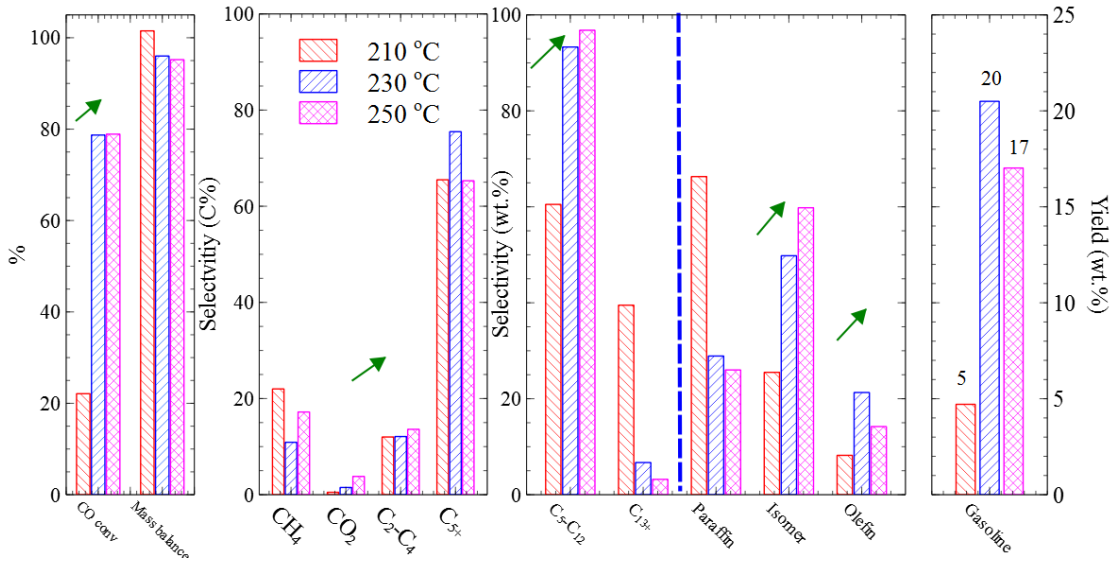

Figure 3-8. Overall performance summary of temperature effect for catalyst with ZSM-5 coating. Reaction conditions as noted in Table 3-4

Table 3-4. Conversion and Selectivity Summary of ZSM-5/Co-Al_2O_3/M Catalyst as a Function of Temperature. Reaction conditions: Catalyst loading: 2.9 g, Co loading: 3.3 wt.%, Pressure: 12 bar, H_2/CO ratio: 2:1, Syngas flowrate: 35 ml/min, Time on stream: 48 h. Reference commercial selectivities are reported in Table 3-3

T (°C)	CO Conv. (%)	Product selectivity (C%)				Oil phase selectivity (wt.%)		Oil product selectivity (wt.%)			Mass Balance (%)
		CH_4	CO_2	C_2-C_4	C_{5+}	C_5-C_{12}	C_{13+}	Paraffins	Isomers	Olefins	
210	22.1	22.0	0.5	12.0	65.5	60.5	39.5	66.3	25.5	8.2	101.5
230	78.7	10.9	1.5	12.1	75.5	93.3	6.7	28.9	49.8	21.3	96.0
250	78.9	17.2	3.8	13.6	65.3	96.8	3.2	26	59.8	14.2	95.2

The liquid product selectivity as a function of temperature is shown in Figure 3-9. The liquid hydrocarbons from experiments at 230 °C and 250 °C were distributed within gasoline range carbon numbers. The liquid product from the 210 °C experiments follows the ASF distribution

with up to C_{23} products identified. This is in agreement with the known Co-catalyzed FTS optimal temperature. Increasing the temperature enhanced the activity of the ZSM-5 layer in cracking lengthy hydrocarbon chains, while isomer and olefin selectivity also improved. At the higher temperature, higher carbon number products isomerized more extensively. Liquid products that do not precisely follow the ASF distribution were formed at 230 °C and 250 °C.

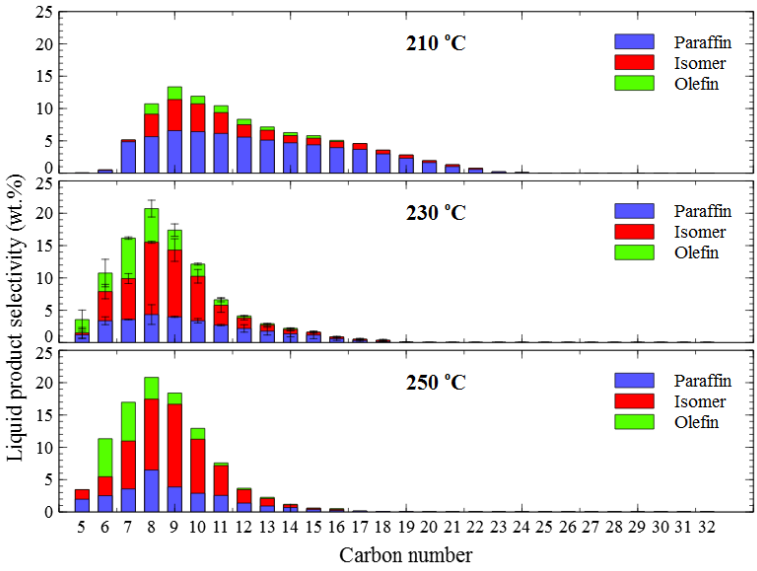

Figure 3-9. Liquid hydrocarbons selectivity from FTS at different temperatures. Reaction conditions as noted in Table 3-4

In summary, ZSM-5 coated catalysts produced more isomers and olefins in the liquid product, improving its quality at higher temperature. However, the high temperature also promoted FTS side reactions and favored undesired gas products. A moderate temperature should be chosen for maximum gasoline production. In this work, it was 230 °C.

3.4.3 Pressure Effect on ZSM-5 Coated Monolith Catalyst Performance

The effect of pressure on FTS over the ZSM-5 coated monolith catalysts is summarized in Table 3-5 and Figure 3-10. CO conversion decreased with increasing pressure, which indicated limitations of mass and heat transfer introduced by the ZSM-5 layer and the liquid products layer formed during the reaction. The selectivity to CH_4, CO_2 and C_2-C_4 hydrocarbons showed a

monotonic decline with increasing pressure (Figure 3-10). This is common and reasonable for the effect of pressure on FTS [121,146]. C_{5+} molar selectivity reached the highest at 20 bar, while gasoline selectivity was highest at 12 bar. With the ZSM-5 catalyzed cracking becoming less favorable at higher pressures, longer hydrocarbon chains formed at 20 bar. Although the total C_{5+} selectivity increased with pressure, the gasoline yield exhibited a peak at 12 bar. At 6 bar, fewer long-chain hydrocarbons were formed (leading to fewer gasoline-range products from ZSM-5 cracking); while at 20 bar, too many long-chain hydrocarbons were produced resulting in plugging and deteriorating the ZSM-5. Paraffin selectivity increased with pressure, while isomers and olefins decreased. This is due to more severe reabsorption and decreased chain branching reactions. Chain branching has been reported to become less favorable at high pressure, while this trend is opposite for reabsorption [39,147]. Reabsorption of olefins can result in longer paraffin chains. Within the tested pressures, 12 bar showed the highest gasoline yield.

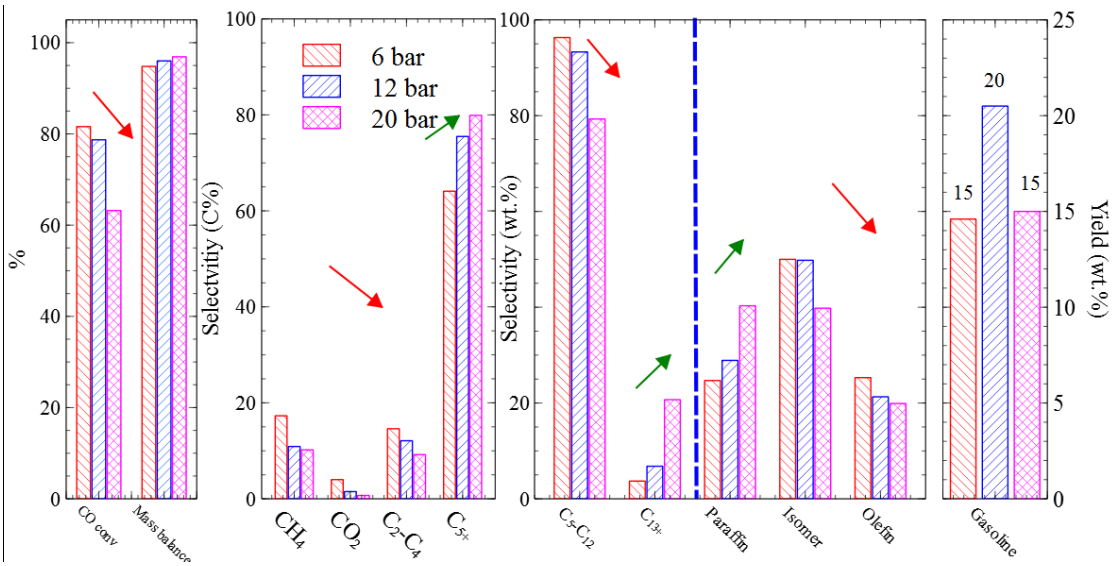

Figure 3-10. Overall performance summary of pressure effect for catalyst with ZSM-5 coating. Reaction conditions as noted in Table 3-5

Table 3-5. FTS Performance Summary of ZSM-5/Co-Al_2O_3/M Catalyst at Different Pressures. Reaction conditions: Catalyst loading: 2.9 g, Co loading: 3.3 wt.%, T: 230 °C, H_2/CO ratio: 2:1, syngas flowrate: 35 ml/min, Time on stream: 48 h. Reference commercial selectivities are reported in Table 3-3

P (bar)	CO Conv. (%)	Product selectivity (C%)				Oil phase selectivity (wt.%)		Oil products selectivity (wt.%)			Mass Balance (%)
		CH_4	CO_2	C_2-C_4	C_{5+}	C_5-C_{12}	C_{13+}	Paraffins	Isomers	Olefins	
6	81.6	17.3	4.0	14.6	64.1	96.3	3.7	24.7	50	25.3	94.8
12	78.7	10.9	1.5	12.1	75.5	93.3	6.8	28.9	49.8	21.3	96.0
20	63.2	10.2	0.7	9.2	79.9	79.3	20.7	40.3	39.8	19.9	96.9

The distribution of liquid hydrocarbons is plotted in Figure 3-11. Higher pressure was shown to favor the formation of longer chain hydrocarbons. Hydrocarbon chains reached C_{21+} at 20 bar, while the vast majority was smaller than C_{12} at 6 bar. Selectivity to isomers and olefins decreased with pressure. This is in agreement with Sarkari et al. [30] who reported that olefin reactivity increased because of the condensation of the hydrocarbons at high pressure. Since the ZSM-5 cracking and isomerization are significant but not dominant at 230 °C, the pressure had a relatively more pronounced effect on the liquid product distribution. Low pressure favored the production of smaller hydrocarbons, in the gasoline range. It also favored the production of undesired gas, in lieu of gasoline yield. In this work, pressure of 12 bar was found to be best for high yields to high octane rating gasoline. Overall, the structured catalysts show a peak in conversion and selectivity at 230 °C, a temperature slightly higher than what is commercially exercised (220 °C for Co catalysts), but at significantly lower pressure (12 bar compared to 20-30 bar in commercial applications). This reduction in pressure requirements, may be beneficial from the process economics and environmental perspectives, as lower pressures should decrease the operating cost and energy requirements of the FTS process.

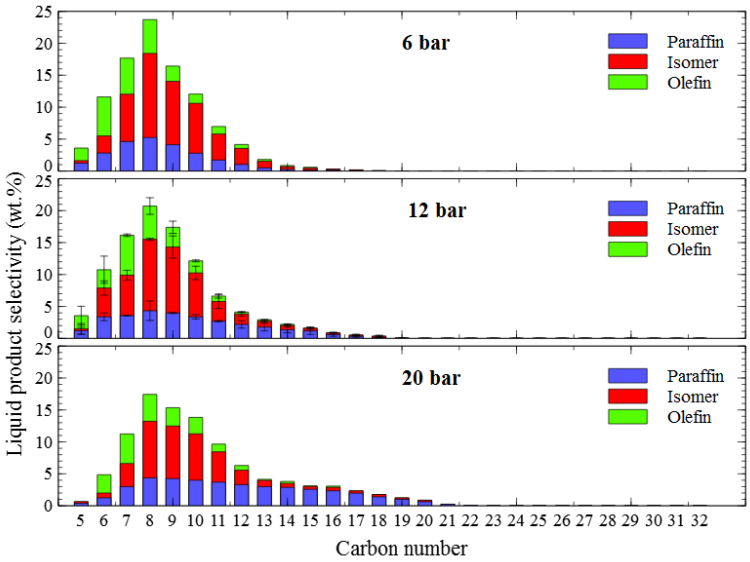

Figure 3-11. Liquid hydrocarbon selectivity from FTS at different pressures. Reaction conditions as noted in Table 3-5

3.5 Conclusions

A novel structured catalyst for in-situ FTS product upgrading to gasoline-range hydrocarbons was synthesized. This catalyst was tested to explore the hypothesis that combination of the intensified process efficiency of monolith with the isomerization and cracking capacity of ZSM-5 can enhance FTS selectivity to gasoline range products. Monolith-supported Co catalysts coated with ZSM-5 showed high FTS selectivity to gasoline range products (C_5-C_{12}) at 230 °C and 12 bar. Gasoline selectivity was found to be as high as 93.3 wt.% within the 75.5 % C_{5+} oil product and CO conversion was as high as 78.7 %. The addition of ZSM-5 on the monolith catalyst not only improved the gasoline selectivity but also gasoline quality, in terms of olefin and isomer composition. Investigation of the temperature effect on catalyst performance showed that the liquid product selectivity shifted to hydrocarbons of lower carbon numbers with the increase of temperature. CO_2 selectivity increased sharply with temperature, because of the enhancement of the water gas shift reaction. More isomers and olefins were produced over the ZSM-5-coated monoliths at high temperatures, but at the expense of the liquid product yield. Increasing reaction pressure led to higher selectivity to heavy hydrocarbons. Low pressure favored the production of isomers and olefins. High pressure was shown to introduce diffusion limitations to the ZSM-5 layer of the FTS catalysts synthesized. A moderate pressure of 12 bar was proposed to favor gasoline production.

Chapter 4

FISCHER-TROPSCH SYNTHESIS IN MONOLITH CATALYSTS COATED WITH HIERARCHICAL ZSM-5

4.1 Introduction

Fischer-Tropsch synthesis (FTS) is a well-known process for the production of diesel and heavy wax-range hydrocarbons. The hydrocarbon distribution from FTS can be altered by varying operating conditions and the type of catalyst used [148–150]. FTS has become reinvigorated because of the discovered massive deposits of North American natural gas, which can be easily converted to synthesis gas (CO and H_2). From synthesis gas, FTS offers a viable process for the production of liquid fuels, which in turn addresses the issue of limited transportation resources in remote locations. Considering the demand in transportation fuels and their environmental impact when produced from fossil fuels, FTS is a promising alternative to produce transportation hydrocarbons free of sulfur and nitrogen. Moreover, FTS can be adapted to a carbon neutral process, where the synthesis gas can be produced from the gasification of renewable biomass resources which again are often found in remote locations [151,152].

To improve FTS performance for liquid fuel production, the development of active and stable catalysts with high wax selectivity is crucial [34,153], since wax can be transformed into liquid fuel easily with a downstream upgrading process. Transition metals are frequently applied as the FTS catalyst active phase, and the choice of metal is largely dependent on the operating conditions. Among all metals, Co is considered the most suitable low-temperature FTS catalyst due to its high activity, relatively low price, favorable selectivity to long linear paraffins and low water-gas shift (WGS) activity [153]. Chain growth probability is one of the factors affecting low-temperature FTS performance. Factors that affect chain growth probability include Co crystallite size, Co

dispersion, properties of the catalyst support (e.g., surface area and pore volume) and the solid phase interactions [154–156]. Alumina (Al_2O_3) is a commonly used support for Co-based FTS catalysts, due to its strong interaction with Co oxides, resulting in small crystallite size and enhanced reducibility [85,157,158].

There are two commercially viable routes to make FTS a gasoline selective process: (1) *ex-situ* hydrocracking of the wax product to produce fuel in the middle distillate range, or (2) *in-situ* conversion using a zeolite co-catalyst [159]. Significant work has been performed on the latter for the *in-situ* conversion of heavy wax to gasoline [25,81,144,160]. Li et al. [89] tailored an encapsulated catalyst with H-β zeolite shell over Co/Al_2O_3 catalyst, which increased the molar ratio of isoparaffin to normal-paraffin by 64% compared with simple mechanical mixing of Co/Al_2O_3 and H-β zeolite. During the process, the zeolite acid sites provided hydrocracking and isomerization of long-chain normal paraffins, thus improving gasoline production and quality. Zola et al. [161] studied FTS performance for Co supported on different zeolites. They found that zeolite ZSM-5 is ideal due to its small pores and shape selective pore structure, which limits the growth of the product chain length and coke formation. They also suggested that the production of long chain hydrocarbons could be related to the three-dimensional pore system and secondary porosity.

In-situ upgrading with a zeolite co-catalyst has been explored in physical mixtures of ZSM-5 and Co catalysts [89,125,159,162]. However, the success of this method is limited due to the non-ideal ZSM-5 confinement, where large portions of the long linear hydrocarbons will diffuse through the edge of ZSM-5 without undergoing further isomerization and hydrocracking [163]. To address this challenge, Tsubaki and coworkers prepared multi-functional ZSM-5 zeolite-encapsulated catalysts, that increased gasoline selectivity and octane number [87,89,164–166]. However, the addition of the zeolite layer on Co/SiO_2 catalysts resulted in lower CO conversion and high CH_4 selectivity

compared with the plain Co/SiO_2 catalysts, most likely due to the higher diffusivity of H_2 relative to CO within the narrow ZSM-5 micropores, and a consequent increase in the local H_2/CO ratio [167]. CH_4 is an undesirable product because it is a relatively low value product and is formed at the expense of valuable liquid hydrocarbons [27]. In previous work [168], we have prepared a layered monolith catalyst composed of cordierite, Co/Al_2O_3 and ZSM-5 with microporosity. These bifunctional catalysts demonstrated excellent selectivity to gasoline-range hydrocarbons. However, CO conversion was limited most likely due to transport limitations from the bulk through the zeolite to the active phase.

One potential solution to the mass transfer limitation problem is the application of mesoporous ZSM-5 with a hierarchical structure to formulate a bifunctional co-catalyst. The mesoporous structure and high surface area of hierarchical ZSM-5 co-catalysts have shown high catalytic activity and relaxed diffusion limitations of reactants and products [123,167,169]. With isomerization, hydrocracking ability and elevated mass transfer, mesoporous ZSM-5 coated FTS catalysts could produce high quality middle distillates, with considerable isomer yields, while maintaining high CO conversion. Therefore, in this work we studied the feasibility of combining a monolith support, with a highly active Co/Al_2O_3 phase, and a hierarchical ZSM-5 membrane coating, with the objective of manufacturing a highly active and gasoline-selective FTS catalyst.

4.2 Experimental

4.2.1 Monolith Catalyst and Hierarchical ZSM-5 Preparation

Monolith-supported catalysts were prepared using a method described in detail in [168] and summarized here. The cordierite monolith substrate was composed of $2MgO:2Al_2O_3:5SiO_2$ (Corning, 200 cpsi). To fit the monolith catalyst in the fixed bed reactor (1/2'' ID), the monolith

substrate was first shaped to 6×6 cells with a blade, and then the four corners were eliminated. The finished monolith support was about 1.4 g in weight and 3'' in length. A thin Al_2O_3 layer was first deposited on the monolith by wash-coating in an Al_2O_3 slurry. After each coating, the substrate was dried at 80 °C for 1 h. To keep the alumina layer thickness constant, the procedure was repeated until each monolith was loaded with about 0.5 g Al_2O_3 coating. After coating with Al_2O_3, the catalysts were calcined at 400 °C for 2 h. With the Al_2O_3 layer constructed, active Co sites were deposited by immersing the support in a $Co(NO_3)_2 \cdot 6H_2O$ solution. The material was then calcined at 400 °C for 2 h, and the procedure was repeated until the desired Co loading was achieved. The outer zeolite layer was deposited by immersing the catalyst in a zeolite slurry, made by mixing 10 g ZSM-5 (Zeolyst International CBV8014, Si/Al of 80) with 35 ml DI water. The final co-catalysts were dried at 80 °C for 1 h and calcined at 400 °C for 2 h before FTS testing.

Mesoporous ZSM-5 (Meso-ZSM-5) was prepared by alkaline mediated desilication of the parent ZSM-5 zeolite (Zeolyst International CBV8014, 418 m^2/g surface area, Si/Al = 80) [170–172]. Prior to alkaline treatment, the parent ZSM-5 was calcined in air at 550 °C for 6 h. Alkaline treatment was accomplished by mixing the calcined zeolite and 0.2 M NaOH at 60 °C for 30 min, followed by three times centrifuging and washing with DI water. The material was converted to the ammonia form by triple-ion exchange in 2 M NH_4NO_3 solution followed by drying at 80 °C for 12 h. The final material was obtained in the H- form by calcination in air at 550 °C. Meso-ZSM-5 was dip coated onto the prepared monolith using the method described above. The layer thickness was controlled by the number of successive dipping cycles.

Table 4-1. Monolith co-catalysts synthesized and loading of each catalyst component

Catalyst	Catalyst weight(g)	Monolith (g)	Al_2O_3 (g)	Co_3O_4 (g)	ZSM-5 (g)
Monolith catalyst w/o ZSM-5	2.26 ± 0.08	1.42 ± 0.03	0.54 ± 0.06	0.20 ± 0.06	--
1.1 g-Micro	2.93 ± 0.03	1.42 ± 0.03	0.40 ± 0.02	0.13 ± 0.02	1.06 ± 0.04
1.1 g-Meso	3.08 ± 0.04	1.46 ± 0.03	0.50 ± 0.04	0.15 ± 0.03	1.07 ± 0.02
1.6 g-Meso	3.78 ± 0.04	1.45 ± 0.02	0.50 ± 0.01	0.16 ± 0.02	1.62 ± 0.03
1.9 g-Meso	4.02 ± 0.03	1.42 ± 0.01	0.51 ± 0.01	0.17 ± 0.02	1.94 ± 0.04

The naming convention for each material prepared in this work follows the form XX g-Type, where XX represents the weight of the zeolite deposited on the outside of the catalyst, indicative of layer thickness, and Type represents whether that zeolite deposited was mesoporous (Meso) or the parent microporous (Micro) ZSM-5. Table 4-1 reports the catalysts prepared and the mass-loading of each component on each catalyst. Monolith without (w/o) ZSM-5 coating, 1.1 g-Micro- and 1.1 g-Meso-ZSM-5 co-catalysts were tested in lab-scale FTS experiments to compare performance with and without ZSM-5 coating and the effect of the introduction of mesopores. The catalysts noted in the table (as 1.1 g-Meso, 1.6 g-Meso and 1.9 g-Meso) were tested to study the effect of the thickness of the mesoporous ZSM-5 layer. The 1.6 g-Meso-ZSM-5 catalyst was then used to study the pressure effect on FTS performance.

4.2.2 FTS Lab-scale process

A fixed bed stainless steel reactor was used in this work with 1/2'' ID and 12'' length. Each structured catalyst was loaded in the fixed bed and supported with quartz wool at both ends. The location of the co-catalysts was within the middle range of the tube furnace to ensure small temperature gradients. A thermocouple was inserted at the top of the reactor bed for accurate temperature measurement and control. The co-catalysts were reduced *in-situ* with 50 ml/min pure

H_2 at 400 °C for 12 h, at ambient pressure. After activation, the reactor was cooled to 180 °C and purged with pure Argon (Ar, UHP300, Airgas) for 10 min. Then, the reactor was pressurized with 10 ml/min Ar and 35 ml/min pre-mixed synthesis gas (CO and H_2 with 1:2 ratio). The desired pressure was achieved and controlled by a back-pressure regulator. Most experiments were conducted at 12 bar, unless indicated otherwise. Reactor temperature was maintained at 230 °C for the duration of the experiment. Flow was controlled by a high-pressure mass flow controller (BROOKS 5850S). Ar served as an internal standard (10 mL/min), while syngas flowrate was set to 35 ml/min for all the tests. Each test duration was set to 48 h. Stripping of the catalysts by Ar was carried out after each run at 180 °C for 10 min. The mass balance was calculated for every test to ensure accuracy. Tests within ±5% mass balance error were accepted. The standard deviation of each test was calculated using three different experiments.

Purging and *in-situ* regeneration of the catalysts was performed by first lowering the system pressure to atmospheric and cooling the temperature to 180 °C, followed by 10 min 100 ml/min Ar purging. After purging, 50 ml/min of Air was fed to the fixed bed reactor, while the furnace temperature was increased from 180 °C to 400 °C with 5 °C/min ramp rate and maintained at 400 °C for 1 h to assure the full depletion of liquid hydrocarbon products. The regeneration temperature was carefully chosen based on FTIR and TPO results shown later. After regeneration, the reactor was cooled down to 180 °C and pressurized with Ar and syngas to 12 bar for another FTS test. This completed one regeneration cycle. A total of 4 regeneration cycles were conducted which added up to 250 h on stream.

4.2.3 Product Quantification

Permanent gas products were analyzed online with a micro-GC 4900 (Agilent) equipped with thermal conductive detector (TCD) and two different columns (PPQ and a molecular sieve 5). The unit is capable of quantifying H_2, CO, CO_2, C_1-C_4 paraffin and olefin species. H_2, CO, CO_2 calibration was conducted by mixing pure Ar with each one of the gases, while C_1-C_4 standard gas (paraffin mixture) was used for gas phase hydrocarbon calibration. Olefins were assumed to have similar calibration to the equivalent paraffin [173].

Liquid hydrocarbons and water were collected in a two-trap system. The first trap was kept at 120 °C, while the second trap was at room temperature. Liquid products (hydrocarbons and water) were collected and weighed for the mass balance calculation. Liquid hydrocarbons were decanted from the water phase using a pipette and dissolved in CS_2. The samples were analyzed by gas chromatography (GC) with a flame ionized detector (FID, Agilent 6890) equipped with a HP-5 column. The retention time and calibration curve of each species were calibrated using C_5-C_{40} paraffin standards (Sigma Aldrich). The calibration curves for paraffins were assumed to hold the same for their corresponding isomers and olefins. All of the peaks appearing before the calibrated paraffin were lumped together as isomers, except for the peak right before the paraffin which was determined to be the α-olefin [106]. The peaks appearing after the paraffin peak were lumped together as olefins. Olefins described in this work were the lumped sum of α-olefin and post-paraffin olefins. The detailed protocol used for product analysis can be found in Zhu and Bollas [168].

4.2.4 Characterization Methods

Diffuse Reflectance Fourier Transform Spectroscopy (DRIFTS) was used to investigate the deposition of extra-framework alumina (EFAL) and determine the relative Brønsted and Lewis acidity of the Meso-ZSM-5, compared to the parent. IR spectra were obtained using a Thermo Nicolet 6700 Fourier-transform Infrared Spectroscopy (FTIR) equipped with a Harrick Praying Mantis DRIFTS accessory and reaction chamber. KBr was used as the background for zeolite spectra, and all spectra were recorded using 32 scans at a resolution of 4 cm^{-1}. Calcined samples were degassed at 550 °C under vacuum for 1 h, then cooled to room temperature for analysis. At that point, the samples were heated to 130 °C, and a new background was taken. Pyridine was then dosed into the cell until saturation, followed by evacuation and then heating to 230 °C, to remove physisorbed pyridine. Brønsted and Lewis acidity were determined from the area under the peaks at 1550 cm^{-1} and 1450 cm^{-1}, respectively, and corrected using the extinction coefficients provided by Emeis [107]. Temperature programmed FTIR was conducted with the same set-up. Characterization was carried out at 25 °C, 100 °C, 150 °C, 300 °C, 500 °C and 600 °C respectively for 3 min with N_2 purging.

The layered co-catalysts morphology and elemental properties were characterized with Scanning Electron Microscopy (SEM) and Transmission Electron Microscopy (TEM). For SEM a FEI EFEM Quanta 250 was used equipped with an EDAX Genesis EDS for elemental analysis. TEM was performed in a FEI Talos F200X operating at 200 KV. The co-catalysts were cut with a razor blade and coated with gold prior to SEM imaging. For TEM imaging, The Meso-ZSM-5 layer was peeled off from the rest of the co-catalysts for characterization, while the co-catalyst without the Meso-ZSM-5 layer was crushed for analysis.

The Brunauer-Emmett-Teller (BET) surface area and pore volume were determined using N_2 adsorption/desorption. Isotherms were gathered using a Micromeritics ASAP 2020 Physisorption Analyzer at 77 K. Prior to analysis, samples were degassed at 150 °C for 12 h. Isotherms were gathered for both fresh and spent catalysts to determine the effects of wax formation on pore blockage and catalysts deactivation.

Finally, temperature-programmed oxidation (TPO) was performed using a Netszch STA 449 F3 Jupiter thermogravimetric analyzer. Oxidation was performed in air at a flow rate of 80 ml/min and heating rate of 10 °C/min from room temperature to 1400 °C. The temperature was kept at 1400°C for 30 min to ensure there was no further mass loss.

4.3 Results

4.3.1 Characterization of Meso-ZSM-5

The physical properties of the Micro-ZSM-5 and Meso-ZSM-5 were characterized by N_2 adsorption/desorption, prior to their incorporation in the monolith. The isotherms are shown in Figure 4-1. Meso-ZSM-5 exhibited type H4 hysteresis, indicative of cylindrical mesopores originating at the surface of the material. The presence of hysteresis in N_2 adsorption was due to mesopores [174]. In order to maintain catalyst activity and shape selectivity, it is crucial that micropore volume is not significantly reduced as a result of the desilication process. T-plot micropore volume analysis showed a mild micropore volume reduction (28%) and a significant increase in external pore volume (353%), as shown in Table 4-2. It is hypothesized that the introduction of mesopores of this nature facilitate the transport of CO and H_2 through the zeolite layer, to the Co active sites and will allow the bulky waxes formed from the FTS reaction to reach zeolite acid sites for cracking, thus improving catalyst performance and stability [89,175,176].

Table 4-2. N_2 isotherm properties summary for parent Micro-ZSM-5 and Meso-ZSM-5

Sample	S_{BET} (m^2/g)[a]	V_{micro}[b] ($cm^3\ g^{-1}$)[b]	V_{meso}[c] ($cm^3\ g^{-1}$)[c]	$D_{average}$[d] (nm)	ΔV_{micro}	ΔV_{meso}	BAS[e]	LAS[e]
Micro-ZSM-5	418	0.14	0.08	6.00	--	--	2.70	0.12
Meso-ZSM-5	421	0.10	0.36	15.00	-27.7%	353.1%	2.13	0.16

[a] Surface area obtained from Brunauer-Emmett-Teller (BET) measurements (S_{BET}). [b] t-plot micro-volume (V_{micro}). [c]BJH adsorption pore volume 1.7-500 nm (V_{meso}). [d]BJH adsorption average pore diameter($D_{average}$). [e] Data calculated from DRIFTs-FTIR pyridine titration

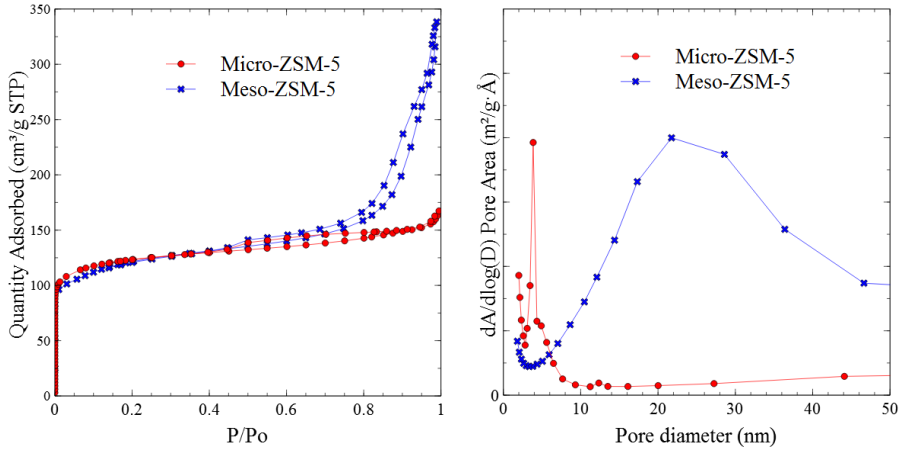

Figure 4-1. Left: N_2 isotherm for parent Micro-ZSM-5 and Meso-ZSM-5. Right: T-plot for parent Micro-ZSM-5 and Meso-ZSM-5

The acidity of the Micro-ZSM-5 and the Meso-ZSM-5 materials was evaluated by collecting FTIR spectra after pyridine adsorption. Prior work has illustrated that ZSM-5 Brønsted acidity plays an important role on product selectivity in hydrocracking and FTS product upgrading [177–179]. Acidity changes usually coincide with a physical modification of ZSM-5. As shown in Figure 4-2, the FTIR spectra of each material after pyridine titration exhibited a peak at 1550 cm^{-1}, representative of Brønsted acidity and a peak at 1450 cm^{-1}, representative of Lewis acidity [180,181]. From Figure 4-2, both the parent Micro-ZSM-5 and the Meso-ZSM-5 materials have significant

levels of Brønsted acidity, and minor levels of Lewis acidity that has been shown to catalyze the water-gas shift reaction [182], an undesirable outcome for FTS. Brønsted acidity decreased by approximately 20%, consistent with the reduction of micropore volume observed from the N_2 sorption data shown in Table 4-2, while Lewis acidity increased only slightly due to the desilication process.

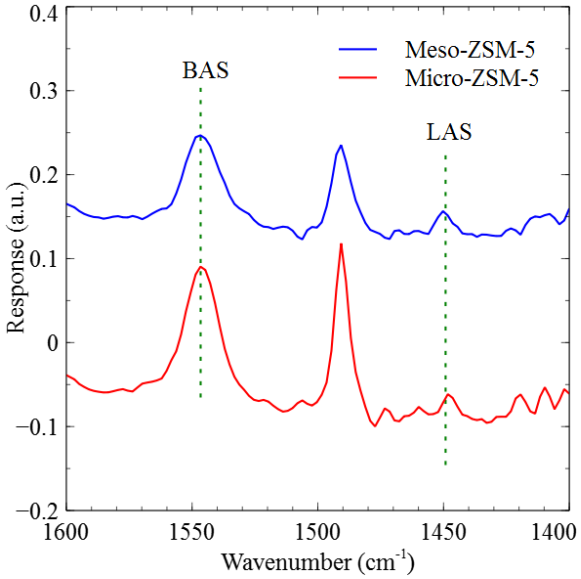

Figure 4-2. DRIFTS-FTIR spectra of Micro-ZSM-5 and Meso-ZSM-5 materials after pyridine titration

4.3.2 SEM and TEM Characterization of the Structure of the 1.1 g-Meso-ZSM-5 co-catalyst

The SEM image and line EDS mapping of the 1.1 g-Meso-ZSM-5 co-catalyst are shown in Figure 4-3. In the SEM image, the layered structure can be clearly viewed. The monolith served as a template for good heat distribution, low pressure drop and short diffusion distance. The Co/Al_2O_3 layer provided active sites for FTS, while the Meso-ZSM-5 outer layer provided shape selectivity and acid sites for hydrocracking and isomerization of the produced long linear hydrocarbons. For the 1.1 g-Meso-ZSM-5 co-catalyst, it can be seen that the layers were thicker at the monolith inside corners, which were around 200 µm thick. The elemental mapping of Figure 4-3 shows that the Si signal had a sharp increase around 60 µm, while the Al showed a high signal

in the range of 30 to 60 µm. The Co signal was present at 10 to 60 µm which was an indication of Co slip to the monolith template mainly due to the wash coating method. Nevertheless, the bulk of Co coincides with the Al_2O_3 layer.

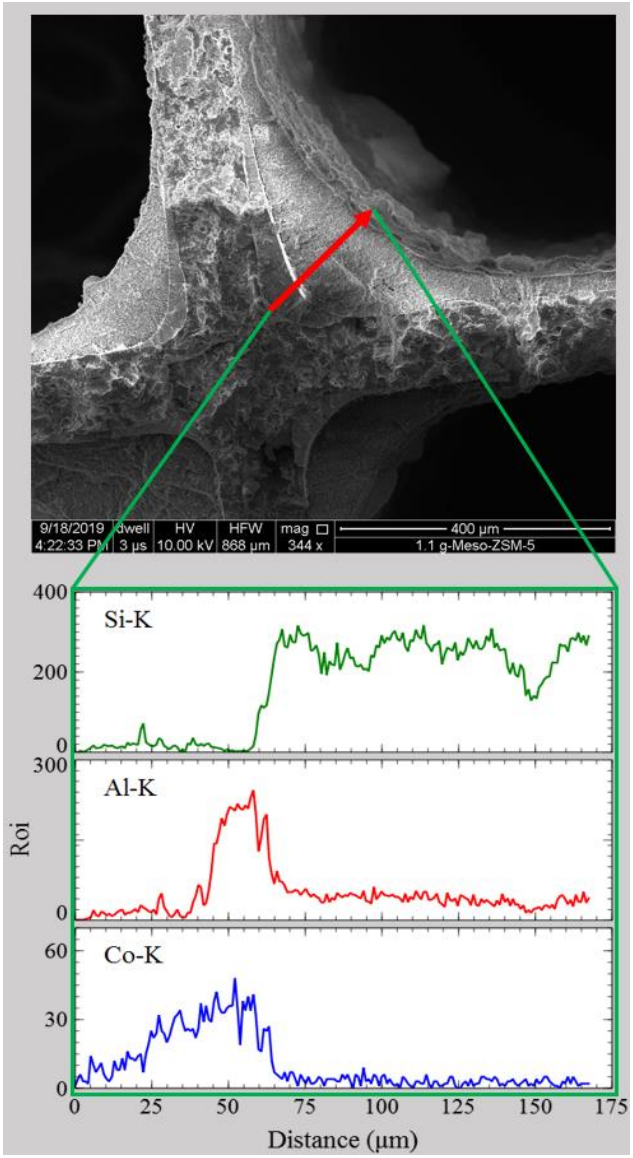

Figure 4-3. Top: SEM image of the 1.1 g-Meso-ZSM-5 co-catalyst. Bottom: Line EDS mapping along the red arrow indicated in the SEM image

The Meso-ZSM-5 layer was peeled off for TEM characterization to explore whether the hierarchical structure of the Meso-ZSM-5 stays intact after catalyst preparation. The TEM image of the peeled Meso-ZSM-5 layer and the elemental mapping of the 1.1 g-Meso-ZSM-5 co-catalyst

without the Meso-ZSM-5 layer are shown in Figure 4-4. Mesopores can be clearly viewed in the right top TEM image. Long channels and irregular circle pores are present, which showcases the good hierarchical structure of the Meso-ZSM-5. From the right bottom elemental mapping, it can be seen that the Co phase, with particle size around 10 nm, is distributed evenly on the Al_2O_3 support, making the catalyst highly active for FTS.

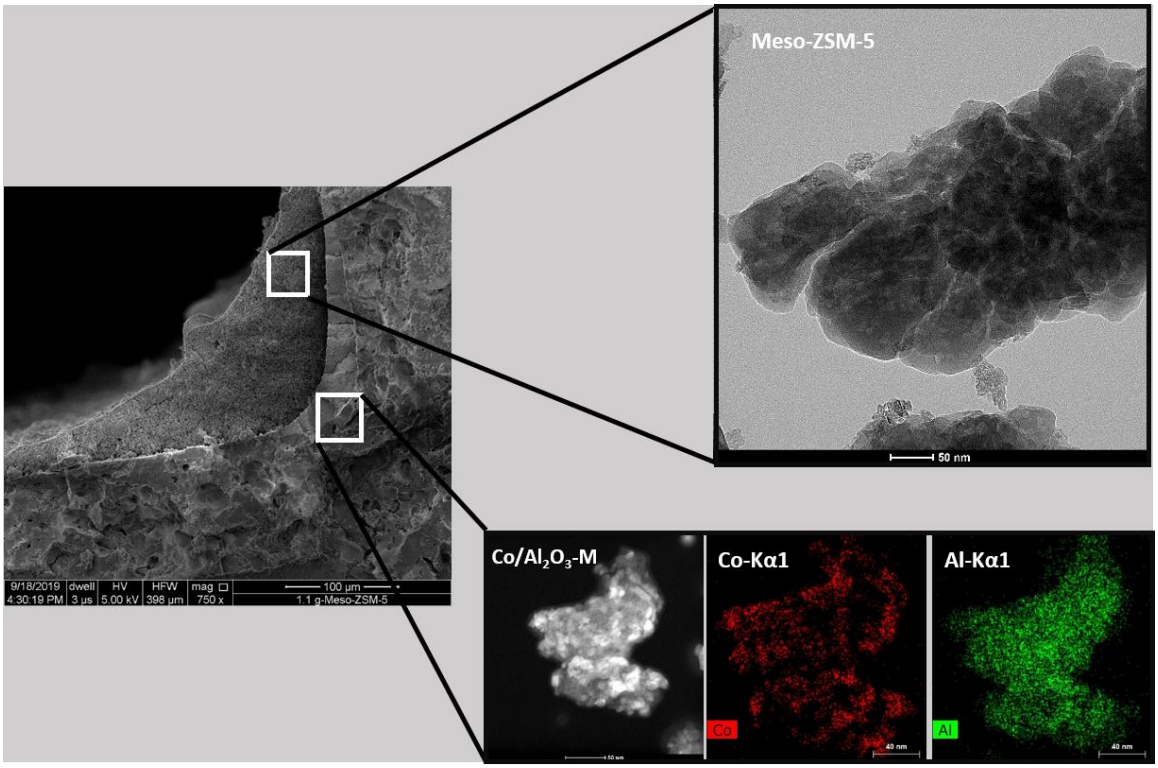

Figure 4-4. Left: SEM image of the layered structure of the 1.1 g-Meso-ZSM-5 co-catalyst. Right Top: TEM image of the Meso-ZSM-5 layer. Right Bottom: Elemental mapping of the 1.1 g-Meso-ZSM-5 co-catalyst without the Meso-ZSM-5 layer

4.3.3 FTS with Meso-ZSM-5 Catalyst

To study the effect of the ZSM-5 outer layer and the introduction of mesopores on FTS performance, control experiments were carried out utilizing three different catalysts: monolith catalysts w/o ZSM-5 coating, 1.1 g-Micro-ZSM-5 catalysts and 1.1 g-Meso-ZSM-5 catalysts. Experiments with the former two catalysts were conducted to study the ZSM-5 outer layer effect

(data are consistent with those presented in [168]), while experiments with the latter two of catalysts were conducted to study the FTS performance with the introduction of mesopores.

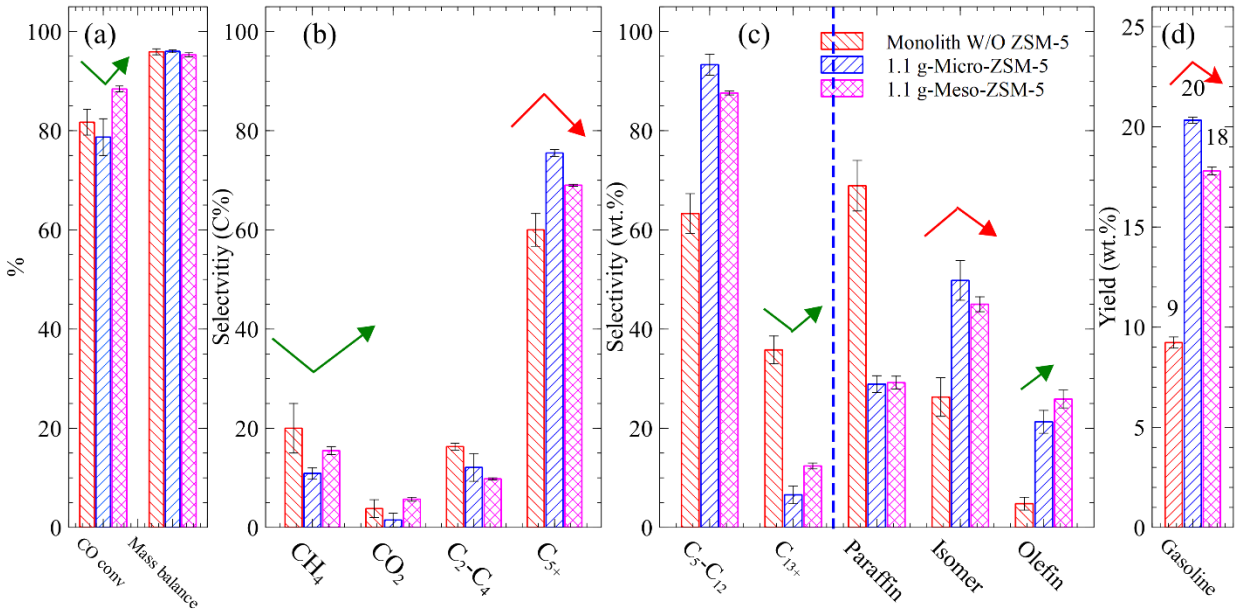

Figure 4-5. Monolith w/o ZSM-5, 1.1 g-Micro-ZSM-5 and 1.1 g-Meso-ZSM-5 catalysts performance comparison. Reaction conditions: T: 230 °C; P: 12 bar; Syngas flowrate: 35 ml/min; Time on stream: 48 h. (Note: C_5-C_{12}, C_{13+} and Paraffin, Isomer, Olefin in subplot (c) in Figure 4-5 are used to show gasoline, non-gasoline selectivity in the oil phase and the oil quality. Gasoline yield in the subplot (d) was calculated by the weight of gasoline produced divided by the total weight of syngas converted. This note holds for the rest of the plots in the paper.)

The performance of the monolith catalyst w/o ZSM-5, the 1.1 g-Micro- and 1.1 g-Meso-ZSM-5 coated co-catalysts is summarized in Figure 4-5. Figure 4-5(a) shows that the introduction of the ZSM-5 outer layer decreased CO conversion, mainly due to the mass transfer limitation originated from the micro-ZSM-5 layer. Compared with the 1.1 g-Micro-ZSM-5 co-catalyst, the 1.1 g-Meso-ZSM-5 catalyst showed 10% higher CO conversion. This was expected because of the improved mass and heat transfer in the mesopores of the Meso-ZSM-5 [178,183–185]. The selectivity of CH_4 and CO_2 showed a slight increase. CH_4 selectivity could be altered by many factors, such as catalyst local hot spots [186,187], diffusion limitations of CO and H_2 and Co interaction with the support [164,188].

Since the diffusion limitation for the micro-ZSM-5 should be relaxed by introducing mesopores, the possible explanation for the increase in the CH_4 and CO_2 could be a mixed effect of hot spots caused by elevated CO conversion and altered ZSM-5 acidity. The selectivity to short-chain hydrocarbons (C_2-C_4) decreased with the introduction of mesopores. Tsubaki et al. [184] attributed this to the weakened micropore catalytic activity, suppressing the light hydrocarbons selectivity of the catalysts due to mesopores. The same trend was also reported in the work of Wang and co-workers [189].

In Figure 4-5(c), the selectivity to gasoline-range hydrocarbons (C_5-C_{12}) was observed to follow the inverse trend of that of CO conversion. The monolith catalysts w/o ZSM-5 achieved a gasoline selectivity of only 64.2 wt.%, showing high selectivity to C_{13+} products, while the 1.1 g-Micro-ZSM-5 co-catalysts had very high gasoline selectivity (93.3 wt.%). With mesoporosity introduced, gasoline selectivity dropped to 87.6 wt.%. The selectivity to C_{13+} products was higher for the 1.1 g-Meso-ZSM-5 co-catalysts compared to that of the 1.1 g-Micro-ZSM-5 co-catalysts. This trend is in good agreement with prior work [184,185,189]. The reason for this trend is that the mesopores led to decreased Brønsted acidity (data in N_2 isotherm properties summary for parent Micro-ZSM-5 and Meso-ZSM-5) and relaxed mass transfer limitations of CO in the 1.1 g-Meso-ZSM-5 co-catalysts, resulting in lower hydrocracking, isomerization and promoting growth of long hydrocarbons. Usually, zeolite materials are utilized in the temperature range of 350-440 °C for crude oil upgrading [146]. Wang et al. [189] and Khodakov et al. [88] conducted experiments showing that hydrocracking and isomerization can also proceed under FTS conditions. The same conclusion was drawn by other researchers [81,156,190]. In regard to the production of paraffins, isomers and olefins, the catalyst w/o ZSM-5 had the highest Paraffins selectivity, while the 1.1 g-Meso-ZSM-5 co-catalysts showed inferior selectivity towards Isomers compared to the 1.1 g-Micro-ZSM-5

co-catalysts. This result supports the previous conclusion made on the Meso-ZSM-5 catalysts being worse at performing hydrocracking and isomerization, since isomers can only be achieved through zeolite isomerization. Since the 1.1 g-Micro-ZSM-5 co-catalyst was better at hydrocracking and isomerization with comparable CO conversion, it achieved the highest gasoline yield at 20 wt.%.

In summary, it was concluded from the control experiments using the monolith catalysts w/o ZSM-5 and the 1.1 g-Micro-ZSM-5 co-catalysts that a CO conversion drop was mainly due to the mass transfer limitation introduced by the micropores of the Micro-ZSM-5 outer layer. After introducing mesopores to the parent Micro-ZSM-5, the 1.1 g-Meso-ZSM-5 co-catalysts relaxed these diffusion limitations. However, the Micro-ZSM-5 desilication process decreased the Brønsted acidity, which limited the isomerization and hydrocracking of long linear hydrocarbon, thus lowering the overall gasoline yield.

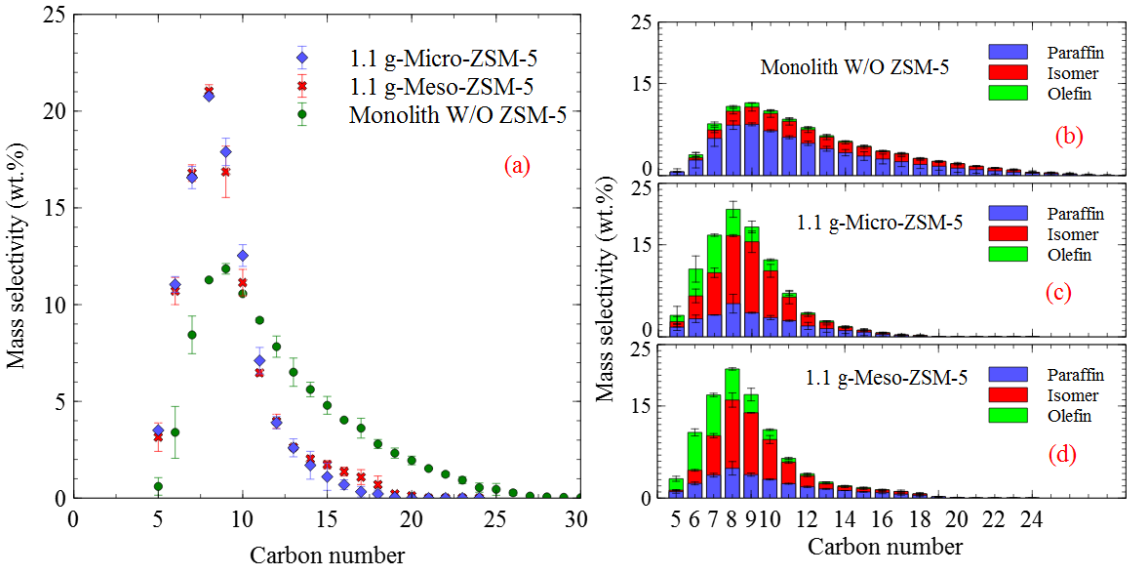

Figure 4-6. (a) Oil carbon number selectivity and paraffin, isomer and olefin selectivity for (b) monolith w/o ZSM-5. (c) 1.1 g-Micro-ZSM-5, and (d) 1.1 g-Meso-ZSM-5 co-catalysts

The mass selectivity of the liquid hydrocarbon products and the selectivity to paraffins, isomers and olefins as a function of carbon number are shown in Figure 4-6(a), and Figs.4-6(b-d) respectively. As shown in Figure 4-6(a), the 1.1 g-Micro-ZSM-5 co-catalysts shifted the oil products from the longer linear hydrocarbons (C_5-C_{26}) achieved by the monolith catalysts w/o ZSM-5 into the range of C_5-C_{18}, peaking in the gasoline-range products (C_5-C_{12}). With the introduction of mesopores, a slight shift in liquid products to the range of C_{14}-C_{18} can be observed for the 1.1 g-Meso-ZSM-5 co-catalysts, evidencing a decline in hydrocracking in the Meso-ZSM-5 outer layer. From Figure 4-6(b-d), the monolith catalysts w/o ZSM-5 produced the smallest amount of isomers and olefins, and the most of paraffins. On the other hand, the 1.1 g-Micro-ZSM-5 and 1.1 g-Meso-ZSM-5 co-catalysts showed comparable reduced selectivity towards paraffins.

It can be concluded from these results that introducing mesopores in the parent Micro-ZSM-5 released mass transfer limitations; however, it was assumed that the decreased Brønsted acidity through the added mesopores negatively impacted hydrocracking and isomerization. A potential solution to this issue is to increase the Meso-ZSM-5 layer thickness in order to increase the reaction path for long linear paraffins hydrocracking and isomerization, thus improving gasoline yield and quality. This hypothesis is explored in the following section.

4.3.4 Meso-ZSM-5 Layer Thickness

The performance of FTS with increasing Meso-ZSM-5 coating thickness is shown in Figure 4-7. The increase of Meso-ZSM-5 coating from 1.1 g to 1.9 g showed no obvious change to CO conversion, indicating that mass transfer limitation is not a dominant. However, the selectivity to C_5-C_{12} range hydrocarbons increased drastically when increasing thickness, from 87.6 wt.% to 97.4 wt.%. Increasing the thickness of the Meso-ZSM-5 led to enhanced hydrocracking and isomerization, and improved gasoline selectivity at high catalyst activity.

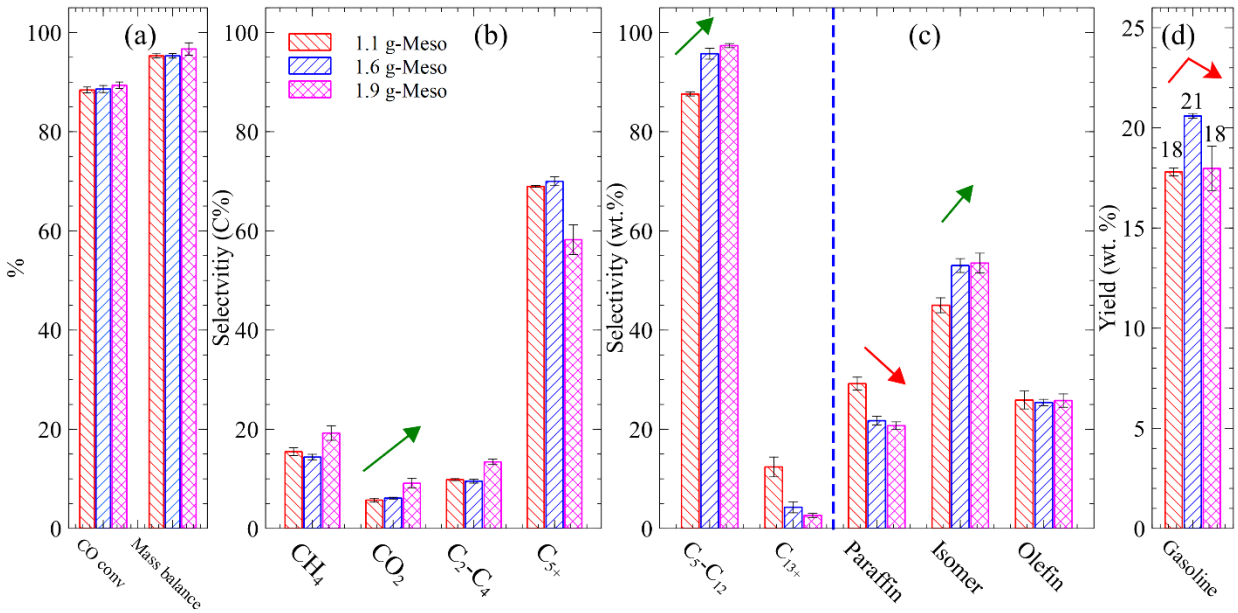

Figure 4-7. Co-catalysts performance with different Meso-ZSM-5 coatings. Reaction conditions: T: 230 °C; P: 12 bar; Syngas flowrate: 35 ml/min; Time on stream: 48 h

As shown in Figure 4-7, the 1.9 g-Meso-ZSM-5 co-catalysts demonstrated the highest selectivity to CH_4, CO_2 and C_2-C_4 gas hydrocarbons, over both the 1.1 g-Meso-ZSM-5 and 1.6 g-Meso-ZSM-5 co-catalysts. The selectivity to C_{5+} hydrocarbons dropped below 60% for the 1.9 g-Meso-ZSM-5 co-catalysts. Tsubaki et al. [164] performed similar work and observed the same increasing trend to CH_4 and C_2-C_4 which were attributed to the enhanced partial pressure ratio of H_2 and CO when the zeolite thickness increased. It is interesting to notice that selectivity to paraffins, isomers and olefins stayed the same for the 1.6 g-Meso-ZSM-5 and 1.9 g-Meso-ZSM-5 co-catalysts, indicating a constant rate of hydrocracking and isomerization reactions. The selectivity to C_5-C_{12} hydrocarbons and isomers maintained the same monotonically increasing trend when increasing the thickness of the Meso-ZSM-5 coating. Overall, increasing the thickness of the Meso-ZSM-5 coating from 1.1 to 1.9 g demonstrated no additional mass transfer limitations, high CO conversion, a slight change to gas species selectivity, and improved gasoline selectivity. For the 1.9 g-Meso-ZSM-5 co-catalysts, although the selectivity to isomers was high, the

selectivity to CH_4, CO_2 and C_2-C_4 gas hydrocarbons is also high, deteriorated the selectivity to C_{5+}. Thus, the highest gasoline yield was obtained from the 1.6 g-Meso-ZSM-5 co-catalysts.

The selectivity to liquid products as a function of the thickness of the Meso-ZSM-5 coating is shown in Figure 4-8. Increasing the Meso-ZSM-5 coating resulted in improved isomer selectivity, with selectivity shifting to lower carbon number hydrocarbons. For the 1.6 g-Meso-ZSM-5 and the 1.9 g-Meso-ZSM-5 co-catalysts, selectivity peaked at C_7, whereas the 1.1 g-Meso-ZSM-5 co-catalysts peaked at C_8. The selectivity to C_5 and C_6 increased for the 1.6 g-Meso-ZSM-5 and the 1.9 g-Meso-ZSM-5 co-catalysts. It is noteworthy that the tail of the hydrocarbons profile as a function of carbon number decreased from carbon number 19 to 15. Isomers selectivity boosted especially from 1.1 g-Meso-ZSM-5 to 1.6 g-Meso-ZSM-5 thickness. The trends in selectivity as a function of carbon number verified the aforementioned assumption of increased hydrocracking and isomerization, with the increase of Meso-ZSM-5 layer thickness.

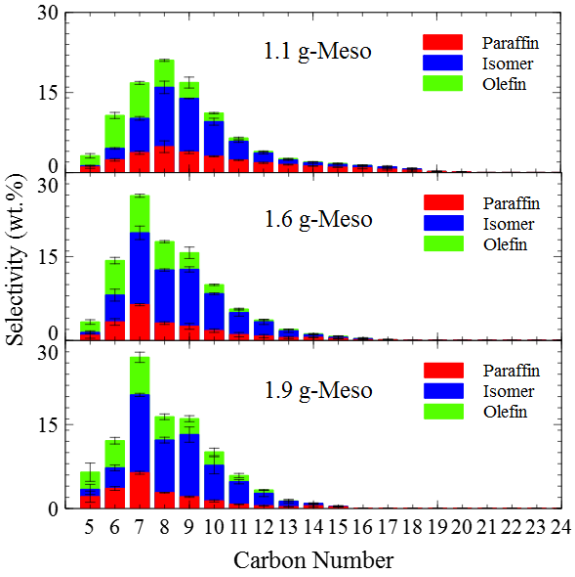

Figure 4-8. Carbon number distribution in the liquid products from different Meso-ZSM-5 loadings

4.3.5 Pressure Effect on 1.6 g-Meso-ZSM-5 Co-catalysts Performance

The 1.6 g-Meso-ZSM-5 catalyst was selected for further study in experiments of increasing pressure. Pressure is a crucial factor in the product distribution of FTS as long linear paraffins tend to form at higher pressures. Based on the good mass transfer, hydrocracking and isomerization characteristics of the 1.6 g-Meso-ZSM-5 co-catalysts, we explored the selectivity and quality of gasoline as a function of pressure in experiments at 6, 12, and 20 bar. The pressure effect on the 1.6 g-Meso-ZSM-5 co-catalysts performance is shown in Figure 4-9. CO conversion increased monotonically with the increase of pressure, in agreement with well-known FTS experience [157,191,192]. Increase in the reaction pressure should lead to liquefaction of gas products, saturation of catalysts pores and decreased mass transfer through the liquefied products layer, resulting to decrease in CO [157]. However, with the majority of liquid products in the C_5-C_{12} carbon range, diffusion limitations through the liquid layer are relaxed. The vapor liquid equilibrium of the measured FTS products was modeled in ASPEN PLUS, using a flash drum model. The flash unit was set to 230 °C and pressure of 6, 12, 20 bar respectively. The status of the FTS products was modeled by using ASPEN PLUS heater model. Conditions and products distribution from experimental work were used as input. The phase of each component as predicted by Aspen Plus is indicated with V for vapor and L for liquid. As shown in Table 4-3, the majority of products are expected to occur in the gas phase at the conditions of the experimental setup used in this work (Liquid products cannot be excluded from the pores of ZSM-5 since the inner pore conditions were not considered in ASPEN PLUS modeling). Increase in pressure results in longer residence times and consequently increased CO conversion.

Table 4-3. Phase status in FTS reactor at different pressures

Phase	6 bar	12 bar	20 bar
V	1	1	1
L	0	0	0
Species	**Mole fraction**		
CO	0.225373	0.085614	0.028614
H_2	0.395395	0.093262	0.041322
H_2O	0.311164	0.673514	0.851043
CH_4	0.038336	0.082416	0.046287
C_2H_6	0.002406	0.006259	0.003533
C_3H_8	0.002587	0.006172	0.002107
C_4H_{10}	0.006078	0.009795	0.003138
C_5H_{12}	0.0015	0.002802	0.002331
C_6H_{14}	0.003023	0.006629	0.003336
C_7H_{16}	0.005637	0.012932	0.007336
C_8H_{18}	0.003156	0.007173	0.003771
C_9H_{20}	0.002633	0.005851	0.003203
$C_{10}H_{22}$	0.001306	0.003535	0.001965
$C_{11}H_{24}$	0.00068	0.001807	0.00126
$C_{12}H_{26}$	0.000368	0.001158	0.000507
$C_{13}H_{28}$	0.000154	0.000501	0.000159
$C_{14}H_{30}$	0.000138	0.000307	8.68E-05
$C_{15}H_{32}$	4.3E-05	0.000173	0
$C_{16}H_{34}$	2.27E-05	7.22E-05	0
$C_{17}H_{36}$	0	2.7E-05	0

The CH_4 and C_2-C_4 selectivity showed a maximum with the increase of pressure. The high selectivity to CH_4 and C_2-C_4 at 6 bar was due to low pressure which favors short chain hydrocarbons formation [30]. At 20 bar, the high selectivity to CH_4 and C_2-C_4 was mainly caused by over-hydrocracking of heavy hydrocarbons at the higher reaction times of the high pressure experiments. At 12 bar, the 1.6 g-Meso-ZSM-5 coated co-catalyst achieved the highest selectivity to C_{5+}.

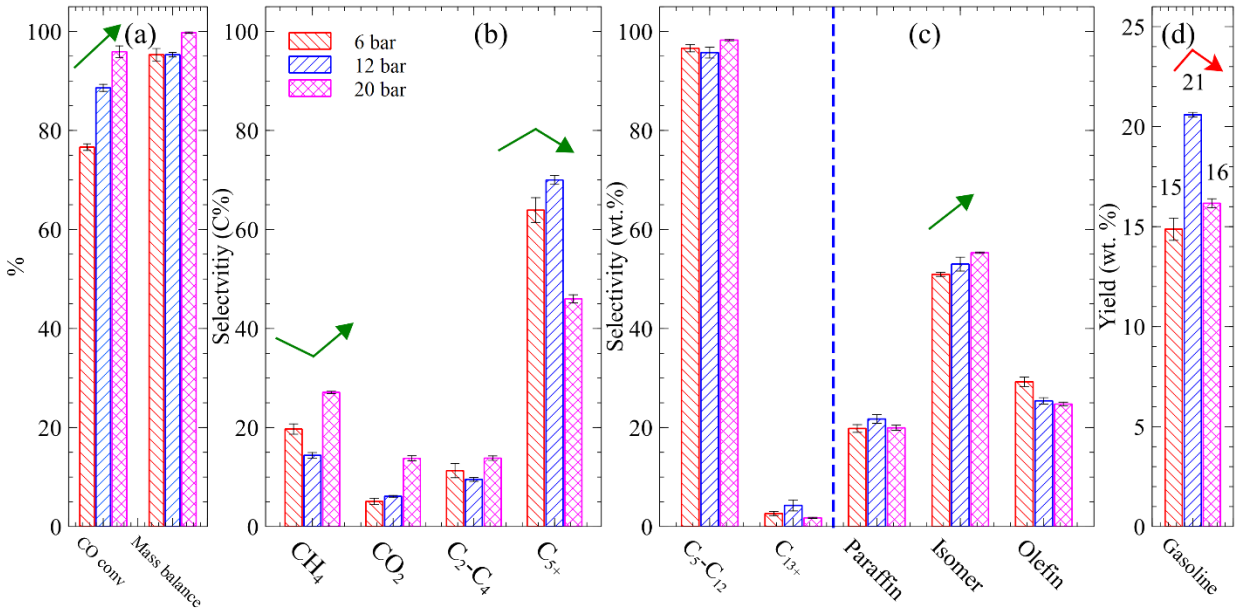

Figure 4-9. Co-catalysts performance of 1.6 g-Meso-ZSM-5 at different pressures. Reaction conditions: T: 230 °C; Syngas flowrate: 35 ml/min; Time on stream: 48 h

As shown in the Figure 4-9, the selectivity to CO_2 increased with the increase of pressure. One possible explanation for this is that the higher pressure favors olefin reabsorption and H_2 consumption, which shifts the water gas shift reaction to the right side, thus increasing CO_2 selectivity [77,193]. Another possible reason for the increased selectivity to CO_2 is the elevated CO conversion which could cause local hot spots in the catalyst, favoring the water gas shift reaction kinetics [157].

The selectivity to C_{5+} decreased with the increase in pressure from 12 to 20 bar. FTS kinetics dictate that heavy hydrocarbons are favorable at high pressure [153]. Clearly, there is an interplay between FTS and hydrocracking on the ZSM-5 pores. The high CH_4, C_2-C_4 and isomer selectivity at 20 bar could be an evidence of excessive ZSM-5 hydro-cracking. Overall, pressure had a complex effect on gasoline yield. Tests at 6 bar showed favorable short chain formation, while tests at 20 bar were dominated by hydro-cracking and water gas shift products. The 1.6 g-Meso-

ZSM-5 catalyst had the best gasoline yield at 12 bar, with high CO conversion, but also the highest yield to isomer products.

The selectivity to paraffins, isomers and olefins for the 1.6 g-Meso-ZSM-5 co-catalysts as a function of carbon number at different pressures is shown in Figure 4-10. With the increase of pressure, there were no significant composition changes that deviate from the conclusions about the pressure effect on gas selectivity. At 20 bar, the C_{15} and C_{16} components disappeared which could be the evidence of ZSM-5 catalyzed cracking.

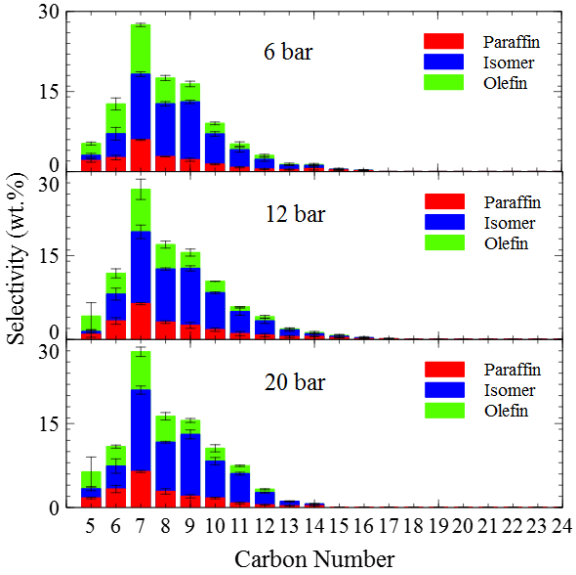

Figure 4-10. Carbon number distribution of the liquid products from the 1.6 g-Meso-ZSM-5 co-catalysts at different pressures

4.4 Catalyst Deactivation

A superior catalyst should possess high activity, selectivity and stability. The monolith catalysts synthesized in this work exhibit high CO conversion (up to 89%) at a relative low temperature (230 °C), with high gasoline selectivity (up to 72%). However, a catalyst stability issue was observed. The CO conversion would gradually decrease with time on stream as shown

in Figure 4-11. To better understand the cause of catalyst deactivation, the spent Meso-ZSM-5 coated co-catalysts were characterized with TPO, FTIR and BET.

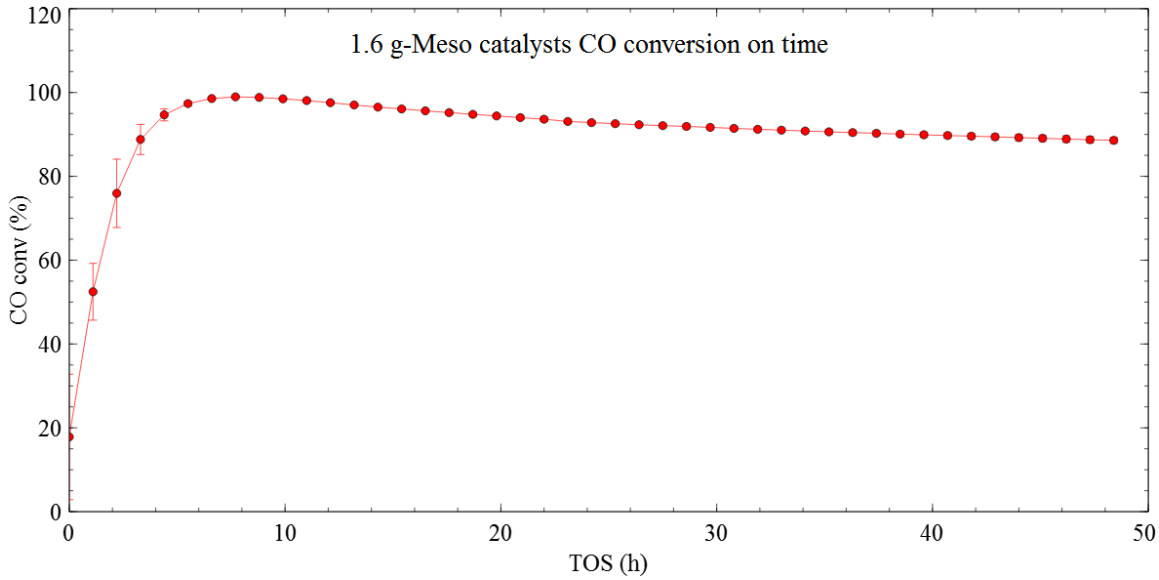

Figure 4-11. 1.6 g-Meso-ZSM-5 CO conversion profile. Reaction condition: T: 230 °C; Pressure: 12 bar; Syngas flowrate: 35 ml/min; Time on stream: 48 h

4.4.1 TPO Characterization

TPO of the spent co-catalysts with different Meso-ZSM-5 loadings was carried out. The TPO for the used 1.6 g-Meso-ZSM-5 co-catalysts is presented as an example in Figure 4-12. Three distinct peaks of the derivative of weight loss were observed due to oxidation at different temperatures. The used co-catalysts showed no weight change when temperature exceeded 600 °C, indicating no further carbon oxidation. The weight loss and corresponding temperature were calculated for each co-catalyst and are shown is Figure 4-13. The first weight loss peaked at around 100 °C and is attributed to water evaporation. The second peak was observed at around 330 °C which is the typical boiling temperature of diesel-range hydrocarbons. The weight loss of each sample at 330 °C was higher than 5 wt.% and the extent of weight loss was consistent with the C_{13+} products selectivity of Figure 4-7. This indicates that diesel-range products were trapped in

the catalysts as residues. The third peak was observed at around 460 °C, and can be attributed to the evaporation and oxidation of the hydrocarbons with carbon number around C_{32}.

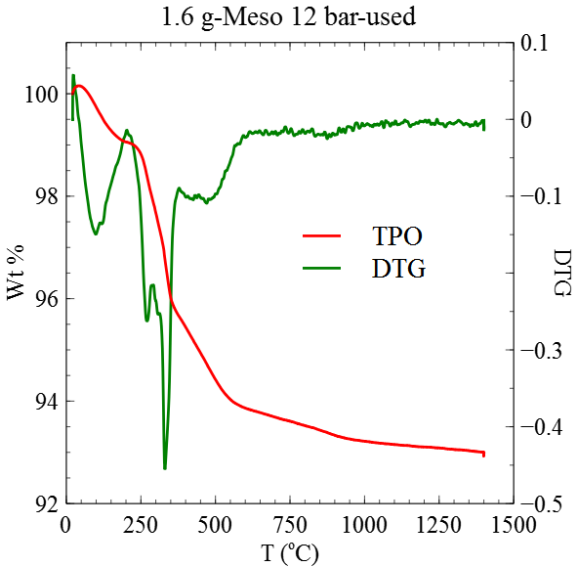

Figure 4-12. TPO and DTG for 1.6 g-Meso-ZSM-5 used co-catalysts

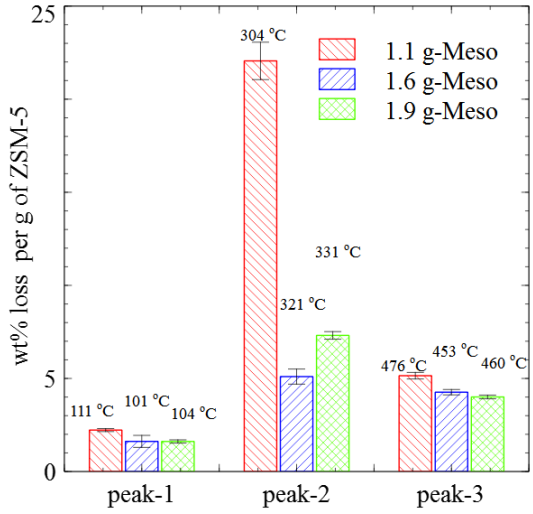

Figure 4-13. TPO weight loss and corresponding TPO peak temperature for used co-catalysts with different Meso-ZSM-5 loading

From the TPO results, it was concluded that there was no solid carbon formed on the catalysts. Hydrocarbons with carbon number around C_{13} were the main residue and products with carbon

number around C_{32} were minor components. This was also confirmed in catalyst regeneration tests presented later in this manuscript.

4.4.2 FTIR Characterization

Figure 4-14 (a) shows the FTIR spectrum of the 1.1 g-Meso-ZSM-5 co-catalyst before and after FTS and Figure 4-14(b) shows the temperature programed FTIR spectrum for the used 1.1 g-Meso-ZSM-5 co-catalyst. Saturated diesel-range hydrocarbons typically have IR peaks in the 2840-3000 cm^{-1} and 1300-1459 cm^{-1} ranges. It can be seen in Figure 4-14(a) that there are no hydrocarbons on the fresh 1.1 g-Meso-ZSM-5 co-catalyst. After FTS, the 1.1 g-Meso-ZSM-5 co-catalyst showed peaks in the range of 2840-3000 cm^{-1}. The FTIR spectra for the rest of the spent co-catalysts (1.6 g and 1.9 g Meso-ZSM-5) were identical with the only difference being the peak area at 2840-3000 cm^{-1}. None of the FTIR spectrum gave peaks related to C=C bonds belonging to poly aromatics or aromatics and peaks commonly attributed to coke [152,194].

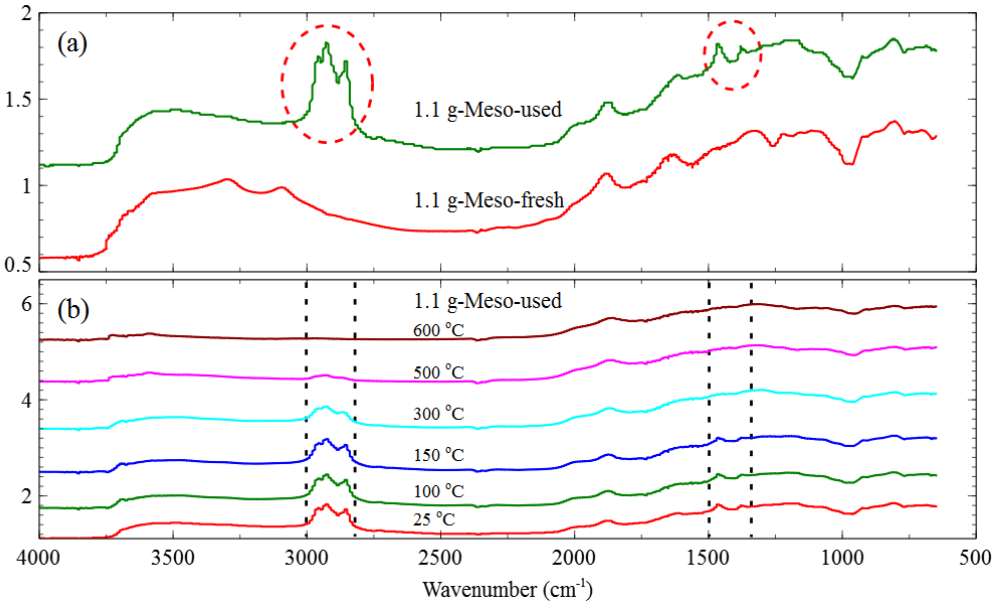

Figure 4-14. (a) FTIR spectra for the 1.1 g-Meso-ZSM-5 co-catalysts before and after FTS reaction. (b) Temperature programed FTIR spectra for the used 1.1 g-Meso-ZSM-5 co-catalyst.

Temperature programmed FTIR was also conducted for the spent 1.1 g-Meso-ZSM-5 co-catalyst. As shown in Figure 4-14 (b), there was no peak area change in the 2840-3000 cm^{-1} range up to 150 °C. From 150 °C to 300 °C, the peak area for diesel-range hydrocarbons decreased. This is consistent with the TPO results discussed earlier. The peaks at 2840-3000 cm^{-1} and 1300-1459 cm^{-1} range basically disappeared when the temperature reached 600 °C.

TPO and FTIR results indicated that co-catalyst deactivation occurs mainly due to saturated diesel-range hydrocarbons. No poly aromatics, aromatics and coke formation was observed. These tests were used to determine a good temperature range for co-catalyst regeneration. The catalysts regeneration temperature was set to 400 °C to evaporate or burn trapped hydrocarbons without affecting the catalysts Co active sites.

4.4.3 BET Characterization

Pore size distribution for the fresh 1.1 g-Meso-ZSM-5 co-catalyst and used co-catalysts with different Meso-ZSM-5 loadings is shown in Figure 4-15. Only the fresh 1.1 g-Meso-ZSM-5 co-catalyst possessed micropores below 2 nm. After FTS reaction, the used co-catalysts with different ZSM-5 thicknesses all showed no pores in the micro range, while the pores in the meso range also decreased compared to the fresh 1.1 g-Meso-ZSM-5 catalyst. The BET data are reported in Table 4-4. The BET surface area for the used co-catalysts with increased ZSM-5 thickness decreased significantly. In summary, FTS caused the complete blocking of micropores and decrease of pore volume in mesopores, which are the main reasons for FTS performance deterioration.

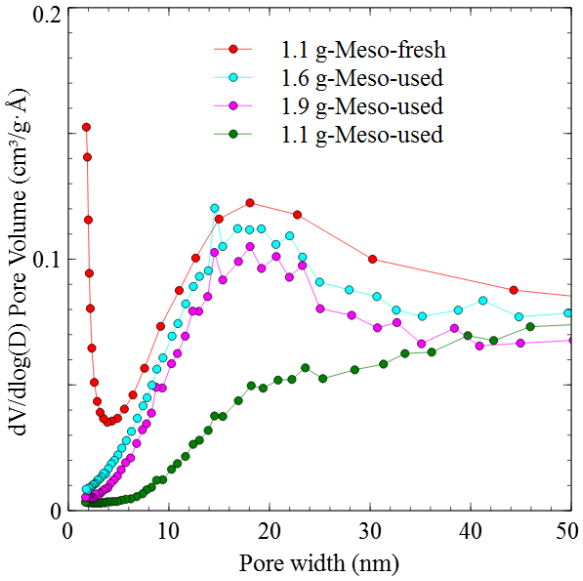

Figure 4-15. Pore size distribution of fresh 1.1 g-Meso-ZSM-5 co-catalyst and used co-catalysts with different Meso-ZSM-5 loadings.

Table 4-4. Data summary for fresh 1.1 g-Meso-ZSM-5 catalyst and used co-catalysts with different Meso-ZSM-5 loadings

Material	**S_{BET} ($m^2\ g^{-1}$)[a]**	**V_{micro} ($cm^3\ g^{-1}$)[b]**	**V_{meso} ($cm^3\ g^{-1}$)[c]**	**$D_{average}$ (nm)[d]**
1.1 g-Meso-fresh	128	0.02	0.16	8.73
1.1 g-Meso-used	10	0.00	0.08	28.22
1.6 g-Meso-used	27	0.00	0.13	17.87
1.9 g-Meso-used	20	0.00	0.11	20.12

[a] Surface area obtained from Brunauer-Emmett-Teller (BET) measurements (S_{BET}). [b] t-plot micropore volume (V_{micro}). [c] BJH desorption mesopore volume (V_{total}). [d] BJH adsorption average pore diameter ($D_{average}$).

4.4.4 Catalysts in-situ regeneration

The co-catalysts were regenerated with oxygen *in-situ* as discussed in the experimental section. The 1.6 g-Meso-ZSM-5 co-catalyst was chosen for an extensive regeneration test. Presented in Figure 4-16, the gap between two runs represents one brief regeneration step. As shown in Figure 4-16, the 1.6 g-Meso-ZSM-5 co-catalyst showed excellent regeneration for up to 250 hrs. The co-catalyst lost activity during each FTS run, but after each *in-situ* regeneration, it

returned to 100% CO conversion at beginning of each run. After nearly 250 hrs on stream, the co-catalysts CO conversion still remained high and replicable of the first run.

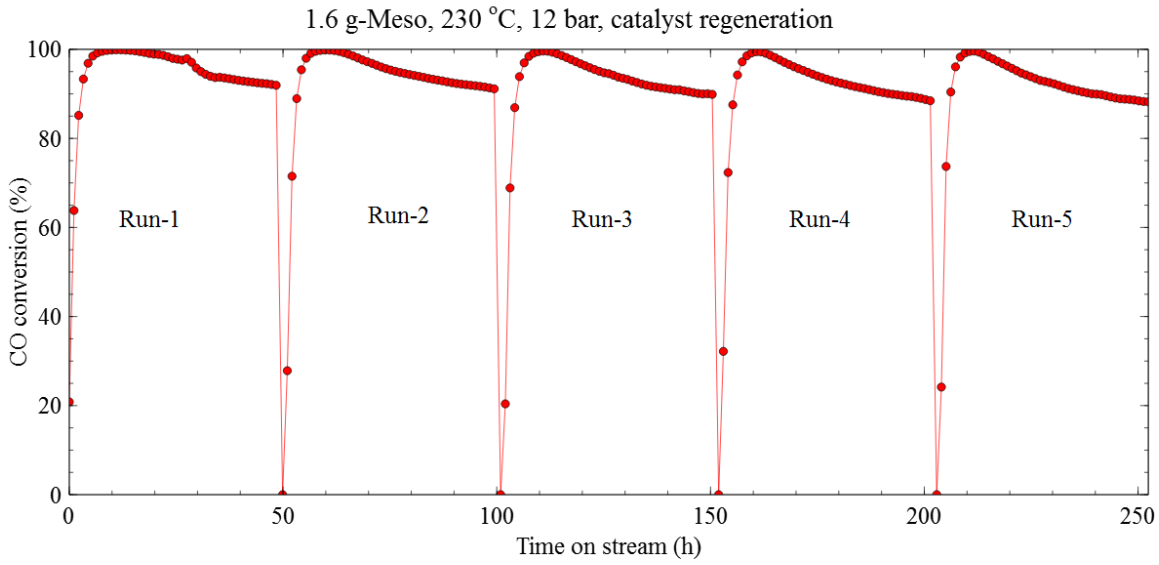

Figure 4-16. Regeneration of the 1.6 g-Meso-ZSM-5 co-catalyst; FTS performance for 250 h on stream.

4.5 Conclusions

A highly active (89% CO conversion), selective (72% gasoline selectivity) and stable (250 h on stream) monolith catalyst coated with hierarchical ZSM-5 was formulated and tested. Compared to the Micro-ZSM-5 coated co-catalysts with the same ZSM-5 loading, the Meso-ZSM-5 coated co-catalysts presented higher CO conversion. This was attributed to the improved mass transfer of CO and FTS products through the mesoporous ZSM-5 layer. Increasing the Meso-ZSM-5 loading from 1.1 to 1.9 g showed a peak in gasoline yield. Gasoline yield first increased due to the improved hydrocracking and isomerization of long linear paraffines in the ZSM-5, and then decreased possibly due to overcracking of the gasoline-range hydrocarbons. FTS at 6 bar was favorable for short-chain hydrocarbons, while at 20 bar hydrocracking and water gas shift reaction products were dominant. The Meso-ZSM-5 co-catalysts peaked gasoline production at 12 bar, at high CO conversion. The stability of the Meso-ZSM-5 co-catalysts was studied. Loss of FTS performance over time was attributed to ZSM-5 pore blocking by saturated long paraffins. *In-situ* regeneration recovered the activity of the co-catalysts to that of the fresh catalyst exhibiting excellent catalyst stability for 250 hrs of testing. The results presented here are an improvement over those in [168] at the expense of higher pressure (enabled by the introduction of mesoporosity to the ZSM-5 layer). Techno-economic analysis is underway to explore the best design for such processes for small-scale FTS.

Chapter 5

TECHONO-ECONOMIC ANALYSIS OF A MODULAR GAS-TO-LIQUID PROCESS TO MONETIZE STRANDED NATURAL GAS

5.1 Introduction

Natural gas (NG) plays an important role in global energy production, accounting for one third of the energy flow [195]. It is also considered the cleanest fossil fuel, with only CO_2 and H_2O as combustion products. NG can be used in many ways, liquefied or pipelined and be used to produce electricity or value added chemicals [196–198]. As an alternative fuel source, NG can be a promising solution to mitigate crude oil crisis and the related environment issues. Although a NG production boom has emerged due to innovating technologies in hydraulic fracturing, horizontal drilling and oil recovery [199], substantial NG is still far from full utilization due to different obstacles, such as remote locations, scarce capacity for commercial gas to liquid (GTL) plant. Those NG reserves are named as "Stranded natural gas (SNG)" [15,200].

SNG is plentiful around the world. It is essentially a wasted resource, by flaring or oil recovery, causing extra anthropogenic CO_2 and capital investment. Technologies to monetize SNG would be highly beneficial. Basically, there are two types of technologies, pipeline, liquefied NG and gas to liquid (GTL) process [197,201,202]. Pipeline and liquefied NG are ways of physical transportation of NG. While GTL process is a route of producing liquid fuels, chemical feedstocks and other products from NG. Usually, three steps are included in GTL: NG is firstly transformed into synthesis gas (syngas, CO and H_2); syngas serves as a feedstock for producing liquid fuels and chemicals and then a upgrading step follows for desired products [15]. The pipeline and liquefied NG technology focuses on the direct usage of NG, while the GTL transforms NG into valued added fuels or chemicals. Pipeline or liquefied NG is not a good option, since most of the stranded NG

wells are in remote areas. Construction of the infrastructures and transportation could be costly, especially for the SNG wells with more than 300 km distance away from the market [203]. GTL process is receiving increased attention in industry and academia, not only because of the NG boom, causing NG price drop, but also its flexibility to produce variety of high value products [204–206]. Besides, clean NG usage with zero or negative carbon emission could be realized with carbon capture and NG dry reforming technology [207–209], which makes GTL more competitive under recent strict regulations. To be profitable, conventional GTL plants have to rely on economy of scale. Currently operating GTL plants are all gigantic. The Shell Middle Distillate (SMDS) plant built in Bintulu, Malaysia in 1993, applying Fischer-Tropsch Synthesis (FTS) technology, has a capacity of 12,500 bpd liquid fuels production; the Methanex GTL plant with 16,000 bpd methanol production capacity [13]; the Escravos GTL plant in Nigeria built by Sasol in Qatar with a capacity of 32,400 bpd FTS liquid; The famous Pearl Plant constructed by Shell and Qatar Petroleum in 2011, equipped with 24 parallel FTS reactors, can reach as high product capacity as 140,000 bpd liquid fuels [197].

In U.S., no big GTL plant is built so far, mainly due to low individual NG well reserve capacity. Shown by EIA report [12], most of the NG wells concentrate on 3000 bpd oil equivalent range, among which most remaining stranded or isolated in remote areas. As an energy-starved and energy imports dependent country [210], monetization of these NG reserves is crucial for mitigating energy crisis, and boosting economy. However, the volumes of the SNG are typically too small to make a large-scale GTL plant profitable. An outstanding advantage of SNG is its low price which can be as low as 0.50 U.S. $/million BTU [211]. This incentivizes companies to exploit new technologies and portfolios to make GTL profitable. Modular GTL plant can be a promising candidate. It is a blocked and containerized units comprised of all the conventional GTL parts,

syngas production, FTS, and upgrading [92]. For a modularized GTL plant, 70 % of the construction is completed before implantation to the NG well site. Shipped by a truck, on-site construction cost can be significantly reduced. Due to the small scale, modular GTL plants have low financial risks, are flexible and can respond rapidly to changes according to market variations [212]. There are mainly two types of technologies used to convert syngas into liquid products in GTL process: NG to oxygenate and NG to liquid hydrocarbons. FTS is used extensively for GTL liquid hydrocarbon fuel production. Compared to oxygenate synthesis, FTS products are highly flexible. FTS can be lumped as low temperature and high temperature FTS. High temperature FTS uses iron as catalyst, suitable for short hydrocarbons formation, while low temperature FTS has cobalt as active phase, favoring long saturated wax production. GTL process with FTS can not only produce gasoline, diesel like transportation fuels, but also high quality waxes, lubes and oils for the use in food, cosmetic and pharmaceutical industry. With respect to fluctuation of market demand, GTL plant with FTS can definitely show more advantages on products variety.

In this work, a modular GTL plant with FTS technology will be formulated and modeled using ASPEN PLUS, aiming for offering a solution to monetize US stranded natural gas. A monolithic bifunctional catalyst formulated in our previous work [168] exhibited high CO conversion with superior gasoline selectivity. Thus, considering the high demand and increasing gasoline price in U.S.. Data from the experimental work will be incorporated to testify its potential for realizing the modular GTL, while a conventional FTS catalyst with products following ASF distribution is used as a benchmark. Technologies that can make GTL modular are considered. Optimization is carried out for better energy usage and liquid fuel production. Economics analysis is performed to invest the profitability. Sensitivity analysis on the plant profitability is carried out by varying feedstock price, plant scale and liquid fuel price.

5.2 Simulations

5.2.1 Process description

Aiming to monetize stranded NG in US, this work takes North Dakoda which has a typical US oil well environment, such as remote areas, lacking of large reserves and power grid, as a modular GTL plant location for modeling. Since the stranded natural gas is from flared and wasted resources, the price for natural gas is set to be zero, unless specified otherwise. Three main blocks for the modular GTL plant were developed in this work as shown in Figure 5-1: synthesis gas generation block, FTS block and upgrading block. The detailed block descriptions will be discussed in the following parts. At the end of the process, two types of products will be generated, gasoline range products (C_5-C_{11}) and diesel range products (C_{12+}).

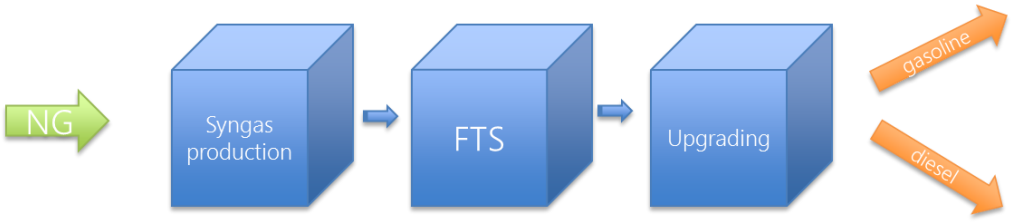

Figure 5-1. Block diagram for the modular GTL plant

5.2.2 Simulation basis

For the calculations here, it is assumed that a desulfurized natural gas is available at 1 bar (gauge) and 25 °C. The natural gas contains 93.9% methane, 3.2% ethane, 0.7% propane, 0.4% n-butane, 1% CO_2 and N_2 as balance which are all in molar basis. This composition has been used extensively in the work of Thomas A. Adams [213,214] and NETL [215]. Simulations were performed using ASPEN PLUS V11. The ASPEN PLUS ECONOMIC ANALYZER (APEA) was used for equipment cost estimation. Peng-Robinson with the Boston-Mathias equation of state was applied for the whole process. A detailed flowchart of the modular GTL plant can be viewed in Figure 5-

2. Three main blocks of the modular GTL plant shown in Figure 5-1 are separated by dashed lines in Figure 5-2. Natural gas is first mixed with steam generated by using the heat recovered from the natural gas burning exhaust. Then the mixed feedstock will be preheated to 500 °C by using the hot products stream from reformer before entering the prereformer. Syngas will be generated inside reformer by steam methane reforming. Syngas generated from steam reforming has a high H_2/CO ratio, while the best H_2/CO ratio for Co-based FTS is about 2. In order to decrease the ratio, a reverse water-gas-shift reactor (RWGSR) is used. Water will be separated before entering the RWGSR, favoring CO formation and decrease energy input at the same time. CO_2 is mixed with the dehydrated syngas and preheated by the hot product stream from RWGSR. Syngas with a H_2/CO ratio of 2 will be generated and dehydrated before entering the FTS reactor. The FTS products then will be separated into three streams, gas products, oil products and water. Gas products will be burned inside the different reactors to provide energy. For the modular GTL plant, structured heat exchanger type reactors will be used for prereformer, reformer, RWGSR and FTS reactor. This type of reactors have reactions going in the tube or shell side and combustion or cooling on the other side to provide or extract heat. To successfully model this type of the reactors, a pseudo furnace was proposed representing the combustion of natural gas and FTS gas products as heating material for the heat exchanger type reactors. Oil products from FTS reactor then will be separated into gasoline and diesel range products using a distillation column which can be transported to oil refinery for further process.

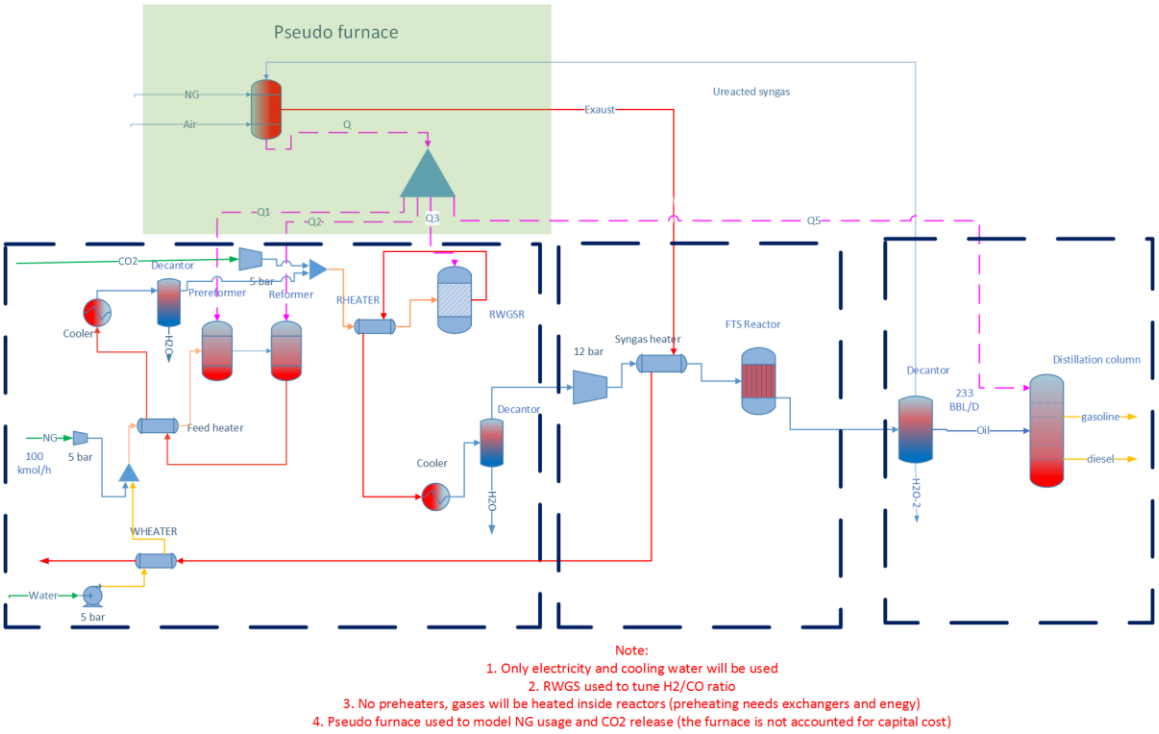

Figure 5-2. Flowchart of the modular GTL plant

5.2.3 Reforming block

Two reactors for NG reforming are employed, a pre-reformer and a main reformer. Pre-reformer is used for the full conversion of C_2-C_4 heavy gas hydrocarbons, avoiding carbon depositions on the following methane reformer nickel type catalysts at high temperature. The pre-reformer in is modeled with a RGibbs reactor model, using the phase and chemical equilibrium calculation option. Temperature is set as 550 °C and pressure as 5 bar, with near full conversion of C_2-C_4, which is a typically used condition [208,216,217]. A nickel based catalyst will be used in pre-reformer. Sensitivity analyses on temperature and pressure are performed to further justify the condition.

There are several technologies can be used for methane reforming to produce synthesis gas: (1) steam methane reforming (SMR) (2) partial oxidation (POX) (3) autothermal reforming (ATR) and (4) dry methane reforming (DMR) [216]. Each of the technology has its own advantages

for synthesis gas production depending on the applications. SMR uses steam and NG as feedstock, no ASU needed, however SMR produces H_2/CO with a ratio of 3 which is suitable for H_2 and methanol production [218]. For FTS usage, the SMR H_2/CO has to be further processed to reach a ratio of 2. POX uses methane and pure oxygen as feedstock. Syngas with a H_2/CO ratio ranging from 1 to 1.6 can be achieved. With a catalyst, POX reaction temperature can be substantially lowered to 1000 K [219]. ATR is considered as the most economic process due to its combined heater and reactor model, yielding high energy and production efficiency. It is a combination of SMR and POX. However, using pure O_2 as a feedstock, an air separation unit (ASU) has to be built which will make GTL plant gigantic and capital consuming. ATR reformer is typically used for large commercial GTL plants. DMR uses CO_2 and CH_4 as feedstock. It can produce syngas with a H_2/CO ratio of 1. DMR has gained increasing attentions due to its mitigation and utilization of greenhouse gases (CO_2 and CH_4), especially under the circumstance of tighter environment regulations on CO_2 emission. DMR opens a route to generate value added fuels and chemicals while contributing to the reduction of CO_2 emissions [220]. SMR and DMR bi-reforming has been extensively studied by researchers. Jonas Baltrusaitis et al. [221] conducted a modeling work to explore the economic feasibility of using DMR to produce syngas compared with SMR and ATR and the lowest annual cost featured a system with both SMR and DMR. Similar work was also conducted by Helen H. Lou et al. [222]. They concluded that SMR + DMR process has a lower carbon footprint compared with SMR alone, while further research needed to be done on DMR catalysts in order to make the process economically competitive. From experiment perspective, George A. Olah and co-workers [223] conducted experiments for methane bi-reforming with a catalyst composed of nickel oxide on magnesium oxide (NiO/MgO) in a tubular flow reactor at elevated pressures (5-30 atm) and temperatures (800-950 °C). They concluded that H_2/CO ratio in the

products can be easily achieved to the desired value of 2 for hydrocarbons synthesis by adjusting the CO_2-to-steam ratio. SMR and DMR can be used in two ways, combined in one reactor [208,216,224] or operated parallel in separated reactors. In this work, a reactor with both SMR and DMR were tested. Nickel type catalysts were used for CH_4 reforming, since steam and CO_2 reforming have similar kinetics on this type of catalysts [223,225]. The use of DMR has several advantages for a modular GTL plant:

(1) Reduced NG usage and CO_2 emissions

(2) Turning CO_2 into valuable chemicals or fuels, lowering CO_2 tax

(3) No need for CO_2 separation column, reduced plant size

The reformer is usually modeled using a REquil reactor, considering the kinetics of the reactions will not be the limiting step at high temperatures. Use of the REquil model will be relative rigorous. The following reactions are used:

$$SMR: \quad CH_4 + H_2O \rightarrow CO + 3H_2 \qquad \Delta H^O_{298K} = 206\ kJ/mol$$

$$DMR: \quad CH_4 + CO_2 \rightarrow 2CO + 2H_2 \qquad \Delta H^O_{298K} = 247\ kJ/mol$$

$$WGS: \quad CO + H_2O \rightarrow CO_2 + H_2 \qquad \Delta H^O_{298K} = -41\ kJ/mol$$

Boudouard reaction can also happen, however, the carbon formation is low at the temperature range in this work [226]. For the work, only the aforementioned three reactions are used. However, the use of DMR with SMR showed one big disadvantage which has not been considered in the reference work [224,227]. DMR is a highly endothermic reaction, while WGS reaction is mildly exothermic. High temperature favors DMR and WGS reaction kinetics at the same time. Although WGS reaction has a low equilibrium constant of 1 at 850 °C, CO_2 residue in the product stream will remain very high caused by the high water content (aforementioned as soot prevention strategy). High CO_2 content can have a negative effect for FTS performance. When CO_2 is smaller

than 5 mol% in the stream, the negative effect is negligible [228–230]. Thus a very complicated and expensive CO_2 separation unit is needed. This will add more complexity and capital cost for the modular GTL plant. To solve this problem, a RWGS reactor with only one reaction was used.

$$RWGS: \qquad CO_2 + H_2 \rightarrow CO + H_2O \qquad \Delta H^O_{298K} = 41\ kJ/mol$$

The type of modular SMR/combustion unit, with alternatively stacked channels derived from plate and fin heat exchanger manufacturing techniques which has been realized by companies as CompactGTL and Velocys [203] will be used for prerefomer, reformer, RWGS and FTS reactors. Reformer temperature of 800 °C was chosen based on a sensitivity analysis displayed in Figure 5-3. As shown, when reformer temperature reaches above 800 °C, there is no big change of CH_4 conversion, H_2 and CO flowrate. H_2/CO ratio also reaches a plateau. Temperature of 800 °C is chosen for minimum energy input and equipment requirement while maintain high CH_4 conversion. This set point matches well with standard experimental temperature, providing high CH_4 conversion while low carbon deposition [231,232]. Increasing pressure will hinder CH_4 conversion due to the volume expansion reactions. Besides, increasing in pressure will dramatically increase temperature requirement for 90% conversion of C_2-C_4 [213]. Many experimental works use atmospheric pressure for steam reforming, however, a pressurized system should be used in practical, considering pressure drops in the equipment. Here, according to sensitivity analysis and practical experience, 5 bar (gauge) is applied to the reformer. In the work, CH_4 conversion of 90% after passing the main reformer is maintained by varying mole flow of steam and reaction conditions. To achieve this goal, a design specification on CH_4 conversion is formulated. The result shows an excess steam usage. It is reasonable since excess steam is beneficial for steam reforming and for preventing carbon formation, while the steam in syngas can also be separated easily using a flash unit.

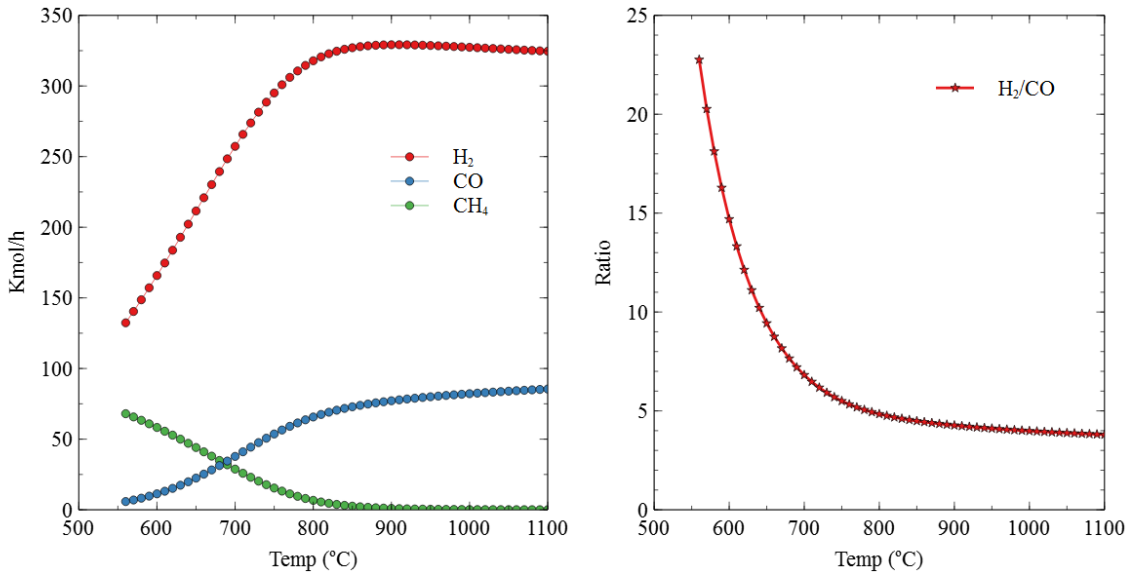

Figure 5-3. Reformer temperature sensitivity analysis. Left: H_2, CO and CH_4 flowrate; Right: H_2/CO ratio

In the RWGS reactor, H_2/CO ratio is tuned by mixing the reformer products with CO_2 which is produced form the combustion of natural gas for heating of different reactors. A design specification by varying CO_2 flowrate and RWGS reactor temperature to achieve H_2/CO ratio of 2, while maintain less than 5 mol% of CO_2 in the product stream. The excess heat in product stream is recovered by preheating the feed stream of RWGS reactor.

5.2.4 FTS block

Cobalt based catalysts will be used in the process, for its high selectivity on liquid hydrocarbons and low water-gas-shift reaction activity. There are different reactor designs for FTS: fixed bed reactors, slurry bed reactors, fluidized bed reactors and Early FTS designs were based on multi-tubular fixed bed reactors (SASOL ARGE) [41], dipped in boiling water for heat removal. However, fixed-beds imposed limits on the minimum applicable catalyst particle size, leading to a compromise between diffusion lengths and acceptable pressure drop. In slurry bed column reactors (SASOL), the bubbling flow ensures good mixing and isothermality. Diffusion

limitations are relaxed by using small catalyst pellets. However, the separation of the waxy product from the catalyst particles is a major limitation. In fluidized-bed reactors (SASOL) [41], small particle size relaxes mass transfer limitations, but the liquid FTS products cause catalyst particle agglomeration and disturb fluidization. Therefore, operating temperatures above the hydrocarbons dew point must be chosen, resulting in chain length growth probability of ~0.7 and selectivity to lighter hydrocarbons. Circulating fluidized bed reactors (Sythol) suffer from attrition, temperature gradients and difficulties in separating waxes from solid catalysts.

As mentioned, the conventional commercial reactors have different types of design problems. Thus, a great amount of research and development effort has been devoted to the development of novel type of reactors. Monolithic structured reactors are a promising solution. Monolithic reactors are well know from gas-solid applications to solve environment related problems, especially the three-way catalytic converter used in the field of car exhaust cleaning, but the application of monolith reactors is rather new to gas-liquid-solid reactions [61]. In contrast to other industrial reactors, monolithic structured reactors can operate at low pressure-drop, high geometric surface-area, high mass-transfer coefficients, and short diffusion lengths. The thickness of cell wall can be adjusted to achieve effectiveness factors close to unity [62–64]. Because of the honeycomb structure with active phase attached on the cell wall, wax separation and catalyst attrition are not of significant concern. Structured catalysts are typically operated adiabatically, resulting in low radial heat transfer and temperatures gradients, but Moulijn and coworkers [61,65,66] and Güttel et al. [67,68] suggested recycling the liquid product and removing reaction heat externally can be realized. Almeida et al. [69] explored FTS in aluminum foams, honeycombs and micro monoliths and measured C_{5+} selectivities of over 50%. They underlined the importance of the catalytic layer thickness of the FTS phase. Visconti et al. [64] showed that heat conduction in

aluminum structured catalysts can be exploited to effectively remove heat. Liu et al. [70,71] showed that C_5–C_{18} selectivity and olefinicity obtained by FTS in monolith catalysts are better than their packed-bed equivalents. They reported high one-pass conversions (~95%) at very low CH_4 selectivities (<10%), which was not possible using conventional fixed beds. In general, structured FTS reactors show superior activity and selectivity, but the importance of temperature profile flattening, through internal or external heat removal is emphasized.

In our previous work [168], a bifunctional structured catalyst consisting of monolith support, Co and ZSM-5 was formulated and tested under normal FTS conditions, aiming at in-situ cracking and isomerization of long hydrocarbons to achieve high gasoline selectivity with premium quality. Temperature and pressure were tuned to achieve the best working conditions for gasoline production. Results showed that the structured bifunctional catalysts had the highest FTS selectivity to gasoline range products (C_5-C_{12}) at 230 °C and 12 bar. The gasoline selectivity and isomers' content significantly increased compared to conventional Co supported on Al_2O_3 catalysts [233,234]. Gasoline selectivity was found to be as high as 93.3 wt.% within the 75.5 % C5+ oil product (mole basis) and CO conversion was as high as 78.7 %. Thus, the FTS reactions performance at 12 bar and 230 °C will be used to model the monolith reactor. Reactions producing C_1 to C_{19} saturated paraffins were added and water gas shift reaction was also considered. The factional conversion for each species is shown in

Table 5-1. The FTS reactor was modeled using a RStoic reactor. Temperature was set as 230 °C and pressure at 12 bar. No pressure drop was assumed and the reactor was cooled by using cooling water extracted from underground or nearby water resources.

Table 5-1. Fractional conversion of all the carbon species used in FTS block

Species	Factional conversion
CH_4	0.085
CO_2	0.012
C_2H_6	0.018
C_3H_8	0.024
C_4H_{10}	0.052
C_5H_{12}	0.020
C_6H_{14}	0.065
C_7H_{16}	0.097
C_8H_{18}	0.122
C_9H_{20}	0.106
$C_{10}H_{22}$	0.074
$C_{11}H_{24}$	0.042
$C_{12}H_{26}$	0.023
$C_{13}H_{28}$	0.015
$C_{14}H_{30}$	0.010
$C_{15}H_{32}$	0.007
$C_{16}H_{34}$	0.004
$C_{17}H_{36}$	0.002
$C_{18}H_{38}$	0.001
$C_{19}H_{40}$	0.000

5.2.5 Upgrading block

A distillation column was modeled using Radfrac model. A rough estimation on the reflux ratio and tray number to achieve 98% C_{11} and 2% C_{12} recovery in distillate was carried out using the DSTWU model. Then, the detailed column diameter, height, reflux ratio and feeding conditions were tuned and optimized in the rigorous Radfrac model.

5.3 Total Capital Investment and Product Cost Estimation

After successful converge of the process, most of the equipment, such as pumps, gas compressors, heat exchangers, decanters and distillation column, were mapped and sized within ASPEN PLUS built in economics analyzer and the equipment costs were calculated using APEN Process Economic Analyzer (APEA). For the equipment cannot be mapped and sized, relative data was acquired from reference papers [224,235,236]. The cost of those equipment was calculated via the six-tenths factor rule (Formula is shown in Eq. 5.1) [237], then the price was updated to the year of 2020, using the price development factor from the annual chemical engineering plant cost index (Shown as Eq. 5.2) [238,239].

$$\frac{Cost_2}{Cost_1} = \left(\frac{Capacity_2}{Capacity_1}\right)^f \tag{5.1}$$

$$\text{Current cost} = \text{Base cost} \times \left(\frac{I}{I_{base}}\right) \tag{5.2}$$

Table 5-2. Six-tenths factors used for bare module equipment cost estimation

Equipment	f	References
FTSR	0.72	[235]
Prereformer	0.6	[227]
Reformer	0.6	[227]
RWGSR	0.65	[235]

Table 5-3. Chemical Engineering Plant Cost Index (CEPCI) changing with year [240,241]

Year	CEPCI
2005	468.2
2006	499.6
2007	525.4
2008	575.4
2009	521.9
2010	550.8

2011	585.7
2012	584.6
2013	567.3
2014	576.1
2015	556.8
2016	541.7
2019	607.5

In Eq. 5.1, $Cost_1$ and $Capacity_1$ are the base equipment cost and capacity, *f* is the exponential factor and the value for different equipment is shown in Table 5-2. For Eq. 5.2, *I* is the Chemical Engineering Plant Cost Index (CEPCI) which is used to update the equipment cost to the nearest year of the plant construction. The CEPCI is shown in Table 5-3.

The sizing effect for the entire plant total bare module cost was estimated using the six-tenths rule with 0.6 of *f*. A preliminary estimate of the total capital investment (TCI) was carried out and the accuracy is about ±30% [237]. A profitability analysis template from Warren D. Seider et al. [237] was used. Before the economics analysis, economic assumptions and base case market prices are summarized in Table 5-4.

Table 5-4. Economic assumptions and base case market prices

		Ref
Assumptions		
Plant lifetime (yrs)	20	[227]
Operation per year (days)	350	[227]
Production capacity	90%	[237]
Start production capacity	50%	[237]
Depreciation schedule	5 year	[237]
Icome tax rate	40%	[227]
Base case market price		
Water	\$1.2E-4 /lb	[237]
Natural gas	\$0	
Gasoline	\$3.25/gallon	[242]
Diesel	\$3.056/gallon	
Cooling water	\$1.2E-5 /lb	[237]
Electricity	\$0.07/kWh	[237]

During the TCI calculation, the cost of the equipment and the cost of its installation were estimated first, then this was added a contingency, cost of the land, royalties, working capital, and the cost for starting up the plant. A total derived bare module factor of 3.21 was used [237]. The total production cost (TPC) was calculated by including operations, maintenance, operating overhead, property taxes and insurance. A 5 year MACRS depreciation was also included to account for the time value of the capital investment. For cash flows calculation, the cumulative net present value (NPV) was shown at a 15% discount rate.

5.4 Preliminary Results and Discussion

Aforementioned, there are typically three blocks for GTL plant, syngas generation block, FTS block and products upgrading block. The investment percentage for the three blocks in the modular GTL is shown in Figure 5-4. Syngas generation account for 46% of the total capital investment due to the three reactors and compressors used. While, the FTS process costs half of the capital investment, mainly due to the high price of FTS reactor. As can be seen in Figure 5-2, there are only three components in the FTS block. Due to the lack of microchannel FTS reactor's price information in open literature, a six-of-tenth factor rule was applied to the reactor from work of C. Zhang et al. [224]. It can be viewed that the products upgrading only accounts for 5% of the total capital investment, due to the use of bifunctional catalysts which has high gasoline selectivity and quality, showing reducing upgrading equipment advantages of modular GTL plant.

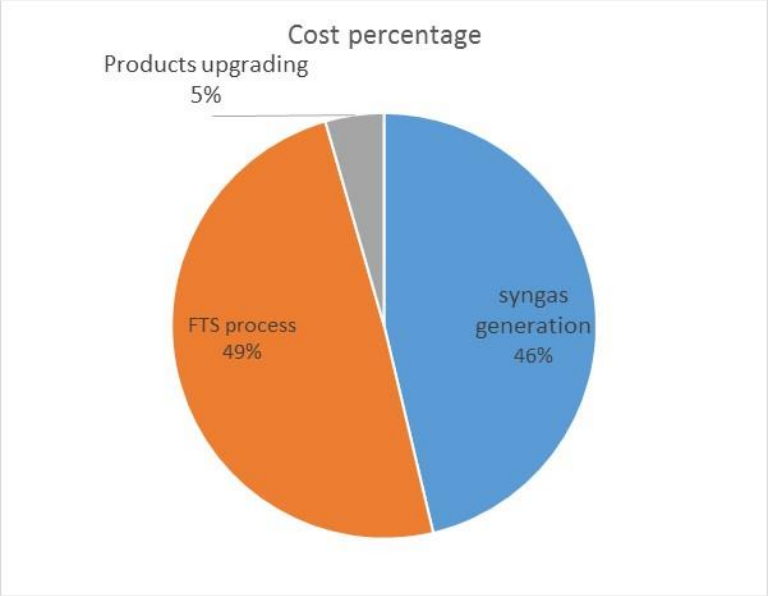

Figure 5-4. Different blocks cost percentage for modular GTL plant

Total product cost percentage for each component of the modular GTL plant is summarized in Figure 5-5. It can be seen that operation and maintenance cost is the main contributor for the total product cost, followed by general expense, utilities, property taxes and insurance and lastly the raw material. The low percentage of raw material is due to none to zero cost of the stranded nature gas. In the work, an economics analysis template [237] for conventional GTL plant was applied which is the reason of high operation and maintenance cost. For modular GTL plant, the operation and maintenance cost can be significantly reduced due to the modularized reactors and equipment. The cost can be reduced by 40% [243]. The result with modified operation and maintenance cost percentage is not shown here, because more accurate data is needed. A more accurate estimation of the operation and maintenance cost will be performed in the future work. Conventional GTL plants are usually large and complicated compared to modular ones which need much more workers and working capital to keep the plant in well working condition. But, Figure 5-5 shows an idea of the contribution of each component for the synthetic oil production cost.

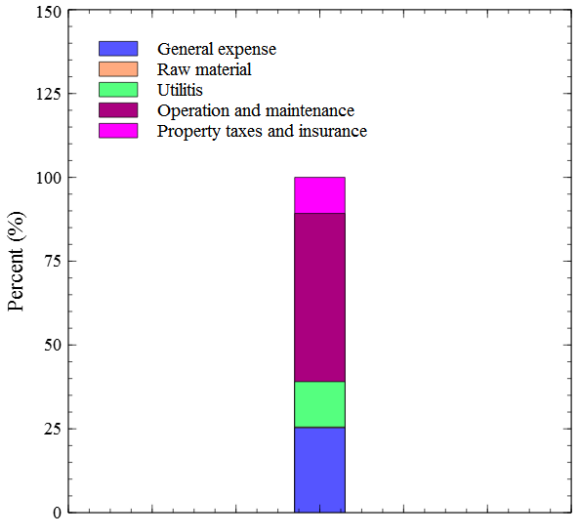

Figure 5-5. Total product cost of the modular plant at 5600 BPD scale

The total capital investment and synthetic oil price change with plant scale is summarized in Figure 5-6. The total capital investment increased from 380 million dollars (MM$) to 800 MM$ when the synthetic oil production increased from 2,200 barrel per day (BPD) to 9,500 BPD. The trend increased less at the high oil production range due to the sixe-to-tenth factor which is the economy of scale. The economy of scale can also be viewed form the decreasing trend of synthetic oil price change with the plant scale. The price decreases from 150 thousand dollar per barrel (M$PB) to 85 M$PB.

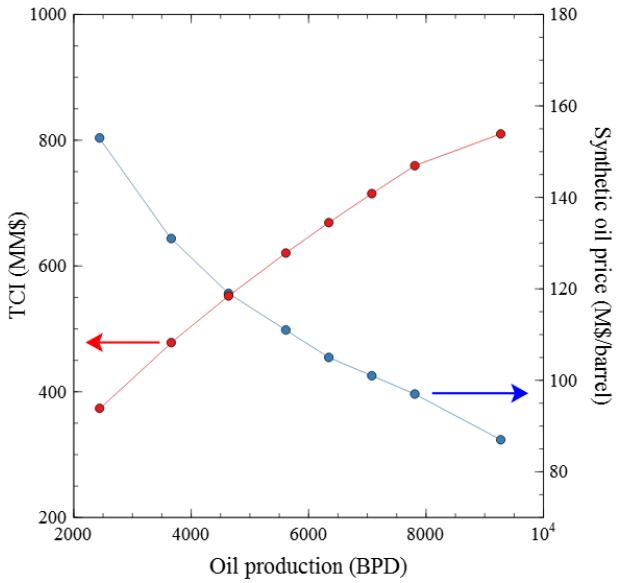

Figure 5-6. Total capital investment and synthetic oil price change with plant scale

Cumulative net present value (CNPV) and iternal rate of return (IRR) at the 20th year are calculated and shown in Figure 5-7. A discount rate of 15% was used for CNPV calculation. When CNPV reaches zeor, the GTL plant will have a break even point which means all of the cost is recovered. It can be seen that the GTL plant has a positive CNPV value when the plant scale is larger than 5,500 BPD. With the increasing of the plant scale, the CNPV show a faster increasing trend at higher plant scale. While IRR basically shows a linear relationship with the increase of the plant scale. From Figure 5-7, we know that, in order to make the GTL plant profitable, the

plant scale has to be larger than 5,500 BPD. The larger the plant is, the higher the IRR will be which means the capitcal cost of the plant can be recovered earllier.

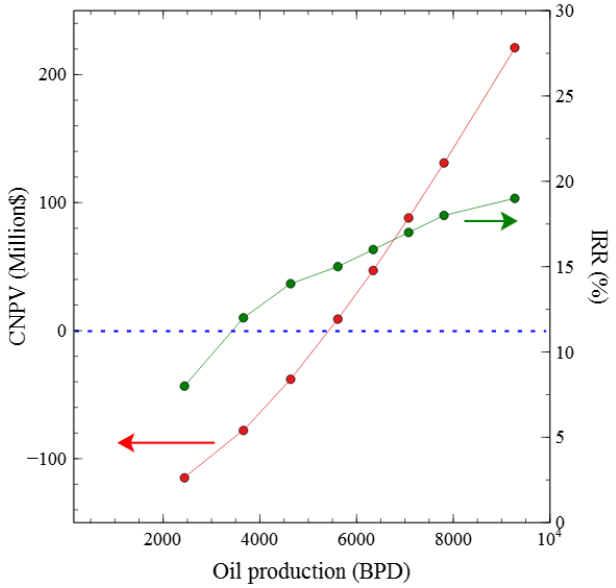

Figure 5-7. Cumulative net present value and internal rate of return change with plant scale

Sensitivity analysis was carried out to show the effect of each cost component on IRR at 5,600 BPD production scale. The result is shown in Figure 5-8. The cost of material and utility cost, operating cost and total permanent cost was increased or decreased by 50% increment up to 150% or down to -150%. It can be seen that the material and utility cost basically shows no effect on the IRR which is reasonable, since the cost of natural gas is zero and there is not too much equipment that will consume much energy. While operating cost shows minor effect on the IRR. The permanent investment has the highest effect. This is because the high capital cost of the purchasing equipment. The IRR can have an about 50% change when the total permanent investment changes by 50%. From the result, we know that, in order to get a higher IRR, more effort needs to be made in decreasing the total permanent investment, either by cutting nonessential equipment or improving process efficiency by intensification.

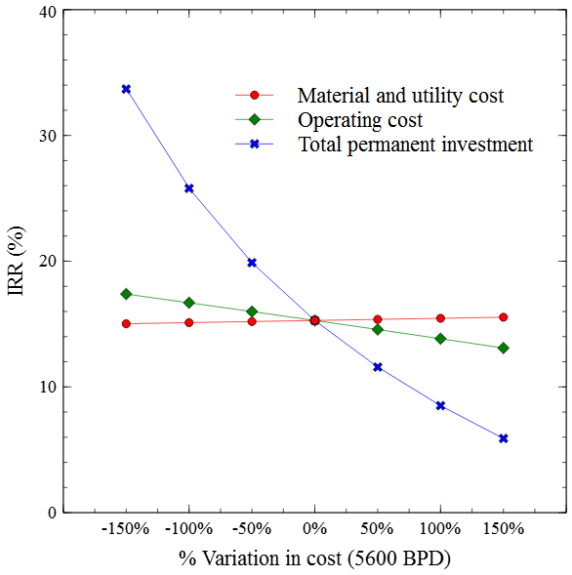

Figure 5-8. Sensitivity analysis on the Internal Rate of Return (IRR) at varied costs

5.5 Conclusions

A preliminary techno-economic analysis for modular GTL plant was carried out in this work. The main advantage for modular GTL plant is that the feedstock has close to zero cost. Other advantages are intensified reactors and reduced equipment which can decrease total capital investment significantly. From the economics analysis, the modular GTL plant can achieve a zero CNPV at 5,500 BPD scale. Any scale larger than that will make the plant profitable. Sensitivity analysis shows that the total permanent investment has the highest effect on IRR. More improvement should be made in decreasing the total permanent investment. However, this scale is still quite large for stranded natural gas well to support in the long run. In this work, operating and some equipment cost are still using conventional GTL template which is not suitable in applying to modular GTL plant. Modular GTL plant has intensified equipment and high flexibility which requires less operating and equipment cost compared to conventional GTL plants. More work will be done in the future focusing on modifying the reduction of operating and equipment cost for modular GTL plant.

Chapter 6

CONCLUSIONS AND FUTURE PERSPECTIVE

6.1 Conclusions

Based on the hypothesis of combining high heat mad mass transfers of monolith support, high long chain hydrocarbons selectivity of Co-based FTS catalysts and the cracking and isomerization of zeolite, a novel structured bifunctional catalyst for in-situ FTS products upgrading to gasoline-range hydrocarbons was synthesized. This catalyst was tested and optimized in a homemade fixed bed reactor. Monolith-supported Co catalysts coated with ZSM-5 showed high FTS selectivity to gasoline range products (C_5-C_{12}) at 230 °C and 12 bar. Gasoline selectivity was found to be as high as 93.3 wt.% within the 75.5 % C_{5+} oil product and CO conversion was as high as 78.7 %. The addition of ZSM-5 on the monolith catalyst not only improved the gasoline selectivity but also gasoline quality, in terms of olefin and isomer composition. Investigation of the temperature effect on catalyst performance showed that the liquid product selectivity shifted to hydrocarbons of lower carbon numbers with the increase of temperature. CO_2 selectivity increased sharply with temperature, because of the enhancement of the water gas shift reaction. More isomers and olefins were produced over the ZSM-5-coated monoliths at high temperatures, but at the expense of the liquid product yield. Increasing reaction pressure led to higher selectivity to heavy hydrocarbons. Low pressure favored the production of isomers and olefins. High pressure was shown to introduce diffusion limitations to the ZSM-5 layer of the FTS catalysts synthesized. A moderate pressure of 12 bar was proposed to favor gasoline production. However, the parent ZSM-5 used has only micro pores with diameter smaller 2 nm. This imposed some extent of mass

transfer barriers shown as a decrease of CO conversion for the bifunctional catalysts. Thus, modification was carried out to increase the mass transfers of the parent ZSM-5.

Mesopores were introduced to the parent ZSM-5 with desilication method. TEM and pyridine adsorption showed that mesopores were successfully made and the acidities of the ZSM-5 did not vary significantly. With the new hierarchical ZSM-5 used as the out layer, a highly active (89% CO conversion), selective (72% gasoline selectivity) and stable (250 h on stream) monolith catalyst coated with hierarchical ZSM-5 was formulated and tested. Compared to the Micro-ZSM-5 coated co-catalysts with the same ZSM-5 loading, the Meso-ZSM-5 coated co-catalysts presented higher CO conversion. This was attributed to the improved mass transfer of CO and FTS products through the mesoporous ZSM-5 layer. Increasing the Meso-ZSM-5 loading from 1.1 to 1.9 g showed a peak in gasoline yield. Gasoline yield first increased due to the improved hydrocracking and isomerization of long linear paraffines in the ZSM-5, and then decreased possibly due to overcracking of the gasoline-range hydrocarbons. FTS at 6 bar was favorable for short-chain hydrocarbons, while at 20 bar hydrocracking and water gas shift reaction products were dominant. The Meso-ZSM-5 co-catalysts peaked gasoline production at 12 bar, at high CO conversion. The stability of the Meso-ZSM-5 co-catalysts was studied. Loss of FTS performance over time was attributed to ZSM-5 pore blocking by saturated long paraffins. *In-situ* regeneration recovered the activity of the co-catalysts to that of the fresh catalyst exhibiting excellent catalyst stability for 250 hrs of testing. The results presented here are an improvement over those in [168] at the expense of higher pressure (enabled by the introduction of mesoporosity to the ZSM-5 layer).

Stranded natural gas has gained increasing attention due to the advance of new technologies and its cheap to zero price characteristics. However, stranded natural gas wells are usually too small to support a commercial GTL plant. Thus, modular small-scale GTL plants are proposed

with intensified process and reduced cost which can make up the loss of size economics of large scale GTL plants. The key for small-scale FTS is the use of intensified reactors to minimum equipment size and reduce capital investment while maintaining high performance. Monolith structured bifunctional catalysts can offer both. High CO conversion and gasoline selectivity can be achieved in one step, resulting no requirement of refining equipment and large scale FTS reactor. With the formulation of monolith structured bifunctional catalysts, techno-economic analysis is performed to explore the best design for such processes for small-scale FTS.

The bifunctional catalysts prepared in the dissertation showed elevated CO conversion and gasoline selectivity, however, flaws were also observed. Facile dip-coating method was used for the bifunctional catalysts preparation. Although a binder was applied to increase the adhesion between each layer, week attachment of the layers were still in presence. No obvious material loss was observed for the bifunctional catalysts during reaction due to the fixed bed regime with minor vibration. But, the layered structure can be easily disturbed while taking the catalysts out of the fixed bed. Besides the adhesion problem, catalysts deactivation is also a big concern. Although a regeneration step was carried out in the dissertation showing that the bifunctional catalysts were completely regenerable, the frequency of regeneration was still too high to a commercial GTL plant. The full deactivation picture is not fully understood yet. Work could be done in the future in terms of improving the Co active sites stability or its self-generation.

6.2 Future Perspective

FTS catalysts have long been an interest in academia and industry research. A catalyst possessing superior activity and high selectivity to certain range products is ideal. There are many factors that can affect catalysts activity and selectivity, particularly catalyst structure parameters. Particle size is among the most significant of these factors.

Significant work has studied Co catalyst particle size effect on FTS performance, CO conversion, selectivity to C_{5+} and stability. Iglesia [154] showed that the surface-specific activity of FTS catalysts is practically constant for particle sizes in the range of 9-200 nm. Smaller Co particles were shown to decrease turn-over frequencies (TOF) and C_{15+} yields [244,245]. Prieto et el. [246] concluded that the higher relative concentration of interfacial sits in small (<10 nm) Co particles is responsible for this phenomenon. However, Breejen et el. [24,247] synthesized Co/SiO_2 catalysts with particle sizes of ~4.6 nm, that displayed high activities, attributed to the very narrow particle size distribution enabled by the mild calcination with NO (instead of air). Thus, it is vital to synthesize a catalyst with controlled particle size and narrow size distribution.

Effort has been done to synthesize well controlled catalyst with narrow size distribution. Lei Ding et el. [248] successfully synthesized a type of raspberry-like silica composite with tunable nickel nanoparticles with a facile one-pot approach. The synthesis procedure is shown in Figure 15. Basically, it is a modified Stober Method. Resorcinol-formaldehyde (RF) polymer was coated on the silica particles surface. Nickel nitrate was added at the same time. Due to the metal chelation effect of the hydroxyl group, Ni was enwrapped in the polymer. Then the material was treated at different temperatures with different ramping rates in N_2 flow. The polymer would decompose and form a carbon layer. Because of the polymer constraint effect, Ni particles were well controlled. The size deviation was within nm. Besides, the Ni particles were all embedded in the carbon layer which were super stable under normal reaction conditions. The catalytic performance was investigated for the reduction of 4-NP. Very stable result was achieved. They stated that the size and density of the nicked nanoparticles could be precisely controlled by adjusting the molar ratio of the nickel salt and RF concentration, or by changing the calcination temperature.

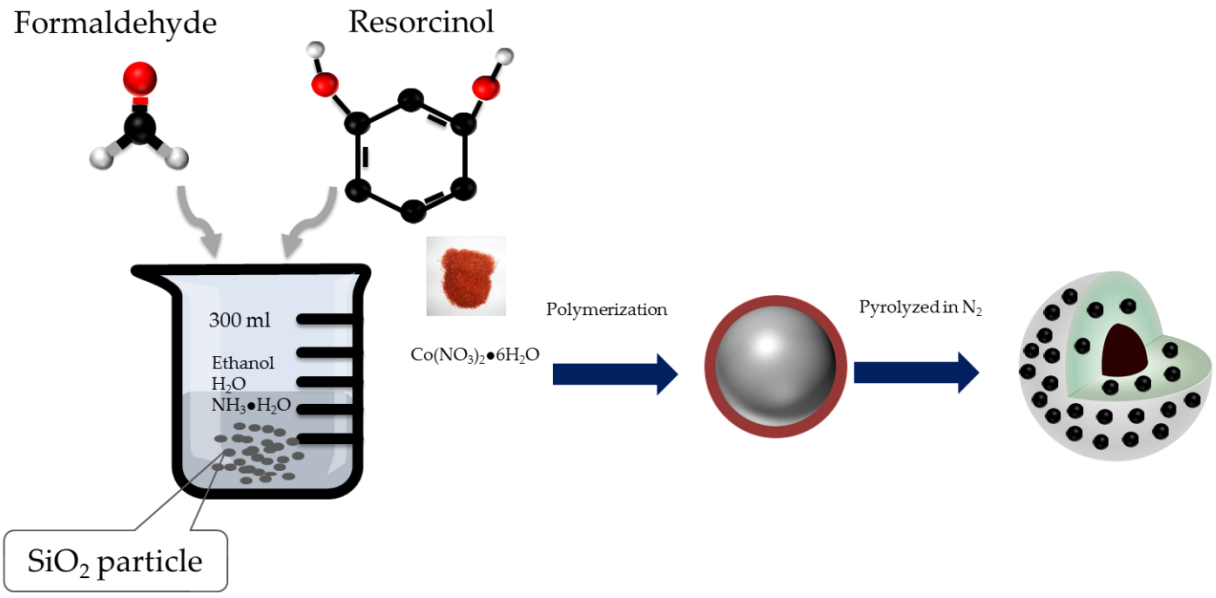

Figure 6-1. The synthesis procedure of raspberry-like silica composite

Other groups [249–252] have done similar research for the synthesis of Fe ,Co and other noble metal nano-particles, achieving stable and high catalysts performace. It can be promising that this process has the potential to formulate a highly stable catalyst with narrow size distribution for FTS. Especially for the use of commercial GTL plant, a shut down time for catalysts regeneration is costly and labor intensive. Thus, a highly stable catalyst with minimum amount of loading of Co with precise size control and narrow size distribution will be synthesized in the future work as shown in Figure 6-1. RF resin will be synthesized and coated on SiO_2 surface with cobalt nitrate added in dropwise. Concentration of the cobalt nitrate will be varied and tested to control the particle size of Co. The catalysts will be tested and evaluated in a fixed bed reactor. TEM, XRD, SEM, TPR and XPS will be used to characterize the particle size, active sites oxidation state, crystallite structure and surface appearance as the work we have done in the dissertation.

APPENDIX I: MISCELLANEOUS INFORMATION AND COPYRIGHT

Monolith structured bifunctional catalyst development, from left to right: Bare monolith, fresh monolith bifunctional catalyst coated with ZMS-5, spent catalysts coated with mirco and meso ZSM-5

FTS liquid products: Left: FTS products from the bifunctional catalysts; Right: FTS products from monolith catalysts without ZSM-5 coating

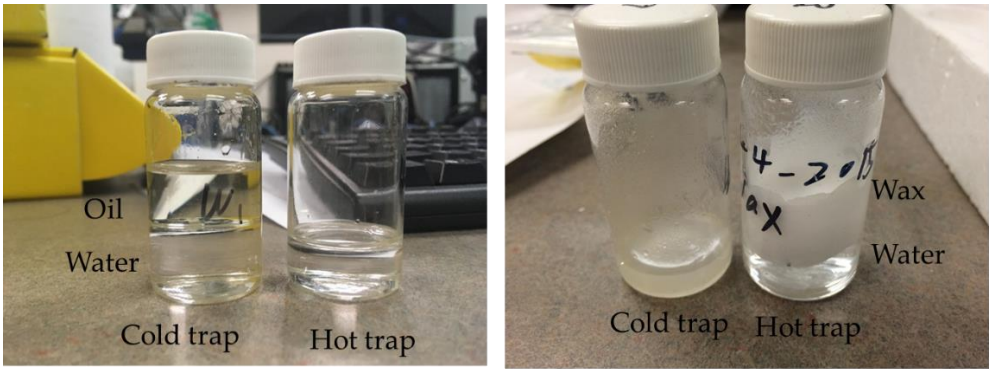

Typical oil products FID signal

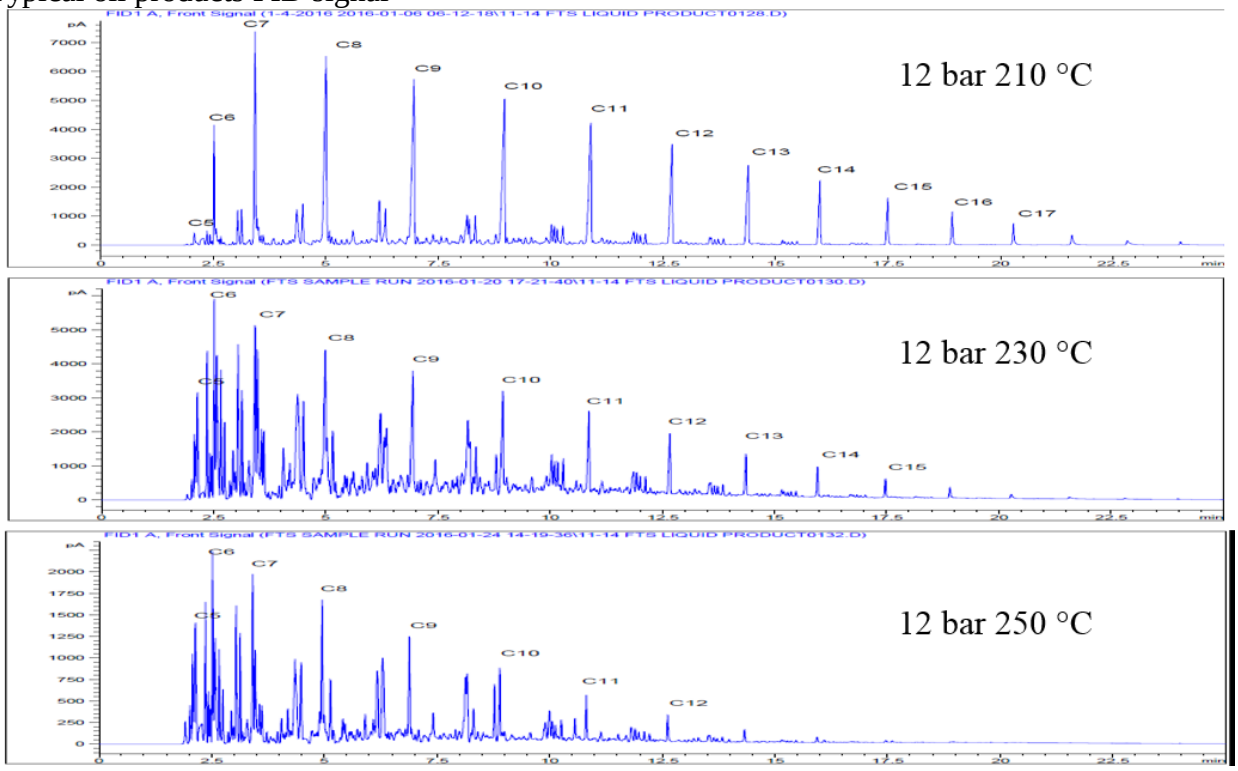

Reprint permission for Figures 3-1 to 3-11 and Tables 3-1 to 3-5

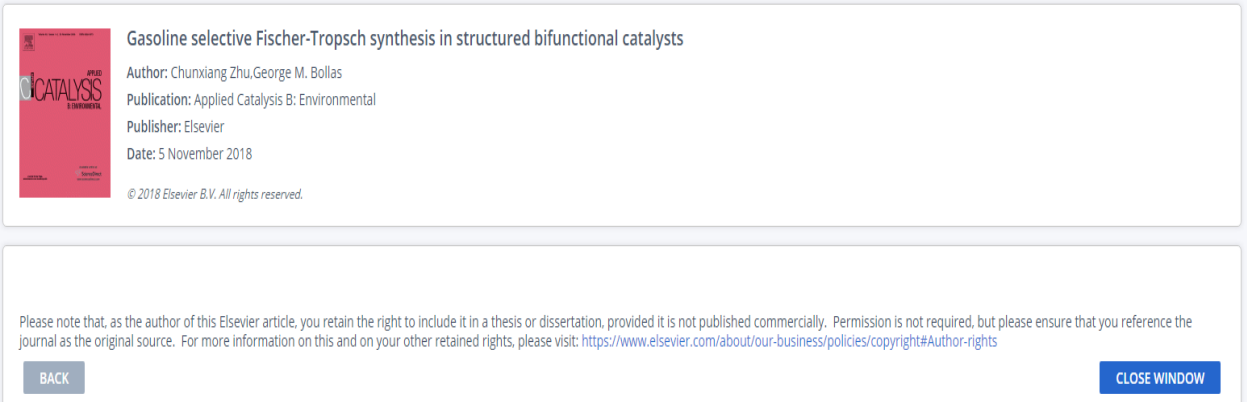

APPENDIX II: PUBLICATIONS AND PRESENTATIONS

Publications

- Zhu, C. & Bollas, G. M. Gasoline selective Fischer-Tropsch synthesis in structured bifunctional catalysts. *Appl. Catal. B Environ.* 235, 92–102 (2018).
- Zhu, C., Gamliel, D., Valla, J. A. & Bollas, G. M. Fischer-Tropsch synthesis in monolith catalysts coated with hierarchical ZSM-5. *Appl. Catal. B Environ.* (in publication)

Conference oral presentations

- Zhu, C., Gamliel, D., Valla, J. A. & Bollas, G. M. Fischer-Tropsch synthesis targeted to gasoline range hydrocarbons. *NECS spring meeting*, UCONN Storrs, 2017
- Bollas, G. M. & Zhu, C., Oxy-fuel co-combustion of coal and biomass in spouted bed reactor. *Clearwater Clean Coal conference*, Florida, Jun 2017
- Gamliel, D., Zhu, C., Valla, J. A. & Bollas, G. M. Monolithic catalysts coated with Hierarchical ZSM-5 for Fischer-Tropsch Synthesis, *AIChE*, 2017
- Zhu, C., Gamliel, D., Valla, J. A. & Bollas, G. M. Gasoline-selective Fischer-Tropsch synthesis with hierarchical ZSM-5 coated monolithic catalysts, *AIChE*, 2016
- Zhu, C. & Bollas, G. M. Fischer-Tropsch synthesis targeted to gasoline range hydrocarbons, *ACS*, Philadelphia, 2016

Posters

- Zhu, C., Gamliel, D., Valla, J. A. & Bollas, G. M. Highly active, selective and stable FTS bi-functional catalyst for gasoline production, *NESC winter meeting*, Worcester, Jan 2020
- Zhu, C. & Bollas, G. M. Fischer-Tropsch synthesis targeted to gasoline range hydrocarbons, *Annual UCONN SoE Poster Competition*, Storrs, CT (2017).

REFERNCES

1. Wikipedia. Petroleum. en.wikipedia.org/wiki/Petroleum (2020).
2. Steven Kettell. Oil crisis economics. www.britannica.com/topic/oil-crisis (2020).
3. Geiger, J. How much crude oil has the world really consumed? oilprice.com/Energy/Crude-Oil/How-Much-Crude-Oil-Has-The-World-Really-Consumed.html (2019).
4. OPEC. OPEC share of world crude oil reserves, 2018. www.opec.org/opec_web/en/data_graphs/330.htm (2018).
5. University of Calgary. Energy education. https://energyeducation.ca/encyclopedia/In_a_barrel_of_oil (2016).
6. EIA. Use of gasoline. https://www.eia.gov/energyexplained/gasoline/use-of-gasoline.php (2019).
7. Eia. Primary Energy Consumption by Source and Sector 2011. (2011).
8. natgas. NaturalGas.org. (2013).
9. Energy, U. E. Natural Gas: Dry vs.Wet. *US Energy Dep. Dev. Corp.* (2013).
10. IEA. *The role of gas in today's energy transitions*. www.iea.org/reports/the-role-of-gas-in-todays-energy-transitions (2019).
11. EIA. *Annual Energy Outlook 2020*. (2020).
12. EIA. *U.S. Crude Oil and Natural Gas Proved Reserves, Year-end 2018*. (2019).
13. Fleisch, T. H., Sills, R. A. & Briscoe, M. D. 2002 - Emergence of the Gas-to-Liquids Industry: A Review of Global GTL Developments. *J. Nat. Gas Chem.* **11**, 1–14 (2002).
14. Khalilpour, R. & Karimi, I. A. Evaluation of utilization alternatives for stranded natural gas. *Energy* **40**, 317–328 (2012).
15. Dong, L., Wei, S., Tan, S. & Zhang, H. GTL or LNG: Which is the best way to monetize 'stranded' natural gas? *Pet. Sci.* **5**, 388–394 (2008).
16. Perego, C., Bortolo, R. & Zennaro, R. Gas to liquids technologies for natural gas reserves valorization: The Eni experience. *Catal. Today* **142**, 9–16 (2009).
17. A Review of Challenges and Opportunities for Stranded Gas Monetisation in the Gulf of Guinea AkaChidike Kanu Sunlink Petroleum Limited, Lagos, Nigeria. 1–8.
18. Society of Petroleum Engineers. Stranded gas. https://petrowiki.org/Stranded_gas (2020).
19. De Klerk, A. Fischer–tropsch process. *Kirk-Othmer Encycl. Chem. Technol.* (2013) doi:10.1002/0471238961.fiscdekl.a01.
20. Dry, M. E. High quality diesel via the Fischer-Tropsch process - A review. *J. Chem. Technol. Biotechnol.* **77**, 43–50 (2002).
21. Van Der Laan, G. P. & BEENACKERS, A. A. C. M. Kinetics and Selectivity of the Fischer–Tropsch Synthesis: A Literature Review. *Catal. Rev. Sci. Eng.* **41**, 255–318 (1999).
22. Jing, Q. Syngas production from reforming of methane with CO_2 and O_2 over Ni/SiO_2 catalysts in a fluidized bed reactor. *Int. J. Hydrogen Energy* **29**, 1245–1251 (2004).
23. Zangouei, M., Razeghi, A., Moghaddam, A. Z. & Omidkhah, M. R. Production of Syngas by Combination of CO2 Reforming and Partial Oxidation of CH4 over Ni/Al2O3 Catalysts in Fixed-bed Reactor. *Int. J. Chem. React. Eng.* **8**, 1–14 (2010).
24. Den Breejen, J. P. *et al.* A Highly Active and Selective Manganese Oxide Promoted Cobalt-on-Silica Fischer–Tropsch Catalyst. *Top. Catal.* **54**, 768–777 (2011).
25. Ngamcharussrivichai, C., Liu, X., Li, X., Vitidsant, T. & Fujimoto, K. An active and selective production of gasoline-range hydrocarbons over bifunctional Co-based catalysts. *Fuel* **86**, 50–59 (2007).

26. Demirbas, A. Progress and recent trends in biofuels. *Prog. Energy Combust. Sci.* **33**, 1–18 (2007).
27. Dalai, A. K. & Davis, B. H. Fischer-Tropsch synthesis: A review of water effects on the performances of unsupported and supported Co catalysts. *Appl. Catal. A Gen.* **348**, 1–15 (2008).
28. Shimura, K., Miyazawa, T., Hanaoka, T. & Hirata, S. Preparation of Co/Al 2 O 3 catalyst for Fischer-Tropsch synthesis: Combination of impregnation method and homogeneous precipitation method. *Appl. Catal. A Gen.* **475**, 1–9 (2014).
29. Abbasi, A., Ghasemi, M. & Sadighi, S. Effect of lanthanum as a promoter on Fe-CO/SioO2 catalyst for fischer-tropsch synthesis. *Bull. Chem. React. Eng. Catal.* **9**, 23–27 (2014).
30. Sarkari, M., Fazlollahi, F., Razmjooie, A. & Mirzaei, A. A. Fisher-Tropsch Synthesis on Alumina Supported Iron-Nickel Catalysts: Effect of Preparation Methods. *Chem. Biochem. Eng. Q.* **25**, 289–297 (2011).
31. Zhang, Q., Kang, J. & Wang, Y. Development of Novel Catalysts for Fischer-Tropsch Synthesis: Tuning the Product Selectivity. *ChemCatChem* **2**, 1030–1058 (2010).
32. Jahangiri, H., Bennett, J., Mahjoubi, P., Wilson, K. & Gu, S. A review of advanced catalyst development for Fischer-Tropsch synthesis of hydrocarbons from biomass derived syn-gas. *Catal. Sci. Technol.* **4**, 2210–2229 (2014).
33. Van Berge, P. J., Van De Loosdrecht, J., Barradas, S. & Van Der Kraan, A. M. Oxidation of cobalt based Fischer-Tropsch catalysts as a deactivation mechanism. *Catal. Today* **58**, 321–334 (2000).
34. Tsakoumis, N. E., Rønning, M., Borg, Ø., Rytter, E. & Holmen, A. Deactivation of cobalt based Fischer–Tropsch catalysts: A review. *Catal. Today* **154**, 162–182 (2010).
35. Zhong, L. *et al.* Cobalt carbide nanoprisms for direct production of lower olefins from syngas. *Nature* **538**, 84–87 (2016).
36. Pedersen, E. Ø., Svenum, I. H. & Blekkan, E. A. Mn promoted Co catalysts for Fischer-Tropsch production of light olefins – An experimental and theoretical study. *J. Catal.* **361**, 23–32 (2018).
37. De Klerk, A. & Furimsky, E. *Catalysis in the Refining of Fischer-Tropsch Syncrude*. (RSC Catalysis Series, 2010).
38. Patzlaff, J., Liu, Y., Graffmann, C. & Gaube, J. Studies on product distributions of iron and cobalt catalyzed Fischer–Tropsch synthesis. *Appl. Catal. A Gen.* **186**, 109–119 (1999).
39. Laan, G. Van der & Beenackers, A. A. C. . Kinetics and Selectivity of the Fischer–Tropsch Synthesis: A Literature Review. *Catal. Rev.* **41**, 255–318 (1999).
40. Lappas, A. A., Dimitropoulos, V. S., Antonakou, E. V., Voutetakis, S. S. & Vasalos, I. A. Design, Construction, and Operation of a Transported Fluid Bed Process Development Unit for Biomass Fast Pyrolysis: Effect of Pyrolysis Temperature. *Ind. Eng. Chem. Res.* **47**, 742–747 (2008).
41. Davis, B. H. Fischer-Tropsch synthesis: Overview of reactor development and future potentialities. *Top. Catal.* **32**, 143–168 (2005).
42. van der Laan, G. P. *Kinetics, Selectivity and Scale Up of the Fischer-Tropsch Synthesis*. *University of Groningen* (1999).
43. Mousavi, S., Zamaniyan, A., Irani, M. & Rashidzadeh, M. Generalized kinetic model for iron and cobalt based Fischer-Tropsch synthesis catalysts: Review and model evaluation. *Appl. Catal. A Gen.* **506**, 57–66 (2015).
44. Qian, W., Zhang, H., Ying, W. & Fang, D. The comprehensive kinetics of Fischer-Tropsch

synthesis over a Co/AC catalyst on the basis of CO insertion mechanism. *Chem. Eng. J.* **228**, 526–534 (2013).
45. Asiaee, A. & Benjamin, K. M. A density functional theory based elementary reaction mechanism for early steps of Fischer-Tropsch synthesis over cobalt catalyst. 2. Microkinetic modeling of liquid-phase vs. gaseous-phase process. *Mol. Catal.* **436**, 210–217 (2017).
46. Zhuo, M., Tan, K. F., Borgna, A. & Saeys, M. Density functional theory study of the co insertion mechanism for Fischer-Tropsch synthesis over co catalysts. *J. Phys. Chem. C* **113**, 8357–8365 (2009).
47. Guedes-Sobrinho, D., Freire, R. L. H., Chaves, A. S. & Da Silva, J. L. F. Ab Initio Investigation of the Role of CO Adsorption on the Physical Properties of 55-Atom PtCo Nanoalloys. *J. Phys. Chem. C* **121**, 27721–27732 (2017).
48. Li, M. R., Chen, J. & Wang, G. C. Reaction Mechanism of Ethanol on Model Cobalt Catalysts: DFT Calculations. *J. Phys. Chem. C* **120**, 14198–14208 (2016).
49. Masters, C. *The Fischer-Tropsch Reaction*. (1979).
50. Blyholder, G. & Emmett, P. H. Fischer-Tropsch synthesis mechanism studies. The addition of radioactive ketene to the synthesis gas. *J. Phys. Chem.* **63**, 962–965 (1959).
51. Blyholder, G. & Emmett, P. H. Fischer-Teopsch synthesis mechanism studies. II. The addition of radioactive ketene to the synthesis gas. *J. Phys. Chem.* **64**, 470–472 (1960).
52. Tau, L. M., Dabbagh, H. A. & Davis, B. H. Fischer-Tropsch Synthesis: Comparison of 14C Distributions When Labeled Alcohol Is Added to the Synthesis Gas. *Energy and Fuels* **5**, 174–179 (1991).
53. Brady, R. C. & Pettit, R. On the Mechanism of the Fischer-Tropsch Reaction. The Chain Propagation Step. *J. Am. Chem. Soc.* **103**, 1287–1289 (1981).
54. Komaya, T. & Bell, A. T. Estimates of rate coefficients for elementary processes occurring during Fischer-Tropsch synthesis over Ru TiO2. *J. Catal.* **146**, 237–248 (1994).
55. Koerts, T., van Wolput, J. H. M. C., de Jong, A. M., Niemantsverdriet, J. W. & van Santen, R. A. Improved activity of a silica supported ruthenium catalyst by carbon monoxide pretreatment. *Appl. Catal. A Gen.* **115**, 315–326 (1994).
56. Wang, C. J. & Ekerdt, J. G. Evidence for alkyl intermediates during Fischer-Tropsch synthesis and their relation to hydrocarbon products. *J. Catal.* **86**, 239–244 (1984).
57. Davis, B. H. Fischer-Tropsch Synthesis: Reaction mechanisms for iron catalysts. *Catal. Today* **141**, 25–33 (2009).
58. Deluzarche, A., Kieffer, R. & Muth, A. Reactions CO, H2 - synthese du methanol sur chromite de zinc etude d'especes chimisorbees a la surface du catalyseur schemas reactionnels possibles. *Tetrahedron Lett.* **18**, 3357–3360 (1977).
59. Sapienza, R. S., Sansone, M. J., Spaulding, L. D. & Lynch, J. F. Novel Interpretations of Carbon Oxide Reductions. in *Fundamental Research in Homogeneous Catalysis* 179–197 (Springer US, 1979). doi:10.1007/978-1-4613-2958-9_13.
60. De Klerk, A. & Furimsky, E. *Catalysis in the Refining of Fischer-Tropsch Syncrude (RSC Catalysis Series)*. (2010).
61. Deugd, R. de, Kapteijn, F., Moulijn, J. A. & de Deugd, R. M. Trends in Fischer–Tropsch reactor technology—opportunities for structured reactors. *Top. Catal.* **26**, 29–39 (2003).
62. de Deugd, R. M., Kapteijn, F. & Moulijn, J. a. Using monolithic catalysts for highly selective Fischer–Tropsch synthesis. *Catal. Today* **79–80**, 495–501 (2003).
63. Kapteijn, F., De Deugd, R. M. & Moulijn, J. A. Fischer-Tropsch synthesis using monolithic catalysts. *Catal. Today* **105**, 350–356 (2005).

64. Visconti, C. G., Tronconi, E., Groppi, G., Lietti, L., Iovane, M., Rossini, S. & Zennaro, R. Monolithic catalysts with high thermal conductivity for the Fischer–Tropsch synthesis in tubular reactors. *Chem. Eng. J.* **171**, 1294–1307 (2011).
65. De Deugd, R. M., Kapteijn, F. & Moulijn, J. A. Using monolithic catalysts for highly selective Fischer-Tropsch synthesis. *Catal. Today* **79**–**80**, 495–501 (2003).
66. De Deugd, R. M., Chougule, R. B., Kreutzer, M. T., Meeuse, F. M., Grievink, J., Kapteijn, F. & Moulijn, J. A. Is a monolithic loop reactor a viable option for Fischer - Tropsch synthesis? *Chem. Eng. Sci.* **58**, 583–591 (2003).
67. Güttel, R., Knochen, J., Kunz, U. & Turek, T. Fischer-Tropsch synthesis on monolith catalysts with recirculation of the liquid. *Fischer-Tropsch-synthese an Monolith. bei rezirkulation der flüssigkeit* **79**, 1295 (2007).
68. Güttel, R., Kunz, U., Turek, T., Bauer, T. & Lange, R. Theoretical studies of the use of monolith reactors in Fischer-Tropsch synthesis. *Theor. Untersuchungen zum Einsatz von Monolith. der Fischer-Tropsch-Synthese* **77**, 1175–1176 (2005).
69. Almeida, L. C., Echave, F. J., Sanz, O., Centeno, M. A., Arzamendi, G., Gandía, L. M., Sousa-Aguiar, E. F., Odriozola, J. A. & Montes, M. Fischer-Tropsch synthesis in microchannels. *Chem. Eng. J.* **167**, 536–544 (2011).
70. Liu, W., Hu, J. & Wang, Y. Fischer-Tropsch synthesis on ceramic monolith-structured catalysts. *Catal. Today* **140**, 142–148 (2009).
71. Liu, W., Wang, Y., Wilcox, W. & Li, S. A compact and high throughput reactor of monolithic-structured catalyst bed for conversion of syngas to liquid fuels. *AIChE Journal* vol. in press (2011).
72. MIT. Monolithic reactor. https://lost-contact.mit.edu/afs/nada.kth.se/amdlinks/pkg/femlab/3.1x/doc/chemmodlib/chem31_ml_reaction5.htm (2020).
73. Avila, P., Montes, M. & Miró, E. E. Monolithic reactors for environmental applications: A review on preparation technologies. *Chem. Eng. J.* **109**, 11–36 (2005).
74. Nijhuis, T. A., Beers, A. E. W., Vergunst, T., Hoek, I., Kapteijn, F. & Moulijn, J. Preparation of monolithic catalysts. *Catal. Rev.* **43**, 345–380 (2001).
75. Hunpinyo, P., Narataruksa, P., Tungkamani, S., Pana-Suppamassadu, K., Chollacoop, N., Sukkathanyawat, H. & Jiamrittiwong, P. *A comprehensive small and pilot fixed bed reactor approach for testing Fischer-Tropsch catalyst activity and performance on BTL route*. *Arabian Journal of Chemistry* (King Saud University, 2013). doi:10.1016/j.arabjc.2013.11.004.
76. Xu, Moulijn, J. A., Xiaoding, X. & Moulijn, J. A. Mitigation of CO2 by Chemical Conversion: Plausible Chemical Reactions and Promising Products. *Energy & Fuels* **10**, 305–325 (1996).
77. Yang, J., Ma, W., Chen, D., Holmen, A. & Davis, B. H. Fischer-Tropsch synthesis: A review of the effect of CO conversion on methane selectivity. *Appl. Catal. A Gen.* **470**, 250–260 (2014).
78. Adeleke, A. A., Liu, X., Lu, X., Moyo, M. & Hildebrandt, D. Cobalt hybrid catalysts in Fischer-Tropsch synthesis. *Rev. Chem. Eng.* (2018) doi:10.1515/revce-2018-0012.
79. Al-Sabawi, M. & de Lasa, H. Modeling thermal and catalytic conversion of decalin under industrial FCC operating conditions. *Chem. Eng. Sci.* **65**, 626–644 (2010).
80. Feng, W., Vynckier, E. & Froment, G. F. Single-event kinetics of catalytic cracking. *Ind. Eng. Chem. Res.* **32**, 2997–3005 (1993).

81. Martínez, A., Valencia, S., Murciano, R., Cerqueira, H. S., Costa, A. F. & S.-Aguiar, E. F. Catalytic behavior of hybrid Co/SiO2-(medium-pore) zeolite catalysts during the one-stage conversion of syngas to gasoline. *Applied Catalysis A: General* vol. 346 117–125 (2008).
82. Li, X.-G. *et al.* Tuning interactions between zeolite and supported metal by physical-sputtering to achieve higher catalytic performances. *Sci. Rep.* **3**, 2813 (2013).
83. Martínez, A. & López, C. The influence of ZSM-5 zeolite composition and crystal size on the in situ conversion of Fischer-Tropsch products over hybrid catalysts. *Appl. Catal. A Gen.* **294**, 251–259 (2005).
84. Zhang, Y., Koike, M., Yang, R., Hinchiranan, S., Vitidsant, T. & Tsubaki, N. Multi-functional alumina-silica bimodal pore catalyst and its application for Fischer-Tropsch synthesis. *Appl. Catal. A Gen.* **292**, 252–258 (2005).
85. Zhang, Y., Nagamori, S., Hinchiranan, S., Vitidsant, T. & Tsubaki, N. Promotional effects of Al2O3 addition to Co/SiO2 catalysts for Fischer - Tropsch synthesis. *Energy and Fuels* **20**, 417–421 (2006).
86. Liu, G., Chen, Q., Oyunkhand, E., Ding, S., Yamane, N., Yang, G., Yoneyama, Y. & Tsubaki, N. Nitrogen-rich mesoporous carbon supported iron catalyst with superior activity for Fischer-Tropsch synthesis. *Carbon N. Y.* **130**, 304–314 (2018).
87. Xing, C. *et al.* Tunable isoparaffin and olefin yields in Fischer-Tropsch synthesis achieved by a novel iron-based micro-capsule catalyst. *Catal. Today* **251**, 41–46 (2015).
88. Prech, J. *et al.* Core-shell metal zeolite composite catalysts for in-situ processing of Fischer-Tropsch hydrocarbons to gasoline type fuels Core-Shell Metal Zeolite Composite Catalysts for In-Situ Processing of Fischer- Tropsch Hydrocarbons to Gasoline Type Fuels. (2020) doi:10.1021/acscatal.9b04421.
89. Li, X., He, J., Meng, M., Yoneyama, Y. & Tsubaki, N. One-step synthesis of H-β zeolite-enwrapped Co/Al2O3 Fischer-Tropsch catalyst with high spatial selectivity. *J. Catal.* **265**, 26–34 (2009).
90. Yang, G., Thongkam, M., Vitidsant, T., Yoneyama, Y., Tan, Y. & Tsubaki, N. A double-shell capsule catalyst with core–shell-like structure for one-step exactly controlled synthesis of dimethyl ether from CO_2 containing syngas. *Catal. Today* **171**, 229–235 (2011).
91. Bao, J., He, J., Zhang, Y., Yoneyama, Y. & Tsubaki, N. A core/shell catalyst produces a spatially confined effect and shape selectivity in a consecutive reaction. *Angew. Chemie - Int. Ed.* **47**, 353–356 (2008).
92. Elvirosa Brancaccio. GTL: Small Scale and Modular Technologies for Gas to Liquid Industry. *Oil Gas Portal* 1–31 (2017).
93. Urban, Z. Modular and Scalable Fischer-Tropsch Reactor for Small-Scale Gas-to-Liquid Production. *Chem. Eng. Technol.* **39**, 2142–2150 (2016).
94. U.S. EIA. The Distribution of U.S. Oil and Natural Gas Wells by Production Rate. 68 (2018).
95. EOG. Satellite-Detected Natural Gas Flaring. https://viirs.skytruth.org/apps/heatmap/flaringmap.html#lat=78.30592&lon=-338.66501&zoom=6&offset=15 (2020).
96. CompactGTL. Resource Opportunity. http://www.compactgtl.com/about/resources/ (2020).
97. CompactGTL. Achievement. http://www.compactgtl.com/about/achievements/ (2020).
98. Cao, C., Hu, J., Li, S., Wilcox, W. & Wang, Y. Intensified Fischer-Tropsch synthesis process with microchannel catalytic reactors. *Catal. Today* **140**, 149–156 (2009).

99. Cao, C., Wang, Y., Jones, S. B., Hu, J., Li, X. S., Elliott, D. C. & Stevens, D. J. Microchannel Catalytic Processes for Converting Biomass-Derived Syngas to Transportation Fuels. in 273–284 (2005). doi:10.1021/bk-2005-0914.ch017.
100. Górak, A. & Stankiewicz, A. Intensified reaction and separation systems. *Annu. Rev. Chem. Biomol. Eng.* **2**, 431–51 (2011).
101. Zhang, Y., Doroodchi, E. & Moghtaderi, B. Chemical looping combustion of ultra low concentration of methane with Fe2O3/Al2O3 and CuO/SiO2. *Appl. Energy* **113**, 1916–1923 (2014).
102. Corbella, B. M., De Diego, L. F., García-Labiano, F., Adánez, J., Palaciost, J. M. & Palacios, J. M. Characterization study and five-cycle tests in a fixed-bed reactor of titania-supported nickel oxide as oxygen carriers for the chemical-looping combustion of methane. *Environ. Sci. Technol.* **39**, 5796–5803 (2005).
103. Rytter, E., Borg, Ø., Enger, B. C. & Holmen, A. A-alumina as catalyst support in Co Fischer-Tropsch synthesis and the effect of added water; encompassing transient effects. *J. Catal.* **373**, 13–24 (2019).
104. Gayán, P., de Diego, L. F., García-Labiano, F., Adánez, J., Abad, A. & Dueso, C. Effect of support on reactivity and selectivity of Ni-based oxygen carriers for chemical-looping combustion. *Fuel* **87**, 2641–2650 (2008).
105. Fu, T. & Li, Z. Highly dispersed cobalt on N-doped carbon nanotubes with improved Fischer-Tropsch synthesis activity. *Catal. Commun.* **47**, 54–57 (2014).
106. Kasht, A., Hussain, R., Ghouri, M., Blank, J. & Elbashir, N. O. Product Analysis of Supercritical Fischer-Tropsch Synthesis : Utilizing a Unique On-Line and Off-Line Gas Chromatographs Setup in a Bench-Scale Reactor Unit. 659–676 (2015) doi:10.4236/ajac.2015.68064.
107. Emeis, C. A. Determination of Integrated Molar Extinction Coefficients for Infrared Absorption Bands of Pyridine Adsorbed on Solid Acid Catalysts. *J. Catal.* **141**, 347–354 (1993).
108. Bell, A. T., Gates, B. C., Ray, D. & Thompson, M. R. *Basic Research Needs: Catalysis for Energy, DOE SC Basic Energy Sciences*. (2008) doi:10.2172/927492.
109. Du, S., Gamliel, D. P., Giotto, M. V., Valla, J. A. & Bollas, G. M. Coke formation of model compounds relevant to pyrolysis bio-oil over ZSM-5. *Appl. Catal. A Gen.* **513**, 67–81 (2016).
110. Du, S., Valla, J. A., Parnas, R. S. & Bollas, G. M. Conversion of Polyethylene Terephthalate Based Waste Carpet to Benzene-Rich Oils through Thermal, Catalytic, and Catalytic Steam Pyrolysis. *ACS Sustain. Chem. Eng.* **4**, 2852–2860 (2016).
111. Dixon, R. K., McGowan, E., Onysko, G. & Scheer, R. M. US energy conservation and efficiency policies: Challenges and opportunities. *Energy Policy* **38**, 6398–6408 (2010).
112. Bang, G. Energy security and climate change concerns: Triggers for energy policy change in the United States? *Energy Policy* **38**, 1645–1653 (2010).
113. de Deugd, R. M., Chougule, R. B., Kreutzer, M. T., Meeuse, F. M., Grievink, J., Kapteijn, F. & Moulijn, J. a. Is a monolithic loop reactor a viable option for Fischer–Tropsch synthesis? *Chem. Eng. Sci.* **58**, 583–591 (2003).
114. Khodakov, A. Y., Chu, W. & Fongarland, P. Advances in the Development of Novel Cobalt Fischer − Tropsch Catalysts for Synthesis of Long-Chain Hydrocarbons and Clean Fuels Advances in the Development of Novel Cobalt Fischer − Tropsch Catalysts for Synthesis of Long-Chain Hydrocarbons and Clean Fue. **107**, 1692–1744 (2007).

115. Marin, R. P. *et al.* Preparation of Fischer–Tropsch Supported Cobalt Catalysts Using a New Gas Anti-Solvent Process. *ACS Catal.* **3**, 764–772 (2013).
116. Pangarkar, K., Schildhauer, T. J., van Ommen, J. R., Nijenhuis, J., Moulijn, J. A. & Kapteijn, F. Experimental and numerical comparison of structured packings with a randomly packed bed reactor for Fischer–Tropsch synthesis. *Catal. Today* **147**, S2–S9 (2009).
117. Kapteijn, F., de Deugd, R. M. & Moulijn, J. A. Fischer–Tropsch synthesis using monolithic catalysts. *Catal. Today* **105**, 350–356 (2005).
118. Botes, F. G. & Böhringer, W. The addition of HZSM-5 to the Fischer – Tropsch process for improved gasoline production. **267**, 217–225 (2004).
119. Guettel, R., Knochen, J., Kunz, U., Kassing, M. & Turek, T. Preparation and Catalytic Evaluation of Cobalt-Based Monolithic and Powder Catalysts for Fischer - Tropsch Synthesis. 6589–6597 (2008).
120. van der Laan, G. P. & Beenackers, A. A. C. M. Intrinsic kinetics of the gas–solid Fischer–Tropsch and water gas shift reactions over a precipitated iron catalyst. *Appl. Catal. A Gen.* **193**, 39–53 (2000).
121. Dry, M. E. The Fischer-Tropsch synthesis. in *Catalysis: Science and Technology Vol. I* (eds. Anderson, J. R. & M., B.) (Springer US, 1981).
122. Dry, M. E. Practical and theoretical aspects of the catalytic Fischer-Tropsch process. *Appl. Catal. A Gen.* **138**, 319–344 (1996).
123. Xing, C., Shen, W., Yang, G., Yang, R., Lu, P., Sun, J., Yoneyama, Y. & Tsubaki, N. Completed encapsulation of cobalt particles in mesoporous H-ZSM-5 zeolite catalyst for direct synthesis of middle isoparaffin from syngas. *Catal. Commun.* **55**, 53–56 (2014).
124. Yang, G., Wang, D., Yoneyama, Y., Tan, Y. & Tsubaki, N. Facile synthesis of H-type zeolite shell on a silica substrate for tandem catalysis. *Chem. Commun.* **48**, 1263 (2012).
125. Tsubaki, N., Yoneyama, Y., Michiki, K. & Fujimoto, K. Three-component hybrid catalyst for direct synthesis of isoparaffin via modified Fischer–Tropsch synthesis. *Catal. Commun.* **4**, 108–111 (2003).
126. He, J. J., Xu, B. L., Yoneyama, Y., Nishiyama, N. & Tsubaki, N. Designing a new kind of capsule catalyst and its application for direct synthesis of middle isoparaffins from synthesis gas. *Chem. Lett.* **34**, 148–149 (2005).
127. Bao, J., He, J., Zhang, Y., Yoneyama, Y. & Tsubaki, N. A Core/Shell Catalyst Produces a Spatially Confined Effect and Shape Selectivity in a Consecutive Reaction. *Angew. Chemie Int. Ed.* **47**, 353–356 (2008).
128. Li, C., Xu, H., Kido, Y., Yoneyama, Y., Suehiro, Y. & Tsubaki, N. A capsule catalyst with a zeolite membrane prepared by direct liquid membrane crystallization. *ChemSusChem* **5**, 862–866 (2012).
129. Klerk, A. de. Fischer–Tropsch fuels refinery design. *Energy Environ. Sci.* **4**, 1177 (2011).
130. Enger, B. C., Fossan, Å. L., Borg, Ø., Rytter, E. & Holmen, A. Modified alumina as catalyst support for cobalt in the Fischer-Tropsch synthesis. *J. Catal.* **284**, 9–22 (2011).
131. Li, X., He, J., Meng, M., Yoneyama, Y. & Tsubaki, N. One-step synthesis of H–β zeolite-enwrapped Co/Al2O3 Fischer–Tropsch catalyst with high spatial selectivity. *J. Catal.* **265**, 26–34 (2009).
132. Yang, G., Xing, C., Hirohama, W., Jin, Y., Zeng, C., Suehiro, Y., Wang, T., Yoneyama, Y. & Tsubaki, N. Tandem catalytic synthesis of light isoparaffin from syngas via Fischer-Tropsch synthesis by newly developed core-shell-like zeolite capsule catalysts. *Catal.*

Today **215**, 29–35 (2013).
133. Liu, J.-Y., Chen, J.-F. & Zhang, Y. Cobalt-imbedded zeolite catalyst for direct syntheses of gasoline via Fischer–Tropsch synthesis. *Catal. Sci. Technol.* **3**, 2559 (2013).
134. Sartipi, S., Makkee, M., Kapteijn, F. & Gascon, J. Catalysis engineering of bifunctional solids for the one-step synthesis of liquid fuels from syngas: a review. *Catal. Sci. Technol.* **4**, 893–907 (2014).
135. Duyckaerts, N., Trotuş, I.-T., Swertz, A.-C., Schüth, F. & Prieto, G. In Situ Hydrocracking of Fischer–Tropsch Hydrocarbons: CO-Prompted Diverging Reaction Pathways for Paraffin and α-Olefin Primary Products. *ACS Catal.* **6**, 4229–4238 (2016).
136. Rytter, E., Tsakoumis, N. E. & Holmen, A. On the selectivity to higher hydrocarbons in Co-based Fischer-Tropsch synthesis. *Catal. Today* **261**, 3–16 (2016).
137. Iglesia, E. Fischer-tropsch synthesis on cobalt catalysts: Structural requirements and reaction pathways. *Stud. Surf. Sci. Catal.* **107**, 153–162 (1997).
138. Iglesia, E., Soled, S. L., Baumgartner, J. E. & Reyes, S. C. Synthesis and Catalytic Properties of Eggshell Cobalt Catalysts for the Fischer-Tropsch Synthesis. *Journal of Catalysis* vol. 153 108–122 (1995).
139. Halmenschlager, C. M., Brar, M., Apan, I. T. & de Klerk, A. Oligomerization of Fischer–Tropsch Tail Gas over H-ZSM-5. *Ind. Eng. Chem. Res.* **55**, 13020–13031 (2016).
140. Ismagilov, Z. R., Matus, E. V. & Tsikoza, L. T. Direct conversion of methane on Mo/ZSM-5 catalysts to produce benzene and hydrogen: achievements and perspectives. *Energy Environ. Sci.* **1**, 526 (2008).
141. Sun, B. *et al.* A highly selective Raney Fe@HZSM-5 Fischer–Tropsch synthesis catalyst for gasoline production: one-pot synthesis and unexpected effect of zeolites. *Catal. Sci. Technol.* **2**, 1625 (2012).
142. Yao, M., Yao, N., Shao, Y., Han, Q., Ma, C., Yuan, C., Li, C. & Li, X. New insight into the activity of ZSM-5 supported Co and CoRu bifunctional Fischer-Tropsch synthesis catalyst. *Chem. Eng. J.* **239**, 408–415 (2014).
143. Sartipi, S., Alberts, M., Meijerink, M. J., Keller, T. C., Perez-Ramirez, J., Gascon, J. & Kapteijn, F. Towards liquid fuels from biosyngas: Effect of zeolite structure in hierarchical-zeolite-supported cobalt catalysts. *ChemSusChem* **6**, 1646–1650 (2013).
144. Sartipi, S., Van Dijk, J. E., Gascon, J. & Kapteijn, F. Toward bifunctional catalysts for the direct conversion of syngas to gasoline range hydrocarbons: H-ZSM-5 coated Co versus H-ZSM-5 supported Co. *Appl. Catal. A Gen.* **456**, 11–22 (2013).
145. He, J., Liu, Z., Yoneyama, Y., Nishiyama, N. & Tsubaki, N. Multiple-functional capsule catalysts: A tailor-made confined reaction environment for the direct synthesis of middle isoparaffins from syngas. *Chem. - A Eur. J.* **12**, 8296–8304 (2006).
146. Brown, S. Catalysis in the refining of fischer-tropsch syncrude. *Platin. Met. Rev.* **55**, 263–267 (2011).
147. Johnson, G. R., Werner, S. & Bell, A. T. An Investigation into the Effects of Mn Promotion on the Activity and Selectivity of Co/SiO 2 for Fischer–Tropsch Synthesis: Evidence for Enhanced CO Adsorption and Dissociation. *ACS Catal.* **5**, 5888–5903 (2015).
148. Yan, Z., Wang, Z., Bukur, D. B. & Goodman, D. W. Fischer-Tropsch synthesis on a model Co/SiO2 catalyst. *J. Catal.* **268**, 196–200 (2009).
149. Martínez, A., López, C., Márquez, F. & Díaz, I. Fischer-Tropsch synthesis of hydrocarbons over mesoporous Co/SBA-15 catalysts: The influence of metal loading, cobalt precursor, and promoters. *J. Catal.* **220**, 486–499 (2003).

150. Tsubaki, N., Sun, S. & Fujimoto, K. Different Functions of the Noble Metals Added to Cobalt Catalysts for Fischer-Tropsch Synthesis. *J. Catal.* **199**, 236–246 (2001).
151. Gamliel, D. P., Du, S., Bollas, G. M. & Valla, J. A. Investigation of in-situ and ex-situ catalytic pyrolysis of miscanthus x giganteus using a PyGC-MS microsystem and comparison with a bench-scale spouted-bed reactor. *Bioresour. Technol.* (2015) doi:10.1016/j.biortech.2015.04.129.
152. Du, S., Sun, Y., Gamliel, D. P., Valla, J. A. & Bollas, G. M. Catalytic pyrolysis of miscanthus × giganteus in a spouted bed reactor. *Bioresour. Technol.* **169**, 188–197 (2014).
153. Dry, M. E. The Fischer-Tropsch process: 1950-2000. *Catalysis Today* vol. 71 227–241 (2002).
154. Iglesia, E. Design, synthesis, and use of cobalt-based Fischer-Tropsch synthesis catalysts. *Appl. Catal. A Gen.* **161**, 59–78 (1997).
155. Song, D. & Li, J. Effect of catalyst pore size on the catalytic performance of silica supported cobalt Fischer-Tropsch catalysts. *J. Mol. Catal. A Chem.* **247**, 206–212 (2006).
156. Sartipi, S., Parashar, K., Valero-Romero, M. J., Santos, V. P., Van Der Linden, B., Makkee, M., Kapteijn, F. & Gascon, J. Hierarchical H-ZSM-5-supported cobalt for the direct synthesis of gasoline-range hydrocarbons from syngas: Advantages, limitations, and mechanistic insight. *J. Catal.* **305**, 179–190 (2013).
157. Khodakov, A. Y., Chu, W. & Fongarland, P. Advances in the Development of Novel Cobalt Fischer—Tropsch Catalysts for Synthesis of Long-Chain Hydrocarbons and Clean Fuels. *ChemInform* **107**, 1692–1744 (2007).
158. Chu, W., Chernavskii, P. A., Gengembre, L., Pankina, G. A., Fongarland, P. & Khodakov, A. Y. Cobalt species in promoted cobalt alumina-supported Fischer-Tropsch catalysts. *J. Catal.* **252**, 215–230 (2007).
159. Botes, F. G. & Böhringer, W. The addition of HZSM-5 to the Fischer-Tropsch process for improved gasoline production. *Appl. Catal. A Gen.* **267**, 217–225 (2004).
160. Liu, S., Gujar, A. C., Thomas, P., Toghiani, H. & White, M. G. Synthesis of gasoline-range hydrocarbons over Mo/HZSM-5 catalysts. *Applied Catalysis A: General* vol. 357 18–25 (2009).
161. S. Zola, A., Bidart, A. M. F., do C. Fraga, A., E. Hori, C., F. Sousa-Aguiar, E. & A. Arroyo, P. Cobalt supported on different zeolites for fischer-tropschsynthesis. *Stud. Surf. Sci. Catal.* **167**, 129–134 (2007).
162. Martínez, A., Rollán, J., Arribas, M. A., Cerqueira, H. S., Costa, A. F. & S.-Aguiar, E. F. A detailed study of the activity and deactivation of zeolites in hybrid Co/SiO2-zeolite Fischer-Tropsch catalysts. *J. Catal.* **249**, 162–173 (2007).
163. Li, Y., Wang, T., Wu, C., Lv, Y. & Tsubaki, N. Gasoline-range hydrocarbon synthesis over cobalt-based Fischer-Tropsch catalysts supported on SiO2/HZSM-5. *Energy and Fuels* **22**, 1897–1901 (2008).
164. Yang, G., He, J., Yoneyama, Y., Tan, Y., Han, Y. & Tsubaki, N. Preparation, characterization and reaction performance of H-ZSM-5/cobalt/silica capsule catalysts with different sizes for direct synthesis of isoparaffins. *Applied Catalysis A: General* vol. 329 99–105 (2007).
165. He, J., Liu, Z., Yoneyama, Y., Nishiyama, N. & Tsubaki, N. Multiple-functional capsule catalysts: A tailor-made confined reaction environment for the direct synthesis of middle isoparaffins from syngas. *Chem. - A Eur. J.* **12**, 8296–8304 (2006).
166. He, J., Yoneyama, Y., Xu, B., Nishiyama, N. & Tsubaki, N. Designing a capsule catalyst

and its application for direct synthesis of middle isoparaffins. *Langmuir* **21**, 1699–1702 (2005).
167. Wang, Y. *et al.* Application of mesoporous ZSM-5 as a support for Fischer-Tropsch cobalt catalysts. *J. Porous Mater.* **22**, 339–345 (2015).
168. Zhu, C. & Bollas, G. M. Gasoline selective Fischer-Tropsch synthesis in structured bifunctional catalysts. *Appl. Catal. B Environ.* **235**, 92–102 (2018).
169. Valero-Romero, M. J., Sartipi, S., Sun, X., Rodríguez-Mirasol, J., Cordero, T., Kapteijn, F. & Gascon, J. Carbon/H-ZSM-5 composites as supports for bi-functional Fischer–Tropsch synthesis catalysts. *Catal. Sci. Technol.* **6**, 2633–2646 (2016).
170. Verboekend, D. & Pérez-Ramírez, J. Design of hierarchical zeolite catalysts by desilication. *Catal. Sci. Technol.* **1**, 879 (2011).
171. Gamliel, D. P., Cho, H. J., Fan, W. & Valla, J. A. On the effectiveness of tailored mesoporous MFI zeolites for biomass catalytic fast pyrolysis. *Appl. Catal. A Gen.* **522**, 109–119 (2016).
172. Gamliel, D. P., Bollas, G. M. & Valla, J. A. Bifunctional Ni-ZSM-5 Catalysts for the Pyrolysis and Hydropyrolysis of Biomass. *Energy Technol.* **5**, 172–182 (2017).
173. Bae, J. S. *et al.* Eco-friendly prepared iron-ore-based catalysts for Fischer-Tropsch synthesis. *Appl. Catal. B Environ.* **244**, 576–582 (2019).
174. Silva, L. S. da, Araki, C. A., Marcucci, S. M. P., Silva, V. L. dos S. T. da & Arroyo, P. A. Desilication of ZSM-5 and ZSM-12 Zeolites with Different Crystal Sizes: Effect on Acidity and Mesoporous Initiation. *Mater. Res.* **22**, (2019).
175. Jin, Y., Yang, G., Chen, Q., Niu, W., Lu, P., Yoneyama, Y. & Tsubaki, N. Development of dual-membrane coated Fe/SiO2 catalyst for efficient synthesis of isoparaffins directly from syngas. *J. Memb. Sci.* **475**, 22–29 (2015).
176. Francis, J., Guillon, E., Bats, N., Pichon, C., Corma, A. & Simon, L. J. Design of improved hydrocracking catalysts by increasing the proximity between acid and metallic sites. *Appl. Catal. A Gen.* **409**–**410**, 140–147 (2011).
177. Firmansyah, M. L., Jalil, A. A., Triwahyono, S., Hamdan, H., Salleh, M. M., Ahmad, W. F. W. & Kadja, G. T. M. Synthesis and characterization of fibrous silica ZSM-5 for cumene hydrocracking. *Catal. Sci. Technol.* **6**, 5178–5182 (2016).
178. Li, J. *et al.* Integrated tuneable synthesis of liquid fuels via Fischer–Tropsch technology. *Nat. Catal.* **1**, 787–793 (2018).
179. Kim, N. Y. *et al.* Synthesis and characterization of Al-modified SBA-15 for Fischer-Tropsch synthesis (FTS) reaction. *Res. Chem. Intermed.* **42**, 319–334 (2016).
180. Lezcano-Gonzalez, I., Deka, U., Arstad, B., Van Yperen-De Deyne, A., Hemelsoet, K., Waroquier, M., Van Speybroeck, V., Weckhuysen, B. M. & Beale, A. M. Determining the storage, availability and reactivity of NH_3 within Cu-Chabazite-based Ammonia Selective Catalytic Reduction systems. *Phys. Chem. Chem. Phys.* **16**, 1639–1650 (2014).
181. Chang, C. C., Cho, H. J., Wang, Z., Wang, X. & Fan, W. Fluoride-free synthesis of a Sn-BEA catalyst by dry gel conversion. *Green Chem.* **17**, 2943–2951 (2015).
182. Djinović, P., Levec, J. & Pintar, A. Effect of structural and acidity/basicity changes of CuO-CeO2 catalysts on their activity for water-gas shift reaction. *Catal. Today* **138**, 222–227 (2008).
183. De Jong, K. P. *et al.* Zeolite y crystals with trimodal porosity as ideal hydrocracking catalysts. *Angew. Chemie - Int. Ed.* **49**, 10074–10078 (2010).
184. Xing, C. *et al.* Hierarchical zeolite y supported cobalt bifunctional catalyst for facilely

tuning the product distribution of Fischer-Tropsch synthesis. *Fuel* **148**, 48–57 (2015).
185. Khodakov, A. Y., Griboval-Constant, A., Bechara, R. & Zholobenko, V. L. Pore size effects in Fischer Tropsch synthesis over cobalt-supported mesoporous silicas. *J. Catal.* **206**, 230–241 (2002).
186. de Klerk, A. Hydroprocessing peculiarities of Fischer-Tropsch syncrude. *Catal. Today* **130**, 439–445 (2008).
187. Yates, I. C. & Satterfield, C. N. Intrinsic Kinetics of the Fischer-Tropsch Synthesis on a Cobalt Catalyst. *Energy and Fuels* **5**, 168–173 (1991).
188. Yang, J., Frøseth, V., Chen, D. & Holmen, A. Particle size effect for cobalt Fischer-Tropsch catalysts based on in situ CO chemisorption. *Surf. Sci.* **648**, 67–73 (2016).
189. Peng, X., Cheng, K., Kang, J., Gu, B., Yu, X., Zhang, Q. & Wang, Y. Impact of Hydrogenolysis on the Selectivity of the Fischer-Tropsch Synthesis: Diesel Fuel Production over Mesoporous Zeolite-Y-Supported Cobalt Nanoparticles. *Angew. Chemie - Int. Ed.* **54**, 4553–4556 (2015).
190. Liu, Z.-W., Li, X., Asami, K. & Fujimoto, K. High performance Pd/beta catalyst for the production of gasoline-range iso-paraffins via a modified Fischer-Tropsch reaction. *Appl. Catal. A Gen.* **300**, 162–169 (2006).
191. Tsubaki, N. & Fujimoto, K. Product control in Fischer-Tropsch synthesis. *Fuel Process. Technol.* **62**, 173–186 (2000).
192. Dinse, A., Aigner, M., Ulbrich, M., Johnson, G. R. & Bell, A. T. Effects of Mn promotion on the activity and selectivity of Co/SiO 2 for Fischer-Tropsch Synthesis. *J. Catal.* **288**, 104–114 (2012).
193. Kim, S., Xu, Z., Reddy, G. K., Smirniotis, P. & Dong, J. Effect of Pressure on High-Temperature Water Gas Shift Reaction in Microporous Zeolite Membrane Reactor. (2012) doi:10.1021/ie201452y.
194. Du, S., Valla, J. A. & Bollas, G. M. Characteristics and origin of char and coke from fast and slow, catalytic and thermal pyrolysis of biomass and relevant model compounds. *Green Chem.* **15**, 3214 (2013).
195. EIA, R. *U.S. Energy Flow*. (2018).
196. Liang, F.-Y., Ryvak, M., Sayeed, S. & Zhao, N. The role of natural gas as a primary fuel in the near future, including comparisons of acquisition, transmission and waste handling costs of as with competitive alternatives. *Chem. Cent. J.* **6**, S4 (2012).
197. Wood, D. A., Nwaoha, C. & Towler, B. F. Gas-to-liquids (GTL): A review of an industry offering several routes for monetizing natural gas. *J. Nat. Gas Sci. Eng.* **9**, 196–208 (2012).
198. Faramawy, S., Zaki, T. & Sakr, A. A. E. Natural gas origin, composition, and processing: A review. *J. Nat. Gas Sci. Eng.* **34**, 34–54 (2016).
199. Charles F. Mason, Lucija A. Muehlenbachs, S. M. O. The Economics of Shale Gas Development. *Annu. Rev. Resour. Econ.* **7**, 269–289 (2015).
200. Attanasi, E. & Freeman, P. Role of stranded gas in increasing global gas supplies. *US Geol. Surv. Open-File Rep. 2013-1044* (2013).
201. Onel, O., Niziolek, A. M. & Floudas, C. A. Natural gas to liquid transportation fuels, olefins, and aromatics. *CAMX 2015 - Compos. Adv. Mater. Expo* 1562–1575 (2015).
202. Iglesia, E., Spivey, J. J. & FLeisch T.H. *Natural GAS CONVERSION VI*. (Elsevier, 2011, 2001).
203. Koortzen, J. G., Bains, S., Kocher, L. L., Baxter, I. K. & Morgan, R. A. Modular gas-to-liquid: Converting a liability into economic value. *Ind. Eng. Chem. Res.* **53**, 1720–1726

(2014).
204. Hao, X., Djatmiko, M. E., Xu, Y., Wang, Y., Chang, J. & Li, Y. Simulation analysis of a gas-to-liquid process using aspen plus. *Chem. Eng. Technol.* **31**, 188–196 (2008).
205. Zhou, H., Yang, S., Xiao, H., Yang, Q., Qian, Y. & Gao, L. Modeling and techno-economic analysis of shale-to-liquid and coal-to-liquid fuels processes. *Energy* **109**, 201–210 (2016).
206. J. Otaraku, I. Technical Analysis of the Natural Gas to Hydrocarbon Liquid Process. *Am. J. Chem. Eng.* **3**, 25 (2015).
207. Fazeli, H., Panahi, M. & Rafiee, A. Investigating the potential of carbon dioxide utilization in a gas-to-liquids process with iron-based Fischer-Tropsch catalyst. *J. Nat. Gas Sci. Eng.* **52**, 549–558 (2018).
208. Ha, K. S., Bae, J. W., Woo, K. J. & Jun, K. W. Efficient utilization of greenhouse gas in a gas-to-liquids process combined with carbon dioxide reforming of methane. *Environ. Sci. Technol.* **44**, 1412–1417 (2010).
209. Rafiee, A., Panahi, M. & Khalilpour, K. R. CO2 utilization through integration of post-combustion carbon capture process with Fischer-Tropsch gas-to-liquid (GTL) processes. *J. CO2 Util.* **18**, 98–106 (2017).
210. EIA. U.S. energy facts explained. https://www.eia.gov/energyexplained/us-energy-facts/ (2019).
211. Texas: Zeus Development Inc. *World LNG/GTL Review*. (2001).
212. Baldea, M. & Edgar, T. F. Modular Manufacturing Processes: Status, Challenges, and Opportunities. *AIChE J.* **63**, 4262–4272 (2017).
213. Adams, T. A. & Barton, P. I. High-efficiency power production from natural gas with carbon capture. *J. Power Sources* **195**, 1971–1983 (2010).
214. Salkuyeh, Y. K. & Adams, T. A. Combining coal gasification, natural gas reforming, and external carbonless heat for efficient production of gasoline and diesel with CO2 capture and sequestration. *Energy Convers. Manag.* **74**, 492–504 (2013).
215. Fout, T., Zoelle, A., Keairns, D., Turner, M., Woods, M., Kuehn, N., Shah, V., Chou, V. & Pinkerton, L. *Cost and Performance Baseline for Fossil Energy Plants Volume 1a: Bituminous Coal (PC) and Natural Gas to Electricity Revision 3*. *National Energy Technology Laboratory (NETL)* vol. 1 http://www.netl.doe.gov/File Library/Research/Energy Analysis/Publications/Rev3Vol1aPC_NGCC_final.pdf (2015).
216. Zhang, C., Jun, K. W., Ha, K. S., Lee, Y. J. & Kang, S. C. Efficient utilization of greenhouse gases in a gas-to-liquids process combined with CO_2/steam-mixed reforming and Fe-based Fischer-Tropsch synthesis. *Environ. Sci. Technol.* **48**, 8251–8257 (2014).
217. Christensen, T. S. Adiabatic prereforming of hydrocarbons - An important step in syngas production. *Appl. Catal. A Gen.* **138**, 285–309 (1996).
218. Barelli, L., Bidini, G., Gallorini, F. & Servili, S. Hydrogen production through sorption-enhanced steam methane reforming and membrane technology: A review. *Energy* **33**, 554–570 (2008).
219. Ruckenstein, E. & Hu, Y. H. Methane partial oxidation over NiO/MgO solid solution catalysts. *Appl. Catal. A Gen.* **183**, 85–92 (1999).
220. Jang, W. J., Shim, J. O., Kim, H. M., Yoo, S. Y. & Roh, H. S. A review on dry reforming of methane in aspect of catalytic properties. *Catal. Today* **324**, 15–26 (2019).
221. Baltrusaitis, J. & Luyben, W. L. Methane Conversion to Syngas for Gas-to-Liquids (GTL): Is Sustainable CO2 Reuse via Dry Methane Reforming (DMR) Cost Competitive with SMR and ATR Processes? *ACS Sustain. Chem. Eng.* **3**, 2100–2111 (2015).

222. Gangadharan, P., Kanchi, K. C. & Lou, H. H. Evaluation of the economic and environmental impact of combining dry reforming with steam reforming of methane. *Chem. Eng. Res. Des.* **90**, 1956–1968 (2012).
223. Olah, G. A., Goeppert, A., Czaun, M. & Prakash, G. K. S. Bi-reforming of methane from any source with steam and carbon dioxide exclusively to metgas (CO-2H2) for methanol and hydrocarbon synthesis. *J. Am. Chem. Soc.* **135**, 648–650 (2013).
224. Zhang, C., Jun, K. W., Gao, R., Kwak, G. & Kang, S. C. Efficient utilization of associated natural gas in a modular gas-to-liquids process: Technical and economic analysis. *Fuel* **176**, 32–39 (2016).
225. Wei, J. & Iglesia, E. Isotopic and kinetic assessment of the mechanism of reactions of CH4 with CO2 or H2O to form synthesis gas and carbon on nickel catalysts. *J. Catal.* **224**, 370–383 (2004).
226. Gao, J., Hou, Z., Lou, H. & Zheng, X. *Dry (CO2) Reforming*. *Fuel Cells: Technologies for Fuel Processing* (Elsevier, 2011). doi:10.1016/B978-0-444-53563-4.10007-0.
227. Zhang, C., Jun, K. W., Gao, R., Lee, Y. J. & Kang, S. C. Efficient utilization of carbon dioxide in gas-to-liquids process: Process simulation and techno-economic analysis. *Fuel* **157**, 285–291 (2015).
228. Yao, Y., Hildebrandt, D., Glasser, D. & Liu, X. Fischer-tropsch synthesis using H2/CO/CO2 syngas mixtures over a cobalt catalyst. *Ind. Eng. Chem. Res.* **49**, 11061–11066 (2010).
229. Visconti, C. G., Lietti, L., Tronconi, E., Forzatti, P., Zennaro, R. & Finocchio, E. Fischer-Tropsch synthesis on a Co/Al2O3 catalyst with CO2 containing syngas. *Appl. Catal. A Gen.* **355**, 61–68 (2009).
230. Riedel, T. & Schaub, G. Low-temperature Fischer-Tropsch synthesis on cobalt catalysts effects of CO2. *Top. Catal.* **26**, 145–156 (2003).
231. Al-Fatesh, A. S., Arafat, Y., Atia, H., Ibrahim, A. A., Ha, Q. L. M., Schneider, M., M-Pohl, M. & Fakeeha, A. H. CO2-reforming of methane to produce syngas over Co-Ni/SBA-15 catalyst: Effect of support modifiers (Mg, la and Sc) on catalytic stability. *J. CO2 Util.* **21**, 395–404 (2017).
232. Bian, Z., Suryawinata, I. Y. & Kawi, S. Highly carbon resistant multicore-shell catalyst derived from Ni-Mg phyllosilicate nanotubes@silica for dry reforming of methane. *Appl. Catal. B Environ.* **195**, 1–8 (2016).
233. Lacroix, M. *et al.* Silicon carbide foam composite containing cobalt as a highly selective and re-usable Fischer-Tropsch synthesis catalyst. *Appl. Catal. A Gen.* **397**, 62–72 (2011).
234. Rohr, F., Lindvåg, O. A., Holmen, A. & Blekkan, E. A. Fischer-Tropsch Synthesis over Cobalt Catalysts Supported on Zirconia-Modified Alumina. *Catal. Today* **58**, 247–254 (2000).
235. Adams, T. a., Barton, P. I., Adams II, T. A., Barton, P. I., Adams, T. a. & Barton, P. I. Combining coal gasification, natural gas reforming, and solid oxide fuel cells for efficient polygeneration with CO2 capture and sequestration. *Fuel Process. Technol.* **92**, 2105–2115 (2011).
236. HAMELINCK, C. N., FAAIJ, A. P. C., den Uil, H., BOERRIGTER, H., DENUIL, H. & BOERRIGTER, H. Production of FT transportation fuels from biomass; technical options, process analysis and optimisation, and development potential. *Energy* **29**, 1743–1771 (2004).
237. Seider, W. D. *Product and process design principles: synthesis, analysis and evaluation*

(Fourth Edition). (Wiley, 2016).
238. Scott Jenkins. 2019 CHEMICAL ENGINEERING PLANT COST INDEX ANNUAL AVERAGE. https://www.chemengonline.com/2019-chemical-engineering-plant-cost-index-annual-average/ (2020).
239. Ali P.Laleh. Cost Estimation. *SALVA SOLUTION* http://salvasolution.com/costing.htm (2019).
240. Chegg study. Business type question dealing with scaling the cost of equipment costs. https://www.chegg.com/homework-help/questions-and-answers/buisness-type-question-dealing-scaling-cost-equiptment-costs-purchase-cost-shell-tube-heat-q24919401 (2020).
241. Engineering, C. THE CHEMICAL ENGINEERING PLANT COST INDEX. https://www.chemengonline.com/pci-home (2020).
242. U.S. EIA. Weekly Retail Gasoline and Diesel Prices. https://www.eia.gov/dnav/pet/PET_PRI_GND_DCUS_NUS_A.htm (2020).
243. Tonkovich, A., Mazanec, T. & Jarosch, K. Gas-to-liquids conversion of associated gas enabled by microchannel technology. *Velocys* 1–7 (2010).
244. Reuel, R. C. & Bartholomew, C. H. Effects of support and dispersion on the CO hydrogenation activity/selectivity properties of cobalt. *Journal of Catalysis* vol. 85 78–88 (1984).
245. Meunier, F. C., Verboekend, D., Gilson, J.-P. P., Groen, J. C. & Pérez-Ramírez, J. Influence of crystal size and probe molecule on diffusion in hierarchical ZSM-5 zeolites prepared by desilication. *Microporous Mesoporous Mater.* **148**, 115–121 (2012).
246. Prieto, G., Martínez, A., Concepción, P. & Moreno-Tost, R. Cobalt particle size effects in Fischer–Tropsch synthesis: structural and in situ spectroscopic characterisation on reverse micelle-synthesised Co/ITQ-2 model catalysts. *J. Catal.* **266**, 129–144 (2009).
247. den Breejen, J. P., Sietsma, J. R. a, Friedrich, H., Bitter, J. H. & de Jong, K. P. Design of supported cobalt catalysts with maximum activity for the Fischer-Tropsch synthesis. *J. Catal.* **270**, 146–152 (2010).
248. Ding, L., Zhang, M., Zhang, Y., Yang, J., Zheng, J. & Xu, J. A type of raspberry-like silica composite with tunable nickel nanoparticles coverage towards nanocatalysis and protein adsorption. *Green Chem.* 6282–6290 (2016) doi:10.1039/C6GC01613H.
249. Wang, X., Lu, L. L., Yu, Z. L., Xu, X. W., Zheng, Y. R. & Yu, S. H. Scalable template synthesis of resorcinol-formaldehyde/graphene oxide composite aerogels with tunable densities and mechanical properties. *Angew. Chemie - Int. Ed.* **54**, 2397–2401 (2015).
250. Yang, P., Xu, Y., Chen, L., Wang, X. & Zhang, Q. One-Pot Synthesis of Monodisperse Noble Metal @ Resorcinol-Formaldehyde (M@RF) and M@Carbon Core-Shell Nanostructure and Their Catalytic Applications. *Langmuir* **31**, 11701–11708 (2015).
251. Liu, J., Qiao, S. Z., Liu, H., Chen, J., Orpe, A., Zhao, D. & Lu, G. Q. Extension of the stöber method to the preparation of monodisperse resorcinol-formaldehyde resin polymer and carbon spheres. *Angew. Chemie - Int. Ed.* **50**, 5947–5951 (2011).
252. Zheng, W., Guo, Z., Huang, Z., Zhuang, J. & Yang, W. In-situ preparation of size-tunable gold nanoparticles in porous resorcinol-formaldehyde resin. *Colloids Surfaces A Physicochem. Eng. Asp.* **484**, 271–277 (2015).